

A Decade of Collectivity in Small Systems

JAN FIETE GROSSE-OETRINGHAUS

CERN, 1211 Geneva, Switzerland
jgrosseo@cern.ch

URS ACHIM WIEDEMANN

CERN, 1211 Geneva, Switzerland
urs.wiedemann@cern.ch

Signatures of collectivity, including azimuthally anisotropic and radial flow as well as characteristic hadrochemical dependencies, have been observed since long in (ultra)relativistic nucleus–nucleus collisions. They underpin the interpretation of these collision systems in terms of QGP formation and close-to-perfect fluidity. Remarkably, however, essentially all these signatures of collectivity have been identified within the last decade in collision systems as small as pp and p–Pb, where collective phenomena had been assumed to be absent traditionally. Precursor phenomena may have been found even in ep and e^+e^- collisions. This article provides a complete review of all data on small system collectivity. It reviews model simulations of these data where available. However, in the absence of a phenomenologically fully satisfactory description of collectivity across all system sizes, we focus in particular on the theoretical basis of all dynamical frameworks of collectivity invoked in heavy ion collisions, and their expected scaling with system size. Our discussion clarifies to what extent all dynamical explanations are challenged by the available data.

Contents

1	Introduction	3
2	Measures of collectivity and medium-modifications	5
2.1	Measures of anisotropic flow	6
2.2	Hadrochemical measures of collectivity	12
2.3	Hard processes in small systems	14
3	Experimental Overview	15
3.1	Long-range correlations	15
3.2	Bulk properties	22
3.3	Hard probes	23
3.4	Towards even smaller systems...	26
4	Theory overview	29
4.1	Dynamical frameworks of collectivity	31
4.2	Hydrodynamization and Thermalization - insights from simple models	39
4.3	Model studies and data comparisons	42
4.4	Model comparisons to hadrochemical measures of collectivity	44
5	Concluding discussion and outlook	45

In high-energy physics, we have concentrated on experiments in which we distribute a higher and higher amount of energy into a region with smaller and smaller dimensions. But, in order to study the question of ‘vacuum’, we must turn to a different direction; we should investigate bulk phenomena by distributing high energy over a relatively large volume.

T.D. Lee, 1975

1. Introduction

The LHC discovery of collectivity in small systems relates measurements in proton–proton, proton–nucleus and nucleus–nucleus collisions in a remarkably smooth way without any step-wise discontinuity. In addition to an intense experimental effort at the LHC, it has motivated the study of dedicated small collision systems at RHIC, the re-analysis and re-interpretation of data in e^+e^- and ep collisions, and extensive theoretical work. As this review will emphasize, this discovery impacts both: our understanding of the dynamics of nucleus–nucleus collisions (in which signatures of collectivity have been searched for traditionally) and our understanding of the dynamics of proton–proton collisions (in which signatures of collectivity had been assumed to be absent). To put these LHC measurements into a broader scientific context, we recall the following:

With the discovery of QCD in 1973^{1,2} and with first insights into the QCD phase structure of the strong interactions at finite temperature and density^{3–5}, confinement and the chiral condensate were understood to be characteristics of the QCD vacuum. The strong interactions at finite temperature became calculable, see e.g. Ref. 6. Their physical origin became testable by creating the conditions for the QCD high-temperature phase — the quark–gluon plasma (QGP) — in laboratory-based experiments. As captured succinctly in the above quote of T.D. Lee⁷, this led since the 1980s to research in heavy-ion physics (HIP) that took a different direction from the main efforts of high-energy physics (HEP).

HEP focused on “hard” high-momentum transfer processes that are calculable perturbatively with controlled precision⁸. Aimed initially at establishing QCD as the theory of the strong interactions, this precision frontier is advanced since the 1990s to control as precisely as possible the QCD background on top of which new physics is searched for in collider experiments. Most relevant for this program are processes in which the systematically calculable “hard” short-distance physics factorizes from the “soft” long-distance contributions which are process-independent and thus independent of the partonic environment in which they may occur. Models of soft multi-particle production in HEP multi-purpose event generators were initially based on extrapolating this picture of collinearly factorized QCD beyond its regime of guaranteed validity. Modern model implementations in PYTHIA⁹, HERWIG¹⁰ and SHERPA¹¹ go beyond a purely incoherent superposition of multiple parton interactions (e.g. by implementing color reconnections in hadronization¹²)

but HEP multi-purpose event generators are not partonic transport codes: the partonic fragmentation processes and essential parts of the hadronization process are modeled as in vacuum, i.e., independent of the phase-space density within which they occur.

HIP, in contrast, focuses on testing QCD at finite phase-space density by searching for collective phenomena in soft multi-particle production, and by characterizing the modification of hard processes embedded in dense QCD matter. Throughout the 1980s and 90s, fixed target experiments with ultra-relativistic nuclear beams at the BNL AGS and at CERN SPS searched for signals of the QGP phase transition in terms of step-like structures that would occur in multiple classes of measurements at a common critical energy density^{13,14}. These experiments stated circumstantial evidence for QGP formation based on their discovery of strong sensitivities of soft particle production to the nuclear environment in the collision region¹⁵. However, the original simple search strategy (that was akin of the methodology used to characterize phase transitions in non-evolving solid state physics) had failed. No step-like changes were discovered.

In the early 2000s, due to major theoretical advances^{16–18} and in comparison with RHIC data^{19–22}, it became clear that dissipative fluid dynamics provides a successful phenomenology of soft multi-particle production in heavy-ion collisions^{23,24}. This resulted in a radically different approach towards testing hot and dense QCD. Since dissipative fluid dynamics is formulated in terms of thermodynamic quantities that are calculable from first principles in QCD, the rapid (hydro)dynamic evolution from extreme initial conditions to a diluted final hadronic state was not viewed any more as a confounding factor in testing equilibrium QCD but it became the very tool via which QCD equilibrium properties would reveal themselves. The resulting phenomenology supports the formation of a QCD fluid of close to minimal dissipative properties in which the mean free path of quasi-particles is so short that the very concept of a medium composed of propagating quasi-particles becomes questionable²⁵. It cannot be overemphasized that this HIP perfect fluid picture of nucleus–nucleus collisions is the extreme opposite of the HEP picture for proton–proton collisions. In the HIP case, no degree of freedom propagates through a sizable fraction of the collision region without interaction with the surrounding medium; in the HEP case, all degrees of freedom free-stream and fragment through the entire collision region without interacting with any medium.

These maximally different default pictures for soft multi-particle production in proton–proton (HEP) and nucleus–nucleus (HIP) collisions raise a set of common sense questions, including: Can both pictures be correct? Is there a critical size or density at which a QCD system produced in hadronic collisions transits from free-streaming to fluid-dynamic behavior? Can precursors of fluid dynamics be identified and could they inform us about the QCD non-equilibrium dynamics that leads to fast hydrodynamization and equilibration? All these questions point to the importance of understanding how collectivity and medium-modifications arise

as a function of systems size^a. It is this point that is informed by the LHC discovery of collectivity in small systems. These measurements marked a paradigm shift as, historically, the experimental programs with nuclear beams focused on central collisions of the heaviest nuclei to distribute high energy over the largest achievable volume and to create conditions most favorable for the formation of a QGP. In this context, the study of small collision systems like p–A or pp was seen as a reference for large systems. The aim was to constrain the nuclear dependence of parton distribution functions and to study so-called cold nuclear matter effects³¹, i.e. the particle production expected in the absence of QGP formation. This logic prevailed throughout the CERN SPS and RHIC experimental programs and it was the original motivation for supplementing the LHC heavy-ion program with p–A collisions³². Heavy-ion experiments therefore always had an important small systems program but without the expectation of gaining significant additional understanding about QCD physics at extreme temperature and density. However, with the LHC discovery of long-range correlation structures in pp collisions in 2010³³ and in p–Pb collisions in 2012^{34–36}, for the first time, effects well-known from the study of the QGP, and not accounted for by standard multi-purpose HEP event generators³⁷, occurred in high-multiplicity pp and p–Pb collisions. That the near-side ridge in pp collisions was only the first observation of a completely generic phenomenon, namely small system collectivity, became gradually clear with the observation of similar effects in p–Pb collisions and with the equally unexpected discovery of a second ridge structure on the away side. A new research direction emerged. This manuscript refers to about 200 experimental publications related to small systems, and it reviews the theoretical research motivated by these data. For earlier reviews, see Refs. 38–41.

This review separates the discussion of definitions of measurements in chapter 2, from the discussion of experimental data in chapter 3 and from the discussion of theoretical concepts informed by these data in chapter 4. To the extent possible, the chapters are self-contained. In particular, chapter 2 provides a detailed and necessarily technical discussion of how measures of collectivity are defined. But one may want to skip chapter 2 in a first reading if one is mainly interested in the state of art of experiment or theory.

2. Measures of collectivity and medium-modifications

In the broader physics debate, it has been emphasized repeatedly that “more is different”⁴² in the sense that macroscopic volumes of matter manifest qualitatively new phenomena that are distinct from those that can be discerned in interactions

^aVarying the spatial extension of a system is not the only way of changing conditions of collectivity. For instance, in simple conformal models, the degree to which a collision system develops collective phenomena is known to depend on one dimensionless product of energy density and transverse extension, the so-called opacity^{26–30}. In practice, however, a change of beam particle from Pb to p changes the transverse spatial extension by a factor 10 – to change energy density by a comparable factor is more difficult because of its approximately logarithmic \sqrt{s} -dependence.

among few elementary constituents. In a broad sense, collectivity refers to such phenomena that emerge with increasing size and complexity of a physical system. Emergent collective phenomena pose novel challenges for physics, as they often require distinct experimental techniques for their characterization, distinct theoretical methods for their description and as there is the fundamental challenge of understanding how collectivity in many-body systems emerges from the fundamental degrees of freedom.

In the phenomenological practice of collider physics, a measure of “collectivity” is more than a measurement. It is a measurement supplemented by a baseline that is free of collective phenomena and on top of which “collectivity” can be established. Baselines are chosen to separate microscopic physics (that is thought to arise from the incoherent superposition of elementary interactions) from those qualitatively novel “collective” phenomena that can arise only in sufficiently macroscopic systems. However, the simple idea of separating microscopic from macroscopic physics faces obvious challenges if applied to small mesoscopic systems that interpolate smoothly between the limiting cases of the small and the big.

2.1. *Measures of anisotropic flow*

Hadronic wavefunctions have a finite transverse extent. When they collide, energy is deposited in a finite region of the plane transverse to the beam direction. The shape of this initial *spatial* deposition depends on the kind of hadron or nucleus that is collided, on the impact parameter of the collision and on event-by-event fluctuations. In an azimuthal Fourier decomposition, this spatial information is typically characterized in terms of *spatial* eccentricities ϵ_n . However, what is measured are certain correlations of final azimuthal asymmetries v_n in *momentum* space. If the quanta produced in different positions in the transverse plane would not interact with each other, the measured v_n would not be sensitive to the ϵ_n 's. One important aspect discussing collectivity is to ask: What is the non-trivial collective dynamics that turns spatial gradients and asymmetries ϵ_n into momentum-anisotropies v_n ,

$$\underbrace{\{\epsilon_1, \epsilon_2, \epsilon_3, \dots\}}_{\text{spatial asymmetries}} \xrightarrow[\text{dynamics?}]{\text{which collective}} \underbrace{\{v_1, v_2, v_3, \dots\}}_{\text{momentum asymmetries}} \quad (1)$$

Experimentally, the initial conditions $\{\epsilon_1, \epsilon_2, \epsilon_3, \dots\}$ in (1) can be changed by choosing different nuclear or hadron beams, by varying the centrality of the collision, or by selecting particular event classes via event shape engineering⁴³. As reviewed in the following section 3, a wealth of data maps out the dynamical response (1) as a function of system size. Here, we start by reviewing different experimental definitions of the anisotropic flow coefficients v_n .

If $P(\vec{p}_1, \vec{p}_2)$ is the probability to produce a pair of particles with momenta \vec{p}_1 and \vec{p}_2 in a collision, and if $P(\vec{p}_i)$ is the corresponding probability to produce a single particle with momentum \vec{p}_i , then $P(\vec{p}_1, \vec{p}_2) \neq P(\vec{p}_1)P(\vec{p}_2)$ signals correlated particle production. However, not all correlated production is “collective”. Mea-

tures of anisotropic flow aim at separating few-particle correlations (that originate from microscopic sources like jets or resonance decays, also referred to as non-flow) from collective phenomena (that involve the correlation amongst essentially all particles in an event). Both sources of correlations scale differently with charged event multiplicity^b N . If the correlation function contains a collective phenomenon that affects with signal strength $S_{\text{collective}}$ each particle pair, then it is multiplied by the number of pairs $\frac{N(N-1)}{2}$. This collective contribution dominates parametrically by $O(N)$ compared to the microscopic production, since

$$P(1, 2) = \frac{2}{N(N-1)} \left(\frac{N(N-1)}{2} S_{\text{collective}}(N) + \frac{N}{2} S_{\text{microscopic}} \right). \quad (2)$$

Here, $S_{\text{collective}}$ is a function of N since it depends also on system size. In contrast, the signal strength $S_{\text{microscopic}}$ of microscopic correlations is by definition independent of the environment it is embedded in and it is thus independent of N .

As a next step we discuss **what one would like to measure and what one would like to remove from the measurement**: Ideally, one would like to characterize the azimuthal distribution of particles into Fourier coefficients

$$v_n \equiv \langle \langle e^{in\varphi} \rangle \rangle = \left\langle \int d\varphi e^{in\varphi} \frac{dN}{d\varphi} \right\rangle, \quad (3)$$

where the two brackets denote averages over all particles in an event and over event samples. Then, one would like to remove from the measurement of v_n all physics of microscopic origin, so that it becomes a measure of collectivity. The problem here is two-fold. First, without reference to a physically preferred azimuthal orientation (such as the orientation of the reaction plane), the azimuthal integral will average to zero. Eq. 3 does not correspond to an experimental measurement. To bypass this problem, one constructs azimuthal multi-particle correlations that are independent of overall azimuthal orientation. Second, any subtraction of microscopic physics depends on a assumption of what this microscopic physics is and it is therefore, strictly speaking, a choice. The notion of *pseudorapidity gap* plays in this context a central role. Namely, the two main few-particle correlation phenomena, jets and resonance decays, occur at small angular differences on the near side, i.e. at small $\Delta\eta$ and $\Delta\varphi$, as we will see later in the left panel of Fig. 2. Those can therefore be separated from long-range contributions by considering only particle pairs with $|\Delta\eta| > \eta_{\text{gap}}$ (η -gap method). However, a jet has a back-to-back component due to momentum conservation^c leading to a broad away-side structure. This structure cannot be separated through an η -gap and in consequence, a considerable amount of the jet correlation remains.

^bFor reasons of readability, we denote charged-particle multiplicity with N and without the usual subscript “ch”.

^cIn pp collisions, contrary to elementary e^+e^- collisions, the parton-parton scattering frame is not the lab frame and therefore the back-to-back side of the jet is found at $\Delta\varphi = \pi$ but at different $\Delta\eta$.

What one measures and what one removes from the measurement.

In the following, we summarize different procedures that are in use to quantify azimuthal correlations and that are used to reduce few-particle correlations in these measurements.

(1) *Near-side ridge yields*

Measurements of near-side ridge yields are arguably the simplest way of bypassing the above-mentioned problem that jet-like correlations lead to a broad away-side structure. As basic e^+e^- or pp inspired calculations and Monte Carlo simulations do not have a mechanism which produces near-side long-range correlation, the yield measurement carries a strong physics message. Some uncertainties remain from the definition of the baseline of the combinatorial background, and one may underestimate this yield at low p_T where the away-side peak is wide in azimuth. Also, from the ridge yield alone one cannot extract v_n coefficients while the converse is possible.

(2) *Event-plane method*

In this method⁴⁴, two different detectors are used. Typically, a forward rapidity detector determines a preferred azimuthal orientation called event plane Ψ_{EP} which in large collision systems is a proxy for the orientation of the reaction plane. This angle is then used to extract Fourier coefficients similar to Eq. 3 from particles measured in a mid-rapidity detector:

$$v_n \equiv \langle \langle e^{in(\varphi - \Psi_{\text{EP}})} \rangle \rangle = \langle \int d\varphi e^{in(\varphi - \Psi_{\text{EP}})} \frac{dN}{d\varphi} \rangle. \quad (4)$$

The rapidity separation of the two detectors allows to reduce non-flow contributions. In small systems such as p-Pb collisions, this method has limitations, since there may not be a clear definition of the reaction plane. For instance, if the system is not rapidity-invariant or if it has small multiplicity, Ψ_{EP} can depend on rapidity. The precision of the event plane depends on the number of considered particles and its resolution is proportional to \sqrt{N} . If the event plane is misestimated, the extracted signal (4) is then reduced as it is averaged out. In practice, if the two used detector systems have a fixed rapidity gap between them by the experiment's design, an experimental study of the signal as function of the rapidity separation is not possible and the associated uncertainties cannot be experimentally assessed.

(3) *Decomposing associated per-trigger yields into Fourier coefficients*

Measuring the distance in azimuth ($\Delta\varphi$) and pseudorapidity ($\Delta\eta$) of a so-called *trigger particle* from a second particle (commonly referred to as *associated particle*), one constructs the normalized per-trigger yield Y_N for events of multiplicity N

$$\frac{1}{N_{\text{trig}}} \frac{dN_{\text{assoc}}}{d\Delta\varphi d\Delta\eta} \equiv Y_N \equiv J_N(\Delta\varphi, \Delta\eta) + N \left[1 + \sum_n 2v_n^2 \cos n\Delta\varphi \right]. \quad (5)$$

This quantity is normalized as particle yield, i.e. an integral over a certain phase space region expresses the number of associated particles to each trigger particle. This method does not require to determine an event plane, as pointed out e.g. in Ref. 45. To characterize a collective component in terms of Fourier coefficients v_n and to distinguish it from a jet-like component $J_N(\Delta\varphi, \Delta\eta)$ due to microscopic interactions, one then exploits that both contributions should scale differently with event multiplicity. To this end, one chooses a factor a such that the jet-like near-side contribution cancels in the difference between two different multiplicities N and M

$$\Delta Y(\Delta\varphi) = Y_N - a Y_M, \quad (6)$$

and one decomposes this difference in terms of flow coefficients v_n . This subtraction assumes that the away-side structures scale in the same way with a as the near-side structures. Two different subtraction techniques have been used regularly:

- (a) *The low-multiplicity subtraction method*^{34,35} assumes that the collective component vanishes at low multiplicity M and extracts the v_n 's from the ansatz

$$\Delta Y(\Delta\varphi) = G' + N \sum_n 2v_n^2 \cos(n\Delta\varphi).$$

- (b) *The template method*⁴⁶ assumes that the collective component is significant at low multiplicity and extracts the v_n from the ansatz^d

$$\Delta Y(\Delta\varphi) = G \left(1 + \sum_n 2v_n^2 \cos(n\Delta\varphi) \right).$$

To illustrate the subtle differences between both subtraction methods, one may consider the case that $a = 1$ and that the values of the flow coefficients $v_{n,N}$ in (5) vary with multiplicity like $v_{n,M}^2 = \alpha_N v_{n,N}^2$. For the two methods, the measured $v_{n,\text{method}}^2$ deviates then from the true $v_{n,N}^2$ like

$$\frac{v_{n,\text{low mult subtraction}}^2}{v_{n,N}^2} = \frac{N - \alpha_N M}{N} \quad \text{versus} \quad \frac{v_{n,\text{template}}^2}{v_{n,N}^2} = \frac{N - \alpha_N M}{N - M}.$$

If one of these ratios equals unity then the “true” signal $v_{n,N}^2$ for the n -th harmonic at multiplicity N is returned by the chosen method. The low-multiplicity subtraction is correct for $\alpha_N = 0$, and the template method is correct of $\alpha_N = 1$. As illustrated in Fig. 1, the larger a true collective component will be at low multiplicity, the more it will be underestimated by the low-multiplicity subtraction method and the more it will be overestimated

^dFor pedagogical reasons we present here the typical simultaneous fit of a , G and v_n in several steps.

by the template method. This also becomes apparent in measurements if both methods are applied to the same dataset. For instance this explains the differences seen at low event multiplicity in the v_2 measurements displayed later in Fig. 5. In the limit of high multiplicity, the results of both methods converge. However, the discussion of what constitutes collectivity at small multiplicity requires a particularly critical assessment of the method employed since even qualitatively different conclusions may be reached at face value. We therefore suggest to make the differences explicit in the nomenclature, for instance by using $v_{n,\text{low mult subtraction}}$ and $v_{n,\text{template}}$.

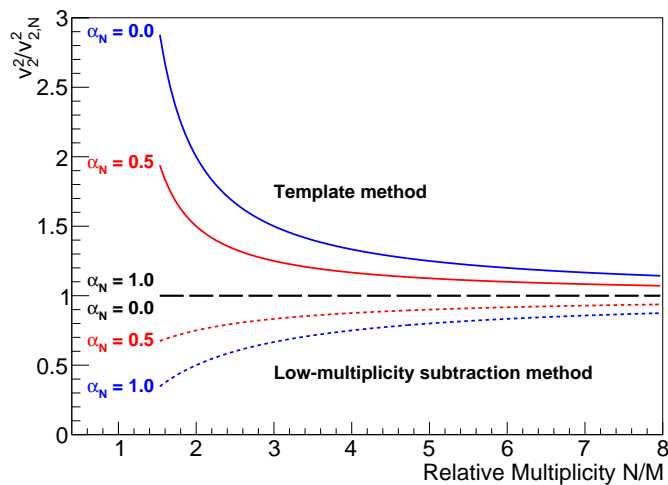


Fig. 1. Ratio of the measured v_2^2 to the true v_2^2 as a function of relative multiplicity N/M for different cases of α_N ($v_{2,M}^2 = \alpha_N v_{2,N}^2$). The solid lines in the upper part show the template method where the v_2 is exact or overestimated depending on α_N , while the dashed lines in the lower part show the low-multiplicity subtraction method where the v_2 is exact or underestimated depending on α_N . Each of the two methods is exact only for a single α_N and the two values are maximally different.

(4) *Two-particle cumulant flow $v_n\{2\}$ and higher orders $v_n\{2m\}$*

The azimuthal angles of all pairs (1, 2) in an event can be directly used to compute a cumulant^{47,48}:

$$\langle\langle e^{in(\varphi_1 - \varphi_2)} \rangle\rangle = v_n\{2\}v_n\{2\} + \underbrace{\langle e^{in(\varphi_1 - \varphi_2)} \rangle_{\text{micro}}}_{\sim O(1/N_s)}, \quad (7)$$

where the brackets denote averages over all particles in an event and over event samples. Non-flow effects are assumed to result only from correlations between pairs of particles that both originate from the same microscopic source. If there are N_s such sources in an event, the second “non-flow” contribution is parametrically $O(1/N_s)$ smaller. The first collective con-

tribution dominates the measured two-particle correlation if the observed signal satisfies $v_n\{2\} \gtrsim O(1/N_s^{1/2})$.

The cumulant method may be regarded as being theoretically preferred since it has the important property that the sensitivity to “non-flow” few-particle correlations can be systematically reduced by purely statistical arguments. To this end, one studies connected $2m$ -point correlation functions (“cumulants”). For instance, the fourth order cumulant reads

$$\begin{aligned} \langle\langle e^{in(\varphi_1+\varphi_2-\varphi_3-\varphi_4)} \rangle\rangle_c &\equiv \langle\langle e^{in(\varphi_1+\varphi_2-\varphi_3-\varphi_4)} \rangle\rangle - \langle\langle e^{in(\varphi_1-\varphi_3)} \rangle\rangle \langle\langle e^{in(\varphi_2-\varphi_4)} \rangle\rangle \\ &\quad - \langle\langle e^{in(\varphi_1-\varphi_4)} \rangle\rangle \langle\langle e^{in(\varphi_2-\varphi_3)} \rangle\rangle \\ &= -(v_n\{4\})^4 + O\left(\frac{1}{N_s^3}\right). \end{aligned} \quad (8)$$

In general, cumulants are constructed such that a non-flow correlation that manifests itself only on the level of $(2m-2)$ -particle correlations does not manifest itself in the $(2m)$ -th cumulant. The signal strength needs to be $v_n\{2m\} > O\left(1/N_s^{(2m-1)/m}\right)$ for flow contributions to dominate the signal. In the phenomenological practice, if the signal $v_n\{2m\}$ stabilizes with increasing m , this is taken as evidence for collectivity. Mathematically, the limit $m \rightarrow \infty$ of these higher-order cumulants corresponds to the so-called LYZ (Lee-Yang-Zero) method⁴⁹. The parametric separation of flow- and non-flow effects via $O\left(1/N_s^{(2m-1)/m}\right)$ power counting is powerful if N_s is large, i.e. if event multiplicities are large. Therefore, the capability of the cumulant method to separate by purely statistical arguments flow from non-flow is limited for small systems.

(5) *Subevent technique*

Higher-order cumulants are computationally intense and naively scale with $O(N^{2m})$. Even for a 4-particle cumulant this is computationally challenging if applied to large event samples. The complexity can be reduced to $O(N)$ by the calculation of so-called Q -vectors whose expressions instead of considering $2m$ particles sum over single particles^{47,50}. As mentioned before, jet-like fragmentation patterns and resonance decays lead mainly to correlations between particles that are close in $\Delta\eta \times \Delta\varphi$. In order to exclude those when computing the Q -vectors, where an η -gap between particles cannot be applied (as only single particles are considered in the calculation), the event is split into several subevents⁵¹, each of which is used for the computation of a Q -vector. The extracted coefficient is then:

$$(v_n\{2, |\Delta\eta| > \gamma\})^2 = \langle\langle e^{in(\varphi_i-\varphi_j)} \rangle\rangle, \quad (9)$$

where all particles i are in the range $\eta > \gamma/2$ while all particles j are in the range $\eta < -\gamma/2$ with $\gamma \geq 0$. Experimentally, one can then test the dependence on γ and if the signal stabilizes with increasing γ , this is taken as evidence for collectivity. It should be noted that regardless how large γ ,

the back-to-back jet structure is not excluded from $v_n\{2, |\Delta\eta| > \gamma\}$, but can be suppressed by extending this method into calculating higher-order cumulants from more than two subevents⁵¹.

This enumeration demonstrates that there are numerous experimental measures for v_n coefficients. Those use different definitions with different underlying assumptions, in particular on what is the definition of the physics in absence of collectivity. Only some of the different methods have separate notation, e.g. $v_n\{2m\}$. Therefore, care has to be taken when comparing different v_n between each other or with theoretical calculations.

2.2. *Hadrochemical measures of collectivity*

Hadrochemistry addresses the question with which relative abundance different hadron species are produced in a collision. What is measured are identified particle yields and their ratios, particle-identified transverse momentum spectra and particle-identified flow coefficients. The baseline on top of which collective effects are established is traditionally chosen to be set by minimum bias pp collisions. There are some technical challenges related to the question of how feed-down contributions from resonance decays are included in or subtracted from particle-identified data⁵², and how the experimental procedure is paralleled in theoretical descriptions. On the modelling side, an additional challenge arises from the incomplete knowledge of short-lived higher mass resonance states which feed down inevitably into the measured yields, see e.g. Ref. 53. In general, however, what is measured is easily stated and it seems unnecessary to describe the definition of hadrochemical measures of collectivity in as much detail as we did for measures of anisotropic flow. In the following, we therefore focus almost exclusively on the physics motivations for which hadrochemical measures of collectivity are studied:

(1) Hadrochemical equilibration

In QCD at sufficiently high energy density, the gluon fusion process $gg \leftrightarrow s\bar{s}$ can drive the strangeness content to chemical equilibrium. The resulting expectation of strangeness enhancement in heavy-ion collisions counts amongst the very first proposed signatures of QGP formation^{54,55}. In nucleus–nucleus collisions, strangeness enhancement (compared to a baseline set by minimum bias pp collisions) is observed in the phase-space integrated relative abundances of all identified strange and multi-strange hadrons at all relativistic center of mass energies from BNL AGS to the LHC⁵⁶. These observations can be accounted for by fitting to a statistical hadronization model that involves two intensive quantities (temperature and a baryo-chemical potential) and one extensive one (volume)^{53,56}. Also the relative abundances of charm and beauty hadrons can be included in the systematics of this statistical hadronization model^{53,57}, if their total production rate is set by initial hard (vacuum-like) processes. That means

that these rates are not thermally produced but statistically distributed.

(2) Particle-identified flow

To the extent to which collective flow is built up in the partonic phase of a collision, all hadron species emerge from the same common flow field u_μ . According to the Cooper-Frye freeze-out prescription, all hadrons will decouple with statistical weights $\exp[-p^\mu u_\mu/T]$ from locally equilibrated patches of a globally expanding system⁵⁸. In analytical blast-wave models⁵⁹ and in fluid-dynamical simulations, this leads to a characteristic mass hierarchy in the p_T -dependent particle-identified flow coefficients $v_n(p_T)$ and in the single inclusive p_T spectra (“radial flow”). These dependencies have been observed in central and semi-peripheral nucleus–nucleus collisions at the CERN SPS, at RHIC and at the LHC for sufficiently small transverse momenta (see Figure 8 and related discussion).

One central question is whether the onset of flow seen in the smallest pp and p–Pb collision systems has the same collective dynamical origin as the flow in nucleus–nucleus collisions. Testing whether anisotropic flow in large and small collision systems shows the same PID-dependence is of obvious interest in this context.

(3) Hadronization mechanisms

The dynamics of hadronization in QCD is not understood. In high-momentum transfer processes where QCD collinear factorization applies, high- p_T partons hadronize the same irrespective of the hard partonic process in which they are produced. Remarkably, also the Lund string⁶⁰ or cluster hadronization models¹⁰ implemented in multi-purpose pp event generators are process-independent in this sense. On the other hand, the observation of significant strangeness enhancement (as well as a suite of other measurements) falsifies the assumption of a process-independent hadronization in nucleus–nucleus collisions. Hadronization in a dense nuclear environment leads to a characteristically different hadrochemical composition compared to that in the vacuum. One important question is whether a process-independent hadronization mechanism of bulk-particle production can also be falsified in small pp and p–Pb collision systems.

There are process-dependent hadronization models that are sensitive to the environment in which hadronization occurs. In particular, in recombination models hadrons result from combining valence-like partons that are produced within the same collision in different partonic interactions^{61,62}. Signatures of recombination are normally searched for at intermediate transverse momenta ($2 \lesssim p_T \lesssim 5$ GeV). The reason is that this mechanism cannot be dominant for soft bulk particle production as it reduces the number of independent degrees of freedom and thus entropy. Also, fragmentation from a high- p_T power-law tail dominates over recombination from a low- p_T exponential slope^{61,62}. One qualitative prediction of recombination is a characteristic baryon-meson splitting as a consequence of the different num-

ber of valence-like quarks that need to be combined. It is of obvious interest to study whether this baryon-meson separation persists across system size.

2.3. *Hard processes in small systems*

In sufficiently central nucleus–nucleus collisions, essentially all high- p_T hadronic final states show numerically large medium-modifications. Our understanding of these jet quenching⁶³ phenomena is based on mechanisms of radiational and collisional parton energy loss that strongly suppress high- p_T colored probes in sufficiently large collision systems. Jet quenching arises from interactions of jets with a medium that exhibits collective phenomena. In theory, there is therefore a direct relation between jet quenching and flow. If fluid dynamics or kinetic transport is the dynamical origin of flow, then there must be medium interactions with colored degrees of freedom at *all* momentum scales, and thus, there must be jet quenching.

In this context, it is remarkable that in the smallest collision systems (pp, p–Pb), LHC experiments have discovered sizable anisotropic flow without finding evidence for jet quenching. Jet quenching in small systems may have escaped detection so far since effects become smaller with decreasing system size and since systematic uncertainties in measuring jet quenching become more important. If this is so, it calls for studies based on more sensitive observables and supported by more accurate calculations. We therefore comment here on problems related to determining the system size dependence of jet quenching in small systems.

In nucleus–nucleus collisions, one of the simplest and most widely used measures of jet quenching is the nuclear modification factor

$$R_{AA}^{h,j}(p_T, y) \Big|_{\text{cent}} = \frac{1}{\langle T_{AA} \rangle} \frac{\frac{1}{N_{\text{ev}}} \frac{dN_{AA}^{h,j}}{dp_T dy} \Big|_{\text{cent}}}{\frac{d\sigma_{pp}^{h,j}}{dp_T dy}}. \quad (10)$$

This factor compares the number $dN_{AA}^{h,j}$ of charged hadrons (h) or calorimetrically defined jets (j) (produced in AA collisions in some range of transverse momentum p_T and rapidity y) to an equivalent number of such hadrons or jets produced in pp collisions. Here, the equivalent number of collisions $\langle N_{\text{coll}} \rangle = \sigma_{\text{pp}}^{\text{inel}} \langle T_{AA} \rangle$ is the product of the total inelastic pp cross section and the nuclear overlap function $\langle T_{AA} \rangle$. $R_{AA}(p_T, y)$ is typically determined as a function of centrality. Centrality is defined in terms of the fraction of highest multiplicity events (or highest total transverse energy events) of the total inelastic nucleus–nucleus cross section, and it is related to $\langle T_{AA} \rangle$ by Glauber-type models⁶⁴.

For centrality to be a good proxy of system size, event-multiplicity should be tightly correlated to the geometry of the collision and it should not be correlated with the hard process. These assumptions are satisfied approximately in sufficiently large systems but they become problematic in small systems. Estimates of the uncertainties associated to $\langle T_{AA} \rangle$ range from 3% in central to 15% in peripheral Pb–Pb collisions⁶⁵. In addition, in peripheral Pb–Pb collisions (centralities larger

than $\sim 70\%$), Eq. (10) is known to be affected by significant event selection and geometry biases^{66,67}. The centrality dependence of hard processes in p–Pb collisions reveals even larger biases. Some of these biases arise from the larger influence of fluctuations in smaller systems, other biases originate in correlations between the hard process and the global event multiplicity^{68,69}. Finally, the nuclear modification factor (10) measures jet quenching with respect to a baseline set by pp collisions, and it is therefore not a good starting point for analyzing jet quenching in pp collisions.

These findings indicate that the measurement of single inclusive jet or hadron spectra as a function of event multiplicity (centrality) is of limited use for the characterization of jet quenching in the smallest collision systems. For small collision systems, it is clearly problematic to include geometrical information such as $\langle T_{AA} \rangle$ in the definition of jet quenching measures, as such information depends on soft physics models that are difficult to constrain for small systems. One way out is the use of inclusive, minimum bias spectra in light nucleus collisions for which a nuclear modification factor can be defined without reference to soft physics modeling, $R_{AA}^{h,j}(p_T, y) \Big|_{\text{min bias}} = \frac{1}{A^2} \frac{d\sigma_{AA}^{h,j}}{dp_T dy} \Big/ \frac{d\sigma_{pp}^{h,j}}{dp_T dy}$. It has been shown that such inclusive measurements have much smaller uncertainties and that they therefore allow for the unambiguous detection of smaller jet quenching signals in nucleus–nucleus collisions with A as small as oxygen^{70,71}. A second general possibility of detecting signatures of jet quenching in small collision systems is the use of self-normalizing processes such as dijet asymmetries. We recall that the very first proposal of a jet quenching effect in small p \bar{p} collisions made by Bjorken in 1982 was of that type⁷².

3. Experimental Overview

3.1. Long-range correlations

The most prominent and from the point of view of analysis methodology rather simple observation is the one of long-range effects in two-particle correlations (5). QCD effects implemented in standard multi-purpose event generators of proton–proton collisions lead to distinct patterns in these correlations: At small angular distances ($\Delta\varphi \approx 0$ and $\Delta\eta \approx 0$) a so-called *near-side* peak results from jet-like fragmentation and resonance decays. A back-to-back structure from momentum conservation is observed at $\Delta\varphi \approx \pi$, called *away side*. This away-side structure is not concentrated around $\Delta\eta \approx 0$ since the center-of-mass systems of any two partons in a hadronic collision is distributed widely in rapidity. In addition to these expected patterns, Fig. 2 (left panel) shows also positive long-range rapidity correlations for $|\Delta\eta| \gtrsim 2$ on the near side. This was surprising since the known microscopic dynamics operational in proton–proton collisions does not lead to long-range near-side correlations. Fig. 2 displays the first ever observed “collective effect” in proton–proton collisions. At the time, it was based on the first sizable LHC high-multiplicity sample although from today’s perspective this sample is very small.

The second hallmark result was the observation of a double-ridge structure in p–Pb collisions^{34,35}, displayed on the right panel of Fig. 2. For reasons which are detailed in section 2.1, the observation in small systems (contrary to large systems) required to take the difference between high-multiplicity and low-multiplicity collisions. Fig. 2 shows clearly an almost rapidity-independent second harmonic v_2 imprinted on the azimuthal two-particle correlation. This is the telltale sign of an elliptic flow signal that had been observed in heavy-ion collisions at all fixed-target and collider energies. Elliptic flow was thought to arise from the collective dynamical response of a system to pressure gradients related to initial spatial anisotropies ε_2 . However, such a collective effect had not been expected in the small p–Pb collision system. At this moment, the scientific community was convinced that something extraordinary was going on and embarked on understanding if the observed effects were truly of similar nature as in heavy-ion collisions. To this end, studies focused first on characterizing higher order flow harmonics v_n and their relation to finer details ε_n of the initial conditions (for motivation, see the discussion of (1)). Soon after, the searches for high-density QCD phenomena in small systems extended to nearly all areas of heavy-ion physics, see Table 1.

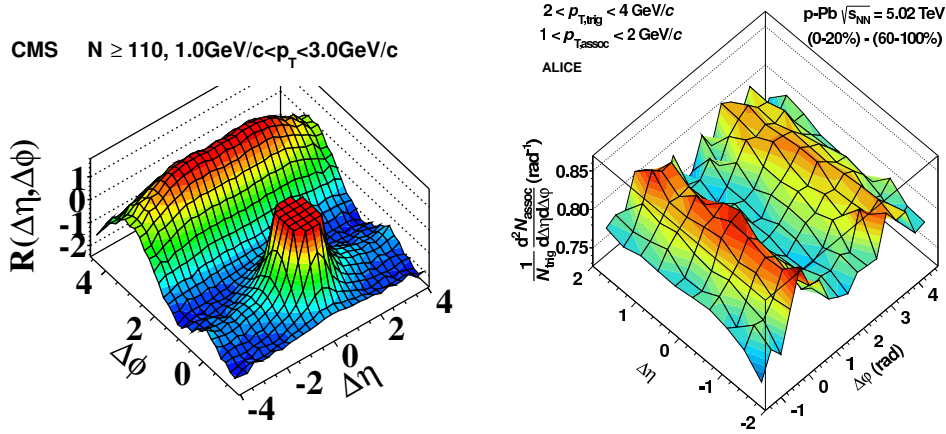


Fig. 2. Two-particle correlation showing the first observation of the long-range correlation on the near side in pp collisions (left panel; Figure from Ref. 33) and the first observation of the double-ridge structure in p–Pb collisions (right panel; Figure from Ref. 35). The left panel shows the two-particle correlation without any subtraction. Hence the near-side jet peak is clearly visible and the the away side is dominated by the jet component. The right panel uses the low-multiplicity subtraction described in section 2.1 which effectively reduces the jet component. This results in an almost complete suppression of the near-side jet peak allowing one to observe two ridges. The right panel is normalized as per-trigger yield, while the left panel uses a relative normalization, see Ref. 33 for details.

Azimuthal anisotropies The observed long-range structures are quantified by decomposing the per-trigger yield into Fourier coefficients v_n , see Eq. 5. The first

Table 1. Summary of observables or effects in Pb–Pb, Xe–Xe and Au–Au collisions, as well as in high multiplicity p–Pb, a–A and pp collisions. References to key measurements are given. See text for details. Table adapted from Ref. 99 and extended by publications of the last 5 years.

Observable or effect	Pb–Pb, Xe–Xe, Au–Au	p–Pb, a–A (high N)	pp (high N)	Refs.
Near-side ridge yields	yes	yes	yes	33–36,74,76,77,79,79,100
Azimuthal anisotropy	v_1 – v_9	v_1 – v_5	v_2 – v_4	34–36,46,73–89,101,102
Weak η dependence	yes	yes	yes	82,90–98
Characteristic mass dependence	v_2 – v_5	v_2, v_3	v_2	78,81,83,87,103–110
Higher-order cumulants (mainly $v_2\{n\}$, $n \geq 4$)	“4 \approx 6 \approx 8 \approx LYZ” +higher harmonics	“4 \approx 6 \approx 8 \approx LYZ” +higher harmonics	“4 \approx 6”	83,84,88,96,109,111–123
Symmetric cumulants (SC)	up to (5, 3)	only (4, 2), (3, 2)	only (4, 2), (3, 2)	86,88,124–130
Non-linear flow modes	up to v_7	not measured	not measured	89,131,132
Factorization breaking	$n = 2$ –4, {2}, {4}	$n = 2, 3$, {2}	not measured	77,85,133–137
Event-by-event v_n distributions	v_2 – v_4	not measured	not measured	138–140
Flow– p_T correlation	up to v_4	v_2	not measured	141,142
Directed flow (from spectators)	yes	no	no	143
Charge-dependent correlations	yes	yes	yes	144–150
Low p_T spectra (“radial flow”)	yes	yes	yes	52,151–161
Intermediate p_T (“recombination”)	yes	yes	yes	153,156,160,162–166
Particle ratios	GC level	GC level	GC level	153,154,157,158,167,168
Statistical model	$\gamma_s^{\text{GC}} = 1$	$\gamma_s^{\text{GC}} \approx 1$	$\gamma_s^{\text{C}} < 1$	52,161,169–171
HBT radii ($R(k_T)$, $R(\sqrt[3]{N})$)	$R_{\text{out}}/R_{\text{side}} \approx 1$	$R_{\text{out}}/R_{\text{side}} \lesssim 1$	$R_{\text{out}}/R_{\text{side}} \lesssim 1$	172–180
Direct photons at low p_T	yes	not measured	not observed	181–183
v_n in events with Z, jets	not measured	up to v_3	v_2	184–186
Jet constituent v_n	v_2	v_2	v_2 in jet frame	187,188
Jet quenching through R_{AA}	yes	not observed	not observed	65,67,189–204
... through dijet asymmetry	yes	not observed	not observed	205–212
... through correlations	yes (Z–jet, γ –jet, h–jet)	not obs. (h–jet, jet–h)	not measured	204,213–222
... through high p_T v_n and jet– v_n	yes	yes	not measured	184,223–225
Heavy flavour anisotropy	up to v_3 (c), up to v_2 (b)	up to v_2	up to v_2	108,226–248
Quarkonia production	suppressed	suppressed	not measured	232,249–284

measurement of non-zero v_2 and v_3 in p–Pb collisions, shown in Fig. 3, provided another indication that the phenomena seen in small systems are heavy-ion like. Since then, a large number of detailed studies have been done on different coefficients of anisotropic flow. Today, measurements extend up to v_9 in Pb–Pb, v_5 in p–Pb, v_3 in d–Au, and v_4 in pp collisions for charged particles. Fig. 4 shows the state-of-the-art measurement of v_2 in pp, p–Pb and Pb–Pb collisions. These coefficients exhibit a weaker multiplicity dependence in pp and p–Pb collisions than in Pb–Pb collisions where this is closely related to the shape of the overlap region, while v_3 are independent of the collision system as a function of multiplicity^{34–36,46,73–89}. The slight trend of increasing v_2 for decreasing multiplicity in pp collisions is related to the extraction method used, see section 2.1. The sensitivity to the method becomes clear when both methods are applied to the same dataset, which is shown in Fig. 5. The η dependence is overall weak and similar in small and large systems^{82,90–98}.

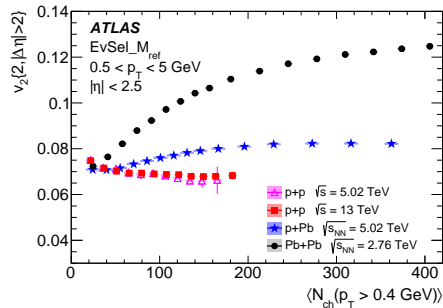
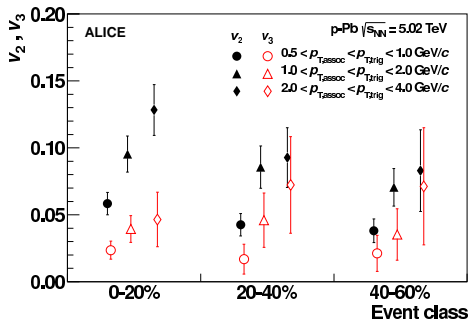


Fig. 3. v_2 and v_3 coefficients extracted from low-multiplicity subtracted two-particle correlations in p–Pb collisions (Figure from Ref. 35). For details on the methodology see Sec. 2.1.

Fig. 4. The v_2 coefficient extracted with the template method in pp, p–Pb and Pb–Pb collisions (Figure from Ref. 84). For details on the methodology see Sec. 2.1.

At RHIC, the influence of the initial geometry has been studied with special collision configurations that favor round (p–Au), elliptical (d–Au) and triangular (^3He –Au) shapes in the initial state. Fig. 6 compares the v_3 coefficients measured by the PHENIX¹⁰¹ and STAR¹⁰² collaborations. The larger signal strength in ^3He –Au as compared to p–Au and d–Au observed by PHENIX¹⁰¹ supports the conclusion that a larger triangular eccentricity leads to a larger triangular v_3 also in these small systems. However, this conclusion is not supported by the STAR¹⁰² data which differ from those of PHENIX by up to a factor 3 in p–Au and d–Au, while they are consistent for ^3He –Au. In model studies, half of this difference could be attributed to the different methods and rapidity ranges^e used in the extraction methods²⁸⁵ but this does not reconcile the different data. The discrepancy is of a qualitative,

^ePHENIX uses the event-plane method with detectors at $-3.9 < \eta < -3.1$ and $|\eta| < 0.35$ while STAR uses the template method with both particles within $|\eta| < 0.9$ and an η gap of 1 unit.

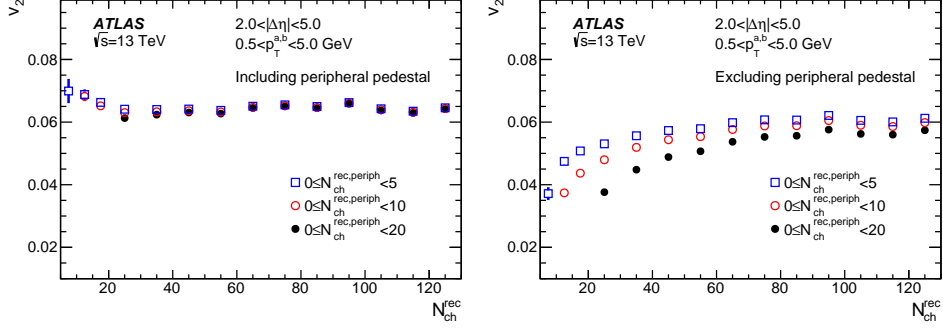


Fig. 5. The v_2 coefficient extracted with the template method (left panel) and the low-multiplicity subtraction method (right panel). The overestimation with the template method and underestimation with the low-multiplicity subtraction method are clearly visible. Figure from Ref. ⁴⁶. For details on the methodology see Sec. 2.1, in particular Fig. 1

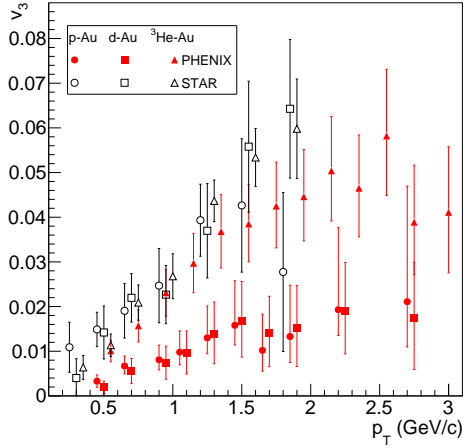


Fig. 6. Comparison of the v_3 measurement of PHENIX¹⁰¹ (red filled symbols) and STAR¹⁰² (black open symbols) in three different collision systems which favor round (p–Au), elliptical (d–Au) and triangular (³He–Au) shapes in the initial state.

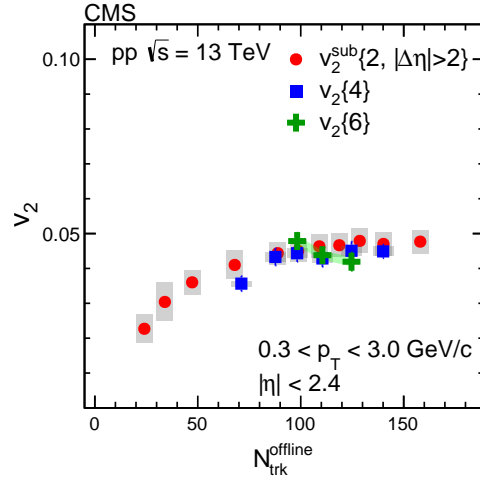


Fig. 7. Higher-order correlations of the v_2 coefficient measured in pp collisions (Figure adapted from Ref. ⁸³).

not only a quantitative nature. To draw lasting physics conclusions from the unique RHIC opportunity of studying these different small collision systems, a resolution of the apparent inconsistencies between STAR and PHENIX remains important.

Multi-particle nature of the observed correlation In heavy-ion collisions, collective phenomena are a correlation between all particles (through common symmetry planes) and therefore correlations are in principle present at all orders. To test

this assumption, higher-order cumulants (see Eq. (8) and following text) have been measured using the Lee-Yang Zeros (LYZ) method and multi-particle correlation techniques with up to 8 particles in both Pb–Pb and p–Pb collisions and up to 6 particles in pp collisions (shown in Fig. 7) for $v_2^{83,84,88,96,111-123}$. The measurements of the cumulants at different orders ($n \geq 4$) are similar within 10% within each collision system. This is a tell-tale sign of collectivity, but it does not identify unambiguously the dynamical mechanism underlying collectivity. From fluid dynamics (see section 4.1.1) to one-hit kinetic theory (see Section 4.1.2), very different dynamical frameworks can lead to correlations amongst essentially all particles in an event.

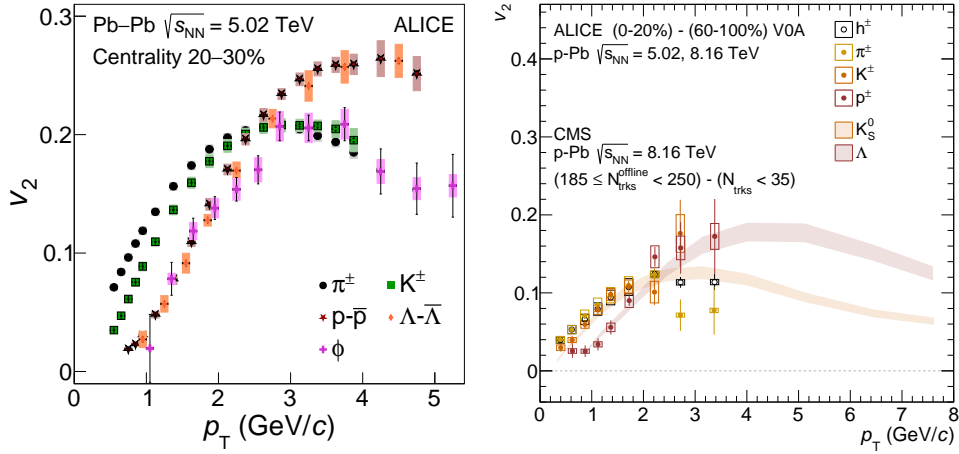


Fig. 8. Compilation of identified-particle v_2 in Pb–Pb collisions (left panel) compared to p–Pb collisions (right panel). Figures from Ref. 171).

Particle-mass dependence Studying the v_n coefficients as a function of p_T for different particle species shows a characteristic mass dependent pattern up to v_5 in Pb–Pb (left panel of Fig. 8), v_3 in p–Pb (right panel of Fig. 8) and other small systems, as well as v_2 in pp collisions where heavier particles are depleted at low p_T ^{78,81,83,87,103–108,110}. If all hadron species were emitted with thermal weight $\exp[-p_\mu u^\mu/T]$ from the same common flow field u^μ , then this would lead to a characteristic $m_T = \sqrt{m^2 + p_T^2}$ -scaling of radial and anisotropic flow (see section 2.2). If, on the other hand, hadron species would result from the recombination of valence-like quarks, then a baryon-meson grouping of observables may be expected. We emphasize that m_T -scaling and baryon-meson grouping are distinct dependencies that cannot be realized simultaneously. Existing data show approximate m_T -scaling at low and approximate meson-baryon grouping at intermediate p_T . Remarkably, essentially the same hadrochemical and p_T -dependencies are observed across all systems from Pb–Pb to p–Pb to pp although both mechanisms may be expected to

depend on system size or phase space density.

The extent to which signatures of collectivity show close commonalities between small and large collision systems had not been expected. Beyond the early findings described above, commonalities have been found by now in a large number of refined measurements listed in Table 1. In the following, we summarize the main experimental conclusions as follows:

Non-linear response Correlations between different anisotropic flow harmonics characterize the non-linear coupling between different collective excitations. In the modelling of heavy-ion collisions, non-linear mode-mode coupling is a generic feature of fluid dynamics^{286–289} where it is found to be sensitive to transport properties. However, non-linear mode-mode coupling is also a generic feature of kinetic transport theory where it persists even in the dilute one-hit approximation^{290,291}, see section 4.1.2 for details. Mixed harmonics or so-called symmetric cumulants have been measured up to SC(5, 3) in Pb–Pb and SC(4, 2) in Au–Au, Xe–Xe, p–Pb and pp collisions^{86,88,124–130}. A further class of observables, linear (v_n^L) and non-linear (v_n^{NL}) flow modes, have been investigated in Pb–Pb collisions up to the seventh order flow harmonic^{89,131,132} but not yet in pp and p–Pb collisions. In general, the measured non-linear response varies only mildly with system size.

More detailed v_n -characterizations Numerous other characterizations constrain the phenomenology of v_n . The factorization of long-range azimuthal two-particle correlations into a product of single particle anisotropies and the breaking of this factorization due to event-plane angle decorrelations in p_T and η has been measured in both Pb–Pb and p–Pb collisions^{85,133,135,136}. Recent measurements show this behavior using four-particle correlators¹³⁷. With the existing data such measurements are not yet possible in pp collisions. It would also be interesting to study event-by-event distributions of v_n coefficients in both p–Pb and pp collisions, which have so far been done in Pb–Pb collisions^{138–140}. The interplay of flow harmonics and radial expansion is studied with correlations of v_n coefficients and the mean p_T event-per-event. The correlation has been measured through modified Pearson correlation coefficient as a function of event activity up to fourth order in Pb–Pb, third order in Xe–Xe collisions and second order in p–Pb collisions^{141,142}. First measurements of higher-order correlations, e.g. $v_2-v_3-p_T$ have been made¹⁴².

Directed flow In Pb–Pb collisions, directed flow of charged particles at mid-rapidity was measured relative to the collision symmetry plane defined by the spectator nucleons, and evidence for dipole-like initial-state density fluctuations in the overlap region was found¹⁴³. In small systems, the concept of directed flow is less clear, especially in pp collisions. If there is collectivity in pp collisions, one could also expect a non-zero directed flow measurement. This is technically challenging since the measurement of the spectator plane is not feasible in small systems and, hence, v_1 could only be measured using higher-order ($n \geq 4$) cumulants which has not been achieved to date.

Charge-dependent correlations The balance function probes the charge creation time and the development of collectivity in the produced system. Its width,

$\langle \Delta\eta \rangle$ and $\langle \Delta\varphi \rangle$, has been measured for charged particles in pp, p–Pb and Pb–Pb collisions^{144,145}. A picture emerges where the system exhibits larger radial flow with increasing multiplicity but also whose charges are created at the later stages of the collision. Charge-dependent azimuthal correlations are measured in both Pb–Pb and p–Pb collisions^{172–174,177}. These studies assess the chiral magnetic effect (CME) and the chiral magnetic wave (CMW) on the produced particles. Their interpretation is still today influenced by strong background contributions, for example from local charge conservation and possibly radial and anisotropic flow.

3.2. *Bulk properties*

Particle spectra and production Particle production yields have been measured for numerous particle species in small and large collision systems^{52,153,154,157,158,161,167–170}. Figure 9 shows the production yields of different identified non-strange, strange and multiple-strange hadrons normalized to the pion yield. As a function of multiplicity, these ratios increase more for strange than for non-strange hadrons, and they increase more for multi-strange hadrons than for strange hadrons^{52,168,169}. That strangeness in nucleus–nucleus collisions is enhanced compared to minimum-bias proton–proton collisions has been observed at all relativistic collision energies at the BNL AGS, the CERN SPS, the RHIC⁵⁶ and now the LHC. Up until today, the factor 25 enhancement of the Ω/π ratio observed by the NA57 Collaboration at the CERN SPS in comparing yields in Pb–Pb and p–Pb collisions is arguably one of the numerically largest medium-modification ever observed in heavy-ion collisions²⁹². The qualitatively novel information of Figure 9 is that this strangeness enhancement sets in smoothly with increasing multiplicity so that even pp collisions show an enhanced strangeness content for higher multiplicity, and p–Pb collisions must not be considered as a baseline in which strangeness enhancement is absent. Moreover, strangeness enhancement shows a universal dependence on event multiplicity irrespective of the collision system. This is in marked contrast to kinetic signatures of collectivity such as elliptic flow (see e.g. Fig. 4) that depend not only on event multiplicity as they contain also spatial information about the collision systems and their centrality dependence.

The p_T spectra of identified particles harden with increasing multiplicity for all studied collision systems. The hardening is stronger for heavier particles^{153,156,160,162–166}. In central nucleus–nucleus collisions, the slopes of soft charged pion, kaon and (anti-)proton p_T spectra are consistent with models in which all hadron spectra are blue-shifted by the same transverse radial flow¹⁵¹. In this framework, a larger radial flow is observed⁵² in pp and p–Pb collisions as compared to Pb–Pb collisions at the same multiplicity.

Source size The measurement of quantum-statistic correlations between pairs of same-charge particles in particular pions at low-momentum transfer allows to assess the size of the emitting source²⁹³. These freeze-out radii are measured in three orthogonal directions (“out”, “side”, “long”). While clearly the expectation is

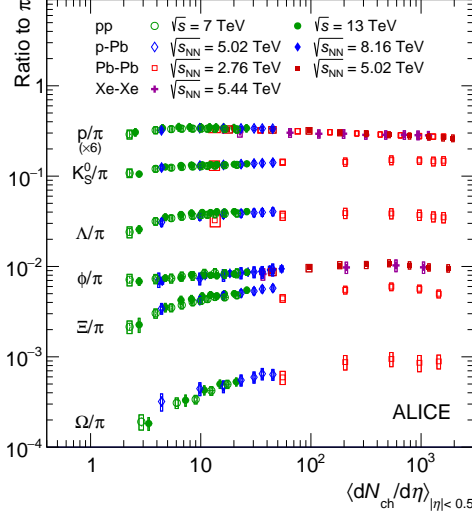


Fig. 9. Particle production yields of strange and non-strange particles normalized to the pion yield as a function of multiplicity in pp, p-Pb, Pb-Pb and Xe-Xe collisions (Figure from Ref. 171).

that these are vastly different in small and large collision systems, their dependence on event and particle pair variables can be compared. The radii scale with $\sqrt[3]{N}$ in all collision systems indicating a constant density at freeze-out and decrease with increasing pair momentum k_T . This is consistent with the expectation that velocity gradients in the collision region should lead to smaller “homogeneity regions” with increasing k_T ²⁹³. The size along the emission direction is similar to the geometric size of the system ($R_{out}/R_{side} \approx 1$) in Pb-Pb collisions^{173,175,176,178,178–180} while this ratio is smaller than unity for both p-Pb and pp collisions^{172–174,177}.

Direct photons Direct-photon measurements have been performed in Pb-Pb and pp collisions in the p_T region sensitive to thermal photon production. For central Pb-Pb collisions, an effective temperature (averaged over the evolution) of about 300 MeV has been extracted from the slope of the photon transverse momentum spectrum^{181,183}. Fluid models that reproduce these spectra start from an initial QGP temperature of more than 400 MeV¹⁸¹ in central Pb-Pb collisions. In pp collisions, no significant direct-photon signal has been identified at low momentum¹⁸². The reported upper bounds lie well above expectations of next-to-leading order QCD. A significant further increase in experimental accuracy would be needed to gain access to a possible thermal component.

3.3. Hard probes

Parton energy loss In nucleus-nucleus collisions, jet quenching and its centrality dependence has been quantified through measurements of the nuclear modification factor R_{AA} (10)^{65,67,189–192,194–196,200–204} as well as correlation measure-

ments^{204,213–215,217–220,222}. Fig. 10 (left panel) shows a strong suppression (R_{AA} as small as 0.13) in central Pb–Pb collisions for charged particles and various identified particles while the R_{AA} for γ is consistent with unity. Also, consistent with the qualitative expectations of parton energy loss, a large asymmetry in back-to-back jet p_T accompanied by slightly modified jet fragmentation functions inside small jet cone sizes ($R = 0.4$) has been observed. The radiated energy appears mostly at large angles ($R > 0.8$)^{205,206,208–212}. Furthermore, in semi-peripheral collisions, reduced but non-zero v_n coefficients have been found to persist up to the highest transverse momenta^{223,224} and di-jet events have been found correlated with elliptic flow²²⁵. These data are interpreted in terms of path-length dependent parton energy loss which in azimuthally asymmetric collision region leads to an azimuthal dependence of high- p_T hadron yields. They illustrate the connection between jet quenching and flow emphasized in section 2.3.

Early data on R_{AA} in Pb–Pb collisions show that a significant suppression $R_{AA} < 1$ persists even in the most peripheral event classes. By now, this phenomenon is understood as an intrinsic selection bias (events with less activity are biased towards larger nucleon–nucleon impact parameter which in turn have less high- Q^2 scatterings)⁶⁷. There is only a tight upper bound but no direct evidence for parton energy loss in the most peripheral Pb–Pb collisions^{67,294}.

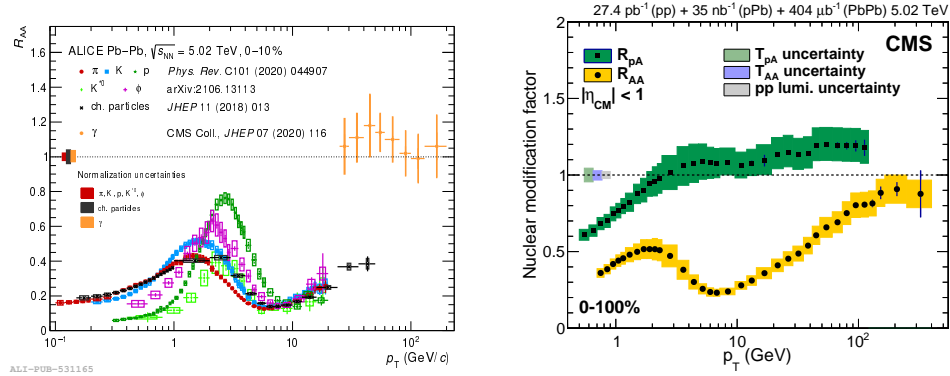


Fig. 10. Left panel: R_{AA} in Pb–Pb collisions for charged particles as well as π , K, p and ϕ compared to γ (Figure from Ref. 171). Right panel: R_{AA} in Pb–Pb collisions for charged particles up to high p_T compared to the result in p–Pb collisions (Figure from Ref. 65).

In p–Pb collisions, measurements of inclusive high- p_T hadron and inclusive jet yields in minimum-bias p–Pb collisions at the LHC are within the current accuracy of approximately 20% consistent with $R_{pPb} = 1$ ^{65,193,197–199,201,203}, see Fig. 10 (right panel). As explained in section 2.3, in small systems, the binning of R_{AA} and other measures of parton energy loss as a function of event activity (centrality) does not necessarily inform us about the system size dependence of jet quenching.

In particular, inclusive jet yields R_{pPb} are strongly suppressed relative to unity in “central” p–Pb collisions, and strongly enhanced in “peripheral” p–Pb collisions¹⁹³, but this is attributed to selection biases²¹⁶ and it does not inform us about the onset of jet quenching in “sufficiently central” p–Pb collisions. Also, signatures of jet quenching are neither observed in inclusive hadron production nor in the dijet transverse momentum imbalance^{197,201,207}. No significant jet quenching effects have been found in p–Pb collisions using correlations by either studying hadron production relative to the jet direction²²¹ or by measuring the semi-inclusive yield of jets recoiling from a high- p_{T} trigger hadron²¹⁶. Ref. 216 sets an upper limit of 400 MeV (at 90% CL) on medium-induced energy transport outside a jet cone with $R = 0.4$. This is about a factor 20 smaller than the magnitude of energy transport from within the jet to outside the jet cone in Pb–Pb collisions²¹³. On the other hand, as mentioned, the presence of energy loss leads to sizable v_{n} coefficients at high- p_{T} ²²³ in Pb–Pb collisions. Surprisingly, non-zero v_2 are measured above 9 GeV/c also in p–Pb collisions despite the lack of other energy-loss signals¹⁸⁴. This indicates that our current understanding of the interplay between jet quenching and flow phenomena is incomplete.

v_{n} in presence of a hard probe. The v_2 measured in events with a Z candidate in pp collisions are identical to the measurement in inclusive events¹⁸⁵. Similarly, selecting events with or without jets in pp collisions does not influence the measured v_2 ¹⁸⁶. Measurements in p–Pb collisions in presence of a high- p_{T} jet are similar to the ones in inclusive events for v_2 and v_3 ¹⁸⁴.

Jet constituent v_{n} Azimuthal correlations have also been measured between jet constituents and the bulk. No significant correlation is found between constituents of high- p_{T} ($p_{\text{T}} > 15$ GeV) jets and the remaining hadrons in the event in pp collisions¹⁸⁶. On the contrary, attempts to isolate jet constituent v_2 in jet-like three-particle correlation in p–Pb show significant non-zero values up to $p_{\text{T}} \sim 8$ GeV/c¹⁸⁷.

v_{n} in jets. In an attempt to identify collective phenomena in the smallest systems, there has been a study of high-multiplicity high-energy ($p_{\text{T}} > 550$ GeV/c) jets with up to 100 charged constituents in the final state¹⁸⁸. Two-particle correlations and v_2 are extracted in a coordinate system defined relative to the jet direction. The measured v_1 , v_2 and v_3 show a distinct trend as a function of multiplicity which is reproduced by Monte Carlo simulations without collective phenomena except at multiplicities above 80 where the trend changes and departs from the Monte Carlo expectation. The authors interpret this result as possible collective phenomena occurring in the dense environment of the jet.

Open heavy flavor and quarkonia Heavy flavor quarks (charm and beauty) are produced in the initial hard scattering and then interact and rescatter with the medium. Thus, also heavy-flavor particles exhibit finite anisotropies as shown with non-zero v_2 measurements for D mesons, J/ψ and HF decay electrons and muons in both Pb–Pb and p–Pb collisions^{108,226–244}. An example is shown in the left panel of Fig. 11. Non-zero v_2 of particles from decays involving bottom quarks are measured in Pb–Pb and p–Pb collisions but with large uncertainties²⁴⁰ in p–Pb collisions,

see also the left panel of Fig. 11. v_2 measurements for Υ are consistent with zero in Pb–Pb collisions^{246,248} and p–Pb collisions²⁴⁵. In pp collisions, significant v_2 for charm are measured at high multiplicity^{240,247} while the v_2 for muons from b decays is consistent with zero²⁴⁷, see the right panel of Fig. 11. Amongst measurements of collectivity seen in Pb–Pb collisions but not yet in smaller systems, there are data on non-zero v_2 for $\psi(2S)$ as well as non-zero v_3 for D mesons and J/ψ .^{238,243,244}

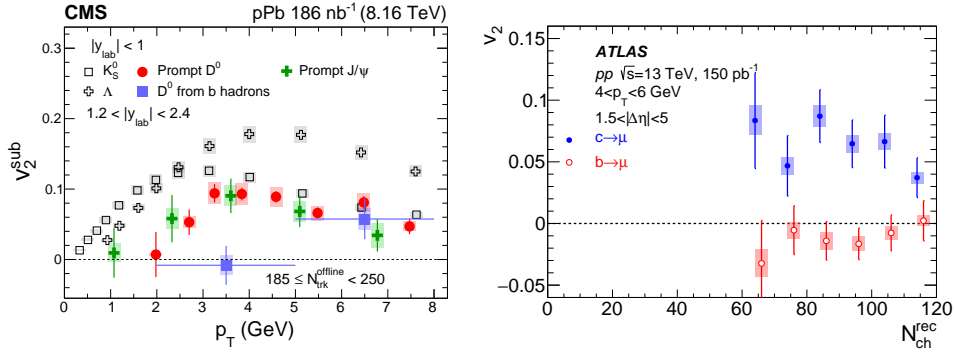


Fig. 11. Left panel: v_2 coefficient of prompt D^0 mesons and J/ψ as well as non-prompt D^0 compared to strange particles as a function of p_T in high-multiplicity p–Pb collisions (Figure adapted from Ref. 240). Right panel: v_2 coefficient of muons from charm and beauty decays as a function of multiplicity in pp collisions (Figure from Ref. 247).

The nuclear modification factor R_{AA} for J/ψ in large systems is enhanced at LHC with respect to RHIC energies^{232,249,250,257,259,261,267,273,276,282,283}. This is qualitatively different from the \sqrt{s} -dependence of $R_{AA}^{J/\psi}$ from CERN SPS to RHIC energies. J/ψ suppression has been expected due to the effect of the medium on the J/ψ binding energy, while the enhancement at LHC energies can be incorporated as a J/ψ regeneration component from deconfined charm quarks²⁸². $\Upsilon(1S)$, $\Upsilon(2S)$ and $\Upsilon(3S)$ production is equally found suppressed in Pb–Pb collisions with respect to the pp reference^{250,251,272,274,277,280,284}.

In p–Pb collisions, J/ψ and $\Upsilon(1S)$ are suppressed relative to pp collisions^{252,254,256,265,266,269–271,275,279,281} which can be attributed to nuclear modification of the gluon PDF¹⁷¹. The production of the excited charmonium state, $\Psi(2S)$ as well as excited bottomonium states $\Upsilon(nS)$, $n \geq 2$ have been measured in both Pb–Pb and p–Pb collisions^{253–255,257,258,260,262–264,268,273,278,281,284} which shows a suppression w.r.t. the ground state.

3.4. Towards even smaller systems...

Studies of the mentioned phenomena have been extended into even smaller systems, by studying low multiplicity pp collisions and by using ultra-peripheral (UPC) heavy-ion collisions where γ –p and γ –Pb processes occur. Furthermore, data of for-

Table 2. Summary of observables measured in γ -p (realized in p-Pb and ep colliders), γ -Pb, low multiplicity pp, e^+e^- and ep collision systems. Low N refers to values close to the minimum-bias multiplicity.

System	Observable		
	Near-side ridge yields	Azimuthal anisotropy (v_n)	Higher-order cumulants
γ -Pb (in Pb-Pb UPC)	observed (template)	up to v_3 (template)	not studied
γ -p (in p-Pb UPC)	not observed	up to $v_3 \approx$ MC (template)	not studied
γ -p (in ep)	not studied	up to $v_2 \approx$ MC	$n = 4 \approx$ MC wrong sign
ep (DIS)	not studied	up to $v_2 \approx$ MC	not studied
pp (low N)	observed	up to v_2 (template)	not studied
ee	limits + hint at 1.02σ	up to $v_3 \approx$ MC	not studied
Refs.	100,295-299	46,83,300,301 298,299,302	301

mer e^+e^- and ep experiments have been re-analyzed where the latter gives access to deep inelastic scattering (DIS) as well as resolved photoproduction resembling γ -p processes. While these studies only cover a fraction of the observables discussed in this section, they provide a number of interesting findings. Table 2 summarizes the current status and a brief overview is given in the following.

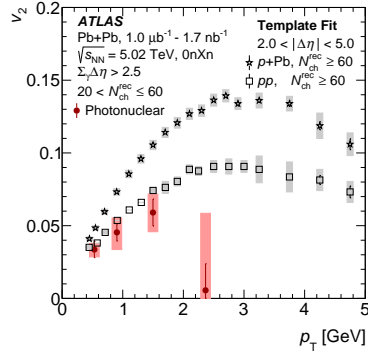


Fig. 12. v_2 coefficient measured in ultra-peripheral γ -Pb collisions compared to the measurement in p-Pb and pp collisions (Figure adapted from Ref. 302).

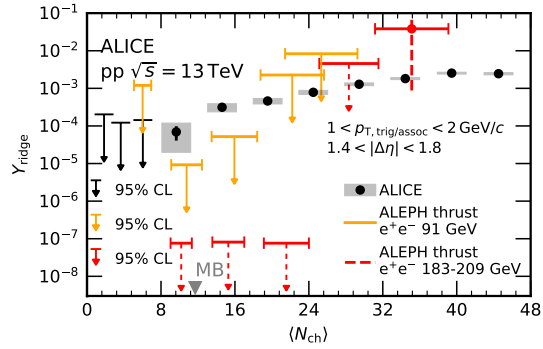


Fig. 13. Near-side ridge yield measured in pp collisions compared to upper limits set in e^+e^- collisions (Figure from Ref. 100).

Ultra-peripheral collisions The electromagnetic cloud traveling with Pb ions in a particle accelerator leads to collisions of photons with beam particles. This allows one to study γ -p (γ -Pb) collisions in a p-Pb (Pb-Pb) collider configuration

in so-called ultraperipheral collisions. Although the study of γ -p processes does not show any near-side ridge structure²⁹⁸, azimuthal Fourier coefficients up to third order have been measured. The positive v_2 is reasonably described by simulations without involving collective phenomena²⁹⁸. The study of γ -Pb collisions shows a different picture: significant non-zero v_2 and v_3 are measured, albeit with the template subtraction method. The v_n are lower than the equivalent measurement at the same multiplicity p-Pb collisions but similar to the ones in pp collisions, see Fig. 12. Contrary to the γ -p result, simulations without a collective component do not reproduce the result, even qualitatively³⁰².

ep collisions Studies in ep collisions in the DIS region find no evidence of a v_2 signal beyond the one expected from momentum conservation and are reproduced by MC generators without involving collective phenomena^{300,301}. In the photoproduction region v_2 is extracted with 2 and 4-particle correlations. No evidence of effects beyond momentum conservation are observed³⁰¹. The 4-particle signal at second order has the opposite sign³⁰¹ to the one observed in high-multiplicity pp to Pb-Pb collisions. The authors of Ref. 301 report their v_2 signal to be consistent with the one in γ -Pb collisions³⁰² and attribute it to jet production unrelated to hydrodynamical behavior.

Low-multiplicity pp collisions While high-multiplicity ridge yields in pp collisions have been the first observation of collective phenomena in pp collisions, see section 3.1, studies at low multiplicity are intrinsically difficult as the signal scales with the square of the particle multiplicity and is dominated by jet fragmentation and resonance decays at low multiplicity. Recently, near-side ridge yields have been measured with great precision to multiplicities lower than the minimum-bias multiplicity¹⁰⁰. Interestingly, significant long-range correlations emerge already at the minimum-bias multiplicity, see Fig. 13. Studies beyond ridge yields, for instance of v_n coefficients are scarce at low multiplicity. Only a v_2 measurement exists in pp collisions just above the minimum-bias multiplicity^{46,83} applying a template subtraction. Higher-order cumulants are only extracted at a multiplicity of 3-4 times the minimum-bias multiplicity at present.

e^+e^- collisions These collisions are free of hadronic effects in the initial state. As such, several mechanisms for collectivity invoked in other collision systems may be difficult to realize in e^+e^- . This makes it particularly interesting to check whether or not precursors of collective effects seen in other collision systems extend to e^+e^- . These collisions have a randomly oriented event topology in the detector, therefore the mentioned studies are performed in the so-called thrust axis which is a proxy for the direction of the hard process occurring in e.g. $e^+e^- \rightarrow q\bar{q}$. Archived ALEPH data as well as data from Belle have been analyzed and limits on near-side ridge yields have been set at collisions energies of about 10.5 GeV^{296,297}, 91 GeV²⁹⁵ and at 183-209 GeV²⁹⁹. In the highest multiplicity studied at 183-209 GeV a non-zero near-side ridge yield has been found at 1.02σ ²⁹⁹, see rightmost ALEPH point in Fig. 13. A special case is the study of $\Upsilon(4S)$ on-resonance data. Here a non-zero near-side yield is found which is however attributed to the special topology in the

decay of the $\Upsilon \rightarrow B\bar{B}$ system and reproduced by Monte Carlo simulations without collective phenomena. Furthermore, v_n coefficients are extracted and compared to MC simulations without collective phenomena which agree except at the largest studied multiplicities²⁹⁹. The statistical precision does not yet allow the conclusion that such phenomena are also found in e^+e^- collisions.

This data allows for a clear comparison to previously mentioned low-multiplicity ridge yields measured in pp collisions. The latter are at least 5σ larger¹⁰⁰ than the ones in e^+e^- collisions^f, see Fig. 13. This demonstrates that additional phenomena are observed in low-multiplicity pp collisions compared to e^+e^- collisions.

4. Theory overview

In the phenomenological discussion of ultra-relativistic nucleus–nucleus collisions, it has been emphasized repeatedly that fluid dynamic models with close-to-minimal dissipative properties can account for a broad range of collective phenomena³⁰³. Data comparisons with iEBE-VISHNU³⁰⁴, superSONIC³⁰⁵, MUSIC³⁰⁶ and other fluid models^{307,308} support this conclusion. However, the physics encoded in such phenomenologically successful “fluid” models goes significantly beyond fluid dynamics^g. It includes suitably chosen initial conditions, hadronization prescriptions, phenomenological choices for kinetic transport in the pre-equilibrium dynamics, and hadronic rescattering. Also the modeling of the fluid dynamic phase itself includes more than fluid dynamics, as explained in section 4.1.1. Early efforts to extend such fluid modeling to small collision systems are reviewed in section 4.3. The current state of the art in model comparisons is set by Bayesian inference techniques³⁰⁹.

The earliest Bayesian analyses of fluid models did not include any data from small systems and they were based on relatively few p_T -integrated measurements^{310–314}. Qualitatively different initial conditions were also studied³¹⁵. Early analyses that included some p–Pb data remained restricted to p_T -integrated quantities³¹⁶. The most complete analysis as of today is given by Trajectum^{317,318}. It includes more than 500 data points on p–Pb and Pb–Pb to overconstrain $O(20)$ model parameters, it extends to p_T -differential information and it has been used to illustrate the physics opportunities of future light ion beams by generating mock data for oxygen–oxygen collisions at the LHC³¹⁹.

Remarkably, the inclusion of data on small collision systems has led so far to no significant additional constraints on the dynamical mechanisms and material

^fTo be specific: The multiplicity range from 8 to 24 charged particles contributes most to this global assessment since ALEPH data allow one to establish the tightest upper bounds in this region. At high multiplicity, the upper bounds are much weaker. While this leaves more room for a potential signal, it must not be interpreted as a signal per se. It needs to be mentioned that the comparison as a function of multiplicity of these different collision systems at very different center-of-mass energies is intrinsically difficult and requires modeling assumptions resulting in a $5\text{--}6.3\sigma$ difference¹⁰⁰.

^gHere and in the following, we put the notion “fluid” in quotation marks to highlight - where required in content - that “fluid” models invoke more than fluid dynamics.

properties invoked to describe successfully central nucleus–nucleus collisions. The reason for this is thought to lie in increased uncertainties associated to the initial conditions of small systems and in an increased sensitivity to final state effects, see section 4.3.2. Within these complex multi-parameter models, our currently limited understanding of such uncertainties seems to offset the discriminatory power which a wider variation of system size could provide^{317,318,320}. A similar statement applies to other complex simulation tools of ultra-relativistic heavy ion collisions such as A Multi Phase Transport (AMPT) model^{321–323}, BAMPS^{324,325} or EPOS^{326,327}. We summarize in section 4.3 to what extent these codes have been compared to measures of collectivity in small systems, but we mention already here that more systematic studies are missing and that no significant further constraints on the dynamical mechanisms underlying collectivity have been reported.

The situation is thus rather peculiar: On the one hand, experiments at the LHC have established the persistence of almost all soft p_T signatures of collectivity across all system sizes from central Pb–Pb down to the low multiplicity pp collisions in which collectivity had not been expected. On the other hand, this wealth of qualitatively novel data does not seem to challenge any of the complex model frameworks used traditionally to simulate soft physics in heavy-ion collisions. The conclusion here is not that fluid-dynamic or transport models of ultra-relativistic heavy-ion collisions naturally explain collectivity in small systems. The conclusion is rather that the predictivity of these models for small systems is sufficiently weak to accommodate existing data.

In this situation, a discussion of what we learn from small system collectivity profits from going beyond mere data-model comparisons. One should ask whether the experimentally established phenomena of collectivity are more generic than the concepts invoked for their explanation. To be specific:

- I The phenomenology of nucleus–nucleus collisions invokes the concept of rapid equilibration – but can this equilibration be rapid enough to explain collectivity down to pp?
- II The phenomenology of nucleus–nucleus collisions invokes fluid dynamics – but what is the smallest droplet to which fluid dynamics applies?
- III The phenomenology of nucleus–nucleus collisions invokes close-to-minimal dissipative properties as the *sine qua non* for numerically large collective effects – but can this be the main cause for collectivity in p–Pb, in pp or even in e^+e^- ?

The field of ultra-relativistic heavy-ion collisions knows of precedents where substantial insights were achieved by going beyond a mere model-data comparison. For instance, two decades ago, a calculation of the viscosity over entropy ratio in a maximally supersymmetric field theory had contributed to revolutionizing heavy-ion phenomenology not because it led itself to a direct data-model comparison, but because it indicated that a hitherto unimagined dynamics could be realized in quantum field theory. In the same spirit, the LHC discovery of collectivity in small systems has triggered since 2010 many studies in theoretically clean simplified set-ups

to understand what is imaginable in terms of fast hydrodynamization, fast kinetic thermalization and fast chemical equilibration, and to what extent fluid dynamic or non-fluid dynamic degrees of freedom are at work in such fast processes. These lines of research are an intrinsic part of the LHC legacy of small system collectivity even if they address often “only” the conceptual and not the phenomenological part of the problem. The present chapter summarizes the most pertinent findings of this broad theoretical research effort. Finally, the last subsection will discuss data-model comparisons.

4.1. Dynamical frameworks of collectivity

Fluid dynamics, kinetic theory and the evolution of initial-state correlations (as well as various non-perturbative mechanisms) are the dynamical frameworks considered for the explanation of collective phenomena in ultra-relativistic nucleus–nucleus collisions. Here, we recall the assumptions on which they are based. This will enable a discussion about their applicability to collective effects in the smallest collision systems.

4.1.1. Fluid dynamic descriptions of collectivity

In nuclear physics, first fluid dynamic formulations of collectivity can be traced back to the liquid-drop model in the 1930s – a very informative account of these earliest developments is given in Ref. 40. In ultra-relativistic heavy ion collisions, it was Bjorken’s work³²⁸ on longitudinally boost-invariant systems that initiated fluid dynamic formulations of the collective expansion.

Fluid dynamics is formulated in terms of thermodynamic quantities, and it emerges in the long wavelength limit of any more complete dynamics. Different derivations of relativistic fluid dynamics exist.

(1) *The thermodynamic (or entropy-wise) derivation*

Fluid dynamics can be derived directly from conservation laws in a gradient expansion. In the simplest case (expansion to zeroth order in gradient), the energy-momentum tensor $T_{\mu\nu} = (\varepsilon + p)u_\mu u_\nu - p g_{\mu\nu}$ depends only on energy density ε , pressure p and three independent components of the local flow field u_μ . The collective dynamics of these five unknowns is fully determined in terms of four constraints from energy-momentum conservation $\nabla_\mu T^{\mu\nu} = 0$ supplemented by the equation of state $\varepsilon = \varepsilon(p)$.

To first order in gradients, the tensor decomposition of $T_{\mu\nu}$ with respect to the flow field u_μ contains a shear viscous term

$$\Pi_{\mu\nu}^{\text{constitutive}} = \eta \left[\Delta^{\mu\alpha} \nabla_\alpha u^\nu + \Delta^{\nu\alpha} \nabla_\alpha u^\mu - \frac{2}{3} \Delta^{\mu\nu} \nabla_\alpha u^\alpha \right], \quad (11)$$

as well as a bulk viscous and a heat conducting one. Here, η denotes the shear viscosity and $\Delta^{\mu\nu}$ is the projector on the subspace orthogonal to u^μ . Remarkably, requiring that entropy increases locally ($\nabla_\mu S^\mu \geq 0$) closes

the dissipative fluid equations to first order in gradients³²⁹. In this sense, dissipative fluid dynamics results solely from the fundamental laws of thermodynamics supplemented by material properties ($\varepsilon = \varepsilon(p)$, η , ...) that are calculable in an equilibrium field theory.

However, implementing the spatial gradients $\nabla_\mu u^\alpha$ in (11) instantaneously would violate causality. Therefore, *causal* viscous fluid dynamics^h specifies how the physical shear viscous tensor $\Pi_{\mu\nu}$ relaxes to its first-order constitutive form $\Pi_{\mu\nu}^{\text{constitutive}}$. This is done by ad hoc assumptions that lie outside the realm of fluid dynamicsⁱ. Israel-Stewart(IS)-type formulations of causal viscous fluid dynamics invoke a simple relaxation time τ_Π ; the temporal decay of a shear viscous excitation takes then the form

$$A_{\text{excitation decay}}(t) \simeq c_{\text{hyd}} \exp\left[-\frac{\eta}{\varepsilon + p} k^2 t\right] + c_{\text{non-hyd}} \exp\left[-\frac{t}{\tau_\Pi}\right]. \quad (12)$$

This time dependence reflects the precise statement that in IS fluid dynamics, the shear viscous channel of the retarded propagator of $T_{\mu\nu}$ has poles at $-i\frac{\eta}{\varepsilon+p}k^2$ and $-i\frac{t}{\tau_\Pi}$, see e.g. Ref. 27 for details. Since hydrodynamics is a gradient expansion, the lifetime of fluid dynamic excitations must grow with the inverse of the squared wave number k^2 . The k -independent decay with lifetime τ_Π is thus explicitly non-fluid dynamic. Israel-Stewart dynamics is fluid dynamics only for sufficiently large wavelengths λ

$$\frac{1}{\tau_\Pi} > \frac{\eta}{\varepsilon + p} k^2 = \frac{\eta}{s} \frac{(2\pi)^2}{T \lambda^2}. \quad (13)$$

(2) *Derivation of relativistic fluid dynamics from transport theory*

In weakly coupled theories, there is a scale separation between the typical size of the wave packet $1/T$ and the mean free path between individual scatterings. Therefore, for time separations much larger than $1/T$, when interference effects between subsequent scatterings can be neglected, the evolution is determined by Boltzmann transport in which collision kernels are given by in-medium scattering processes in the field theory. In QCD, this is the basis of AMY effective kinetic theory (EKT).^{332,333}

In general, Boltzmann transport theory evolves one-point probability densities $f(x, p, t)$ in response to collision kernels.^j Fluid dynamics can be derived by restricting Boltzmann transport to the lowest momentum moments of $f(x, p, t)$, namely the local conserved currents $N_\mu = \int p_\mu f(x, p, t)$ and the

^hOther causal formulations of fluid dynamics are possible^{330,331} but these have not been employed in phenomenological studies so far.

ⁱAs this relaxation dynamics must preserve transversality and orthogonality of $\Pi_{\mu\nu}$, its precise formulation is a bit technical and it will not be given here. For details, see e.g. Eq. (3.12) of Ref. 18.

^jThe evolution of $f(x, p, t)$ is coupled to that of correlated n -point density functions in the so-called BBGKY-hierarchy, and Boltzmann transport results from the truncation of that hierarchy.

energy-momentum tensor $T_{\mu\nu} = \int p_\mu p_\nu f(x, p, t)$. For relativistic dissipative fluid dynamics, this derivation was pioneered by Israel and Stewart³³⁴ (see also Refs. 335–337) and it was adapted to heavy-ion collisions subsequently^{338–341}.

For fluid-dynamic excitations, the kinetic and entropy-wise derivations yield the same equations of motion. However, the spectrum of non-fluid dynamic excitations depends on how the collision kernel is modeled^{342–345} and it differs from that of Israel-Stewart dynamics. In the simplest relaxation time approximation (RTA) of kinetic theory, the non-propagating non-fluid dynamic excitation of IS fluid dynamics in (12) is replaced by propagating quasi-particle excitations with lifetime $\tau_{\Pi} = a \frac{\eta}{sT}$, $a = 5$. In close analogy to IS dynamics, this kinetic evolution will not be governed by fluid dynamic degrees of freedom on length scales λ that are too short to satisfy (13).

(3) *Derivation of relativistic fluid dynamics from quantum field theory*

In general, dissipative transport coefficients can be calculated via the Green-Kubo formula as certain long-wavelength limits of correlation functions in the thermal field theory^{346,347}. For QCD, such transport coefficients have been calculated in finite temperature perturbation theory to (almost) next-to-leading order³⁴⁸, and there are some exploratory studies in lattice QCD^{349,350}. However, nothing is known rigorously about the spectrum of non-fluid excitations in QCD, except that they must exist, and that they may be more complicated than a few well-isolated poles³⁵¹. In this sense, the microscopic structure of the QGP is unknown to date.

In the strong coupling limit of non-abelian quantum field theories with gravity dual, both fluid dynamics and the microscopic dynamics beyond fluid dynamics is known. Dissipative fluid dynamics can be derived from the gradient expansion of gravitational perturbations in the dual classical supergravity theory^{18,352}. String-theory inspired derivations have helped to identify the complete set of allowed second-order transport terms¹⁸, including transport coefficients that can arise only in anomalous fluid dynamics³⁵³ and that can lead to qualitatively novel phenomena such as the chiral magnetic effect³⁵⁴. These anomalous transport coefficients can also be identified in an entropy-wise derivation³⁵⁵.

For $\mathcal{N} = 4$ SYM theory in the limit of strong coupling $\lambda = g^2 N_c \rightarrow \infty$ and large number of colors $N_c \rightarrow \infty$, the relaxation time in (12) is $\tau_{\Pi} = a \frac{\eta}{sT}$ with $a = 4 - \log(4) \approx 2.61$ (see Ref. 25 for a more complete review of relaxation times). The excitation spectrum of non-fluid (so-called quasi-normal) modes is fully known in the strong-coupling limit^{356,357}. The question of how the non-fluid dynamic properties of these non-abelian plasmas change with coupling strength is subject of recent research^{358–361}.

In summary, these findings support the following qualitative statements:

- The fluid dynamic evolution equations for relativistic collective dynamics

are universal: they take the same form, irrespective of whether they are derived from conservation laws (entropy-wise derivation)³⁶², from specific kinetic theories via Grad’s 14 moment expansion³⁶³ or with string-theoretical techniques in strongly coupled QFTs^{18,352}.

- Any dynamics limited to fluid dynamic excitations is acausal. Any causal relativistic collective dynamics exhibits also non-fluid dynamic excitations. These are non-universal and they depend on details of the microscopic dynamics. As non-fluid dynamic excitations must exist, the relevant question is not the qualitative one (to be a fluid or not to be a fluid?), but the quantitative one: to what extent is collectivity dominated by fluid-dynamic or non-fluid dynamic excitations?
- Fluid-dynamic excitations dominate if they are more long-lived than the non-fluid ones. For this to be the case, the wavelengths λ of excitations should satisfy^k

$$\lambda > \sqrt{\frac{\eta (2\pi)^2}{s T} \tau_{\Pi}} = (2\pi) \frac{\eta \sqrt{a}}{s T}. \quad (14)$$

For an almost perfect plasma with $\frac{\eta}{s} = \frac{1}{4\pi}$ and varying a from $a \approx 2.61$ (in $\mathcal{N} = 4$ SYM) to $a = 5$ (in kinetic theory), one finds $\lambda > (0.81 - 1.12) \frac{1}{T}$. In particular, $\lambda > 1$ fm for $T = 200$ MeV. For a less perfect fluid, this bound is more stringent.

According to these numerical estimates, the smallest pp and p–Pb collision systems have an initial transverse extension into which fluid dynamic excitations of wavelength (14) barely fit. For a predominantly fluid dynamic explanation of pp and p–Pb collisions, however, one would require that scales significantly smaller than the transverse system size can be resolved by excitations that propagate fluid dynamically. According to the estimate (14), this must not be taken for granted. Apparently supportive of this parametric statement, there is some evidence that if “fluid” modeling is applied to smaller and smaller systems, then the fluid dynamic aspects of that modeling become less and less relevant (see section 4.3.2 below).

^kConditions for the applicability of fluid dynamics have been formulated alternatively in terms of Reynolds number and Knudsen number, as reviewed succinctly in Ref. 41. Reynolds number is an intrinsically fluid dynamic concept used in the wider rheological practice to discriminate laminar from turbulent flow. Knudsen number measures system size in units of mean free path and thus requires knowledge about which degrees of freedom propagate with which cross section. Both concepts can be generalized⁴¹. Instead, we prefer here to formulate the applicability of fluid dynamics directly in terms of the decay time of non-fluid dynamic modes in (14), as this brings to the forefront what is really experimentally at stage: to learn about the nature of the non-fluid degrees of freedom which are characteristic features of the QGP, to learn about their decay which governs hydrodynamization, and to be open to the logical possibility that over a significant period in the evolution, non-fluid degrees of freedom may be non-negligible and coexistent with the fluid dynamic ones.

4.1.2. Kinetic theory and transport models

The application of kinetic theory to ultra-relativistic heavy-ion collisions is as old as that of fluid dynamics. Around the same time at which Bjorken formulated boost-invariant fluid dynamics, Baym formulated boost-invariant kinetic theory to understand “the approach to thermodynamic equilibrium” of “the excitations present”³⁶⁴. As indicated by this wording, kinetic theory had been viewed from the very beginning as a tool for understanding how and on what time scale equilibrium is achieved (“thermalization”) and how fluid dynamic behavior emerges (“hydrodynamization”). The potential relevance and the potential limitations of formulating small system collectivity in terms of kinetic transport theory may be summarized as follows:

Pro Unlike fluid dynamics, kinetic theory applies to arbitrarily small systems. It is a candidate dynamics that interpolates *smoothly* between free-streaming in sufficiently small and dilute systems (assumed to be realized in multi-purpose event generators for pp collisions) and dissipative fluid dynamics in sufficiently large and dense systems (assumed to be realized in fluid simulations for Pb–Pb collisions). These qualitative features have motivated many recent studies of the onset of collective phenomena in small collision systems (see section 4.2.1).

Con The formulation of kinetic transport theory relies on a scale separation between the size $\sim 1/T$ of quantum mechanical wavepackets and the mean free path between individual scatterings. In the strong coupling limit of quantum field theories with gravity duals, this scale separation is not realized. In high temperature QCD, the scale separation is perturbatively realized and it allows one to derive an effective kinetic theory, called AMY EKT^{332,333}. For phenomenologically relevant values of the running QCD coupling (say $\alpha_s(Q^2 = 2\text{GeV}^2) \simeq 0.3$), a parametrically clean scale separation does not exist. In this case, the use of transport models may still promise qualitative insights but it pushes kinetic theory beyond its region of guaranteed applicability.

In kinetic theory, collective dynamics arises from the microscopic dynamics implemented in the collision kernels of the transport equations. In the phenomenological practice, any formulation of this microscopic dynamics is necessarily incomplete. Without entering what would be an inevitably technical and model-dependent discussion of how different choices of collision kernels are motivated, we highlight here two qualitative insights that have emerged within the last decade:

(1) *Rapid kinetic hydrodynamization and thermalization*

QCD effective kinetic theory, AMY EKT^{332,333} propagates one-point probability densities in response to in-medium $2 \rightarrow 2$ elastic and $1 \rightarrow 2$ LPM collision kernels. It implements the so-called BMSS bottom-up thermalization³⁶⁵ according to which a longitudinally Bjorken-expanding initially

oversaturated system dilutes and becomes undersaturated while $1 \rightarrow 2$ splittings build up a reservoir of soft scattering centers. Subsequent interactions with these soft scattering centers drive the system then to equilibrium. Numerical studies with phenomenologically realized values of α_s have demonstrated^{366,367} that the resulting evolution towards equilibrium can be sufficiently fast to hydrodynamize initial conditions in ultra-relativistic heavy ion collisions efficiently.

Beyond conceptual insights, this line of research has resulted by now in a simulation tool. A linearized version of AMY EKT underlies the KoM-PoST code^{368,369} that sets the current state of the art of modeling the pre-equilibrium stage of “fluid” models. The duration over which pre-equilibrium evolution deviates significantly from viscous fluid dynamics in AMY EKT is comparable to the transverse extent of a pp collision (see discussion of Figure 14 below). This is another indication that if “fluid” models are applied to small systems, the fluid part of their evolution plays an increasingly smaller role for smaller system size. It is in line with the conclusions summarized at the end of section 4.1.1.

Beyond the linearized treatment of KoMPOST, there is a first proof-of-principle study of a Lorentz invariant parton cascade ALPACA that solves the AMY EKT Boltzmann equations³⁷⁰.

(2) *Onset of collectivity in “one-hit” kinetic theory*

Evolving with $2 \rightarrow 2$ Boltzmann transport an expanding mixture of several relativistic massive particle species, it was found early on that a single collision per particle in average can already lead to sizable elliptic flow, with mass ordering between the species³⁷¹. Similar findings were reported for the phenomenologically more complete AMPT code³⁷², emphasizing that the contribution from hydrodynamic-type mechanisms is small, see section 4.3. In a sufficiently small and dilute system, the first correction to free-streaming is obtained by expanding the collective dynamics to first order in the collision term. This is an expansion to first order in opacity, where opacity measures a specific combination of transverse geometric extension and local transverse energy density^{291,373}. In simple kinetic models (isotropization time approximation – ITA), the one-hit approximation leads naturally and for generic reasons to a hierarchy of the linear response coefficients v_n/ε_n in (1) that is in line with experimental observations. Remarkably, also non-linear response coefficients result in one-hit kinematics as a consequence of simple scaling behaviors²⁹⁰. In ITA kinetic theory, non-linear response coefficients like v_4/ε_2^2 or $v_5/(\varepsilon_2\varepsilon_3)$ are found to have the phenomenologically required order of magnitude in one-hit dynamics^{291,373}.

In contrast to fluid dynamics, the region of validity of kinetic theory is not limited to quanta of low momentum. Kinetic theory is thus a framework in which bulk dynamics and the jet quenching of hard processes could emerge as differ-

ent manifestations of the same underlying dynamics. This is particularly apparent in AMY EKT which is known to give rise to fast hydrodynamization while its $1 \rightarrow 2$ Landau-Pomeranchuk–Migdal collision kernel is known³⁷⁴ to implement the BDMPS-Z formulation³⁷⁵ of radiative parton energy loss that underlies many jet quenching formulations.

4.1.3. Initial state quantum interference as a source of collectivity

Both fluid dynamic and kinetic models attribute the observed phenomena of collectivity to final state partonic and hadronic scattering. In contrast, it has been suggested in the context of saturation physics that initial state correlations could be responsible for the flow-like phenomena observed in small systems. With the so-called IP-Glasma model^{376,377}, saturation physics has motivated an ab initio formulation of subnucleon fluctuations. Models within this framework were shown to reproduce di-hadron correlation data in pp^{378,379} and p–Pb³⁷⁹ collisions, and in various small collision systems studied at RHIC³⁸⁰. However, a reassessment of this saturation physics explanation in an independent model implementation³⁸¹ called into question some of the essential elements reported in Ref. 380. In this context, the results of Ref. 380 were referred to as “counterintuitive”.

A short succinct review of the initial state perspective on collectivity in small collision systems can be found in Ref. 382. What is referred to as “glasma graphs” in saturation physics can be viewed as the calculation of quantum interference effects in the superposition of emission amplitudes from different sources. It follows directly from Heisenberg’s uncertainty principle that quantum interference can map spatially anisotropic distributions of these initial sources into momentum anisotropies in the final state. In this sense, non-vanishing elliptic flow from sources correlated in the initial state may be intuitively expected even though the size of their contribution may be difficult to calculate and even though current model implementations may be unsatisfactory.

The phenomenology of ultra-relativistic heavy ion collisions knows of collective effects that are of a pure quantum nature. In particular, HBT correlations are collective in the sense that they are correlations amongst all identical particles in an event and that they persist in the limit of a large number of sources; they also translate spatio-temporal anisotropies into momentum anisotropies²⁹³. Explicit calculations in saturation physics^{379,383} have identified such HBT-like correlations. Different calculational set-ups indicate that momentum anisotropies v_n resulting from quantum interference can persist in the limit of a large number of sources^{384–386} irrespective of whether the conditions for saturation physics are satisfied^{384,387}. However, the size of possible effects depends on assumptions, e.g., about the orientation of color fields³⁸⁸. Also, saturation physics alone cannot be expected to explain all important manifestations of collectivity. In particular, the formalism tends to lead to relatively short-range correlations in rapidity³⁸⁹ and in transverse momenta³⁸⁸, it decreases with increasing system size^{380,390} and it can be washed out by final-state interac-

tions^{320,391}. In addition, it does not address the observed mass ordering of collective flow and it does not explain naturally the system size dependence of flow from small to large systems. In summary, the observed collective phenomena are clearly more generic than their explanation within the framework of saturation physics although, from a theoretical viewpoint, quantum interference can be expected to contribute to momentum anisotropies at some (as yet not fully understood) scale.

4.1.4. *Strings, ropes, shoving, pomerons and all that*

The collective phenomena observed in small systems relate to physics at small momentum transfers which is nominally non-perturbative. Fluid dynamic descriptions aim at capturing this non-perturbative physics in terms of a few transport coefficients; saturation physics aims at capturing it by doing perturbation theory on top of a non-perturbative high-density background; kinetic theory views non-perturbative information as included in the collision kernels. All three frameworks have important limitations if applied to small systems. Also, they do not exhaust the range of non-perturbative concepts that can be motivated within QCD. This subsection reviews other non-perturbative approaches that have been explored in the context of small system collectivity.

In QCD, partonic scatterings separate color charges. Separated color charges are connected via flux tubes that fragment eventually. The description of this non-perturbative dynamics is model-dependent, but it is an essential aspect of QCD. In the so-called Lund string, it is at the basis of a successful hadronization model⁶⁰ that is employed in modern multi-purpose event generators⁹. It has been argued that this string fragmentation must be supplemented by thermal effects to account for the observation of heavy-ion like behavior in the hadrochemical composition of high-multiplicity pp collisions at the LHC³⁷. In inelastic hadronic or nuclear collisions, flux tubes stretch between partons at projectile and target rapidities. With any interaction that shifts the distribution of such flux tubes in the transverse plane, these strings become candidates for long-range rapidity correlations^{392,393}. Such a string shoving mechanism was shown to implement hadrochemical and kinematic signatures of collectivity in small systems³⁹⁴. A related mechanism has been suggested but not worked out in Ref. 395. Even the founding father of fluid dynamic applications to ultra-relativistic heavy ion collisions has argued that while fluid dynamics may account for the observed ridge in nucleus–nucleus collisions, the apparently similar ridge effect in high-multiplicity pp collisions could be due to “a quite different physical mechanism”, namely the collision of aligned flux tubes³⁹⁶.

In general, elevating strings and more complex, spatially extended colored structures (such as ropes, baryon junctions etc.) to dynamical degrees of freedom has a long history in the phenomenological modeling of nucleus–nucleus collisions. Early implementations include the dual parton model³⁹⁷, RQMD³⁹⁸, URQMD³⁹⁹ and extensions of HiJING⁴⁰⁰. Also AMPT enhances its initial energy density significantly with a string melting mechanism⁴⁰¹ and it is thus more than a parton cascade. An-

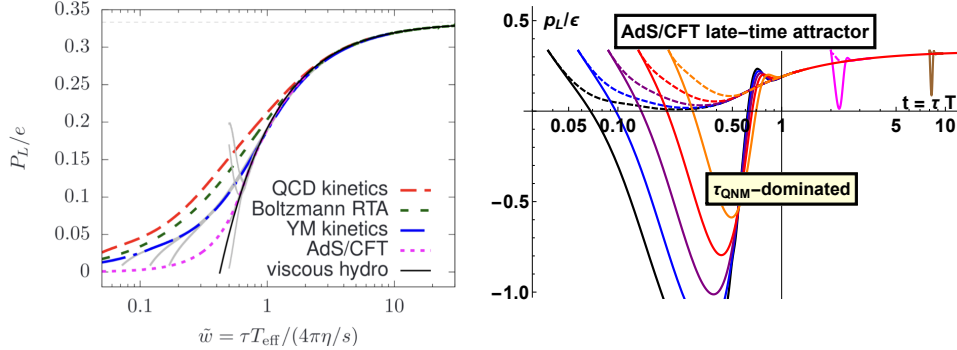


Fig. 14. Evolution of the ratio of longitudinal pressure over energy density in different 1+1D models. Left panel: All microscopic theories (dashed curves) have the same late-time attractor which is relativistic viscous fluid dynamics. All microscopic theories hydrodynamize (i.e. approach this attractor) on the same time scale $\sim (4\pi) \frac{\eta}{sT}$, including variations of initial conditions within the same model (grey lines). Figure taken from Ref. 404. Right panel: Not all microscopic theories have an early time attractor. For the strongly coupled QFT shown here, initial conditions set at five different times and two different choices all hydrodynamize at the time scale $\sim (4\pi) \frac{\eta}{sT}$ without displaying universal behavior at earlier times. Figure taken from Refs. 405. The hydrodynamization scale identified in these studies is consistent with the simple parametric estimate in (14).

other non-perturbative concept that emerges naturally in QCD is that of pomeron exchanges⁴⁰². Such mechanisms have been argued to give rise to fluid dynamic behavior⁴⁰³.

4.2. Hydrodynamization and Thermalization - insights from simple models

In general, collectivity is thought to arise from far out-of-equilibrium initial conditions in a dynamics which thermalizes locally and which thus lends itself eventually to a fluid dynamic description. But in a smaller collision system, any collective dynamics is at work for a shorter time. In the following, we summarize efforts to understand in simplified model set-ups the central question I whether thermalization and hydrodynamization can occur sufficiently quickly for explaining collectivity in the smallest collision systems.

4.2.1. Studies in boost-invariant 1+1 dimensional systems

A dynamical system with boost-invariant initial conditions evolves in a boost-invariant way. Also, if initial conditions are translationally invariant in the transverse plane, this symmetry is preserved throughout the evolution. Invoking both symmetries, the resulting dynamics is essentially 1+1-dimensional. As first realized by Bjorken³²⁸ for hydrodynamics and by Baym³⁶⁴ for kinetic theory, this offers the possibility of formulating technically simple, analytically tractable toy models that share important commonalities with physically realized almost boost-invariant

collision systems.

Timescale of hydrodynamization: Due to the symmetries in 1+1D systems, a very limited set of out-of-equilibrium conditions can be explored: Transverse gradients and density fluctuations are forbidden, conditions with initial eccentricity cannot be initialized and the dynamical mapping (1) from ϵ_n to v_n cannot be explored. However, initial conditions that deviate *locally* from equilibrium can be imposed. In fluid dynamics^{405–408} (in the absence of conserved currents), the only observables are the longitudinal pressure p_L and the energy density ϵ ; both depend only on time, and their ratio can be initialized arbitrarily far away from the equilibrium value $p_L/\epsilon = \frac{1}{3}$. In Boltzmann kinetic theory^{405,407,409–412}, also higher moments of the one-particle distribution function f can be studied. However, the timescales for their relaxation are rather trivially related and numerically comparable to those governing p_L and ϵ ^{405,410,413}. In numerically tractable, strongly coupled field theories with gravity dual^{405,407,414,415}, the evolution is not limited to a one-particle probability distribution and a larger variety of initial conditions may be initiated⁴⁰⁵.

Technically, the question of hydrodynamization amounts to asking on which timescale arbitrarily initialized components of the energy-momentum tensor relax to their constitutive expressions, (such as (11)) in a fluid dynamic gradient expansion. In the simplest 1+1D models (which have only ϵ and p_L as observables), this reduces to the question on which time scale p_L/ϵ reaches the viscous hydrodynamic correction (see black line in the left panel of Fig. 14) to the equilibrium value $p_L/\epsilon = \frac{1}{3}$. The answer is: in a Bjorken expanding system, hydrodynamization occurs on timescales $O\left((4\pi)\frac{\eta}{sT}\right)$. This is so far all microscopic dynamics explored in Fig. 14, irrespective of whether it is strongly coupled or weakly coupled. This answer fully supports the parametric estimate (14) for the limited range of validity of fluid dynamics. In this sense, the problem of hydrodynamization is fully solved in 1+1D.

Early-time and late-time attractors: In the recent literature on hydrodynamization, the more general concept of attractor solutions plays an important role, see Ref. 416 for a broad review with relations to many neighboring fields. Attractors are the particular solutions of a dynamical system to which arbitrary initial conditions within the basin of attraction relax at sufficiently late times. The late-time hydrodynamic attractor is clearly visible in Fig. 14 and it is reached for arbitrary initial conditions. Remarkably, in 1+1D boost-invariant fluid dynamics and kinetic transport, attractor solutions are found not only at late times, but also at arbitrarily early times^{405,407,409–412}. However, the existence of an early-time attractor is not the tell-tale sign of a particularly efficient hydrodynamization. Rather, it is a consequence of the interplay between local interaction and the rapid longitudinal expansion in boost-invariant systems⁴⁰⁵. In kinetic theory, this is a non-interacting free-streaming dynamics that drives the system to negligible p_L , in fluid dynamics, the early time attractor risks being unphysical since longitudinal gradients become arbitrarily large at arbitrarily early time and they thus lie outside a fluid

dynamic description. In strongly coupled quantum field theories, no early time attractor exists and the system hydrodynamizes on the natural time scale $O(1/T)$ on which interactions drive the system to local equilibrium, see Fig. 14. Related findings have been corroborated in QCD effective kinetic theory without^{367,368} and with^{417,418} quark degrees of freedom. In summary, only the late-time attractor is independent of the microscopic dynamics, i.e. universal. It reflects the onset of fluid dynamics. In contrast, the early-time attractor is non-universal and it is not related to the onset of fluid dynamics. Fluid dynamics is not unreasonably effective. Rather, it sets in when standard textbook arguments expect it to set in, namely on scales on which fluid dynamic excitations live longer as non-fluid dynamic ones (see discussion leading to (14)).

The approach of particular initial conditions to known hydrodynamic late-time attractor solutions has also been explored to exhibit the asymptotic nature of the hydrodynamic gradient expansion, to develop resummation techniques^{343,405,411,419–422} and it has been used to illustrate the role of non-hydrodynamic poles in the relaxation to the attractor⁴¹⁵.

4.2.2. Studies in boost-invariant higher-dimensional systems

The fact that arbitrary initial conditions relax to a universal late-time fluid-dynamic attractor solution is equivalent to saying that initial conditions are forgotten. In the boost-invariant 1+1-dimensional systems discussed so far, essentially all measurable quantities forget initial conditions on a hydrodynamization time scale which is significantly shorter than the thermalization time scale at which the system approaches local equilibrium (here $p_L/\varepsilon = 1/3$), see Figure 14. Having identified this universal hydrodynamization time scale in multiple models based on qualitatively different physics assumptions is arguably one of the main insights of these 1+1-dimensional studies. However, while thermalization is about forgetting, hydrodynamization is not. A fluid dynamic evolution that implements the mapping (1) from initial spatial eccentricities ϵ_n to final momentum anisotropies v_n is a dynamics that remembers the initial conditions ϵ_n . The fact that the evolution of 1+1D models forgets any initial condition at late times is not a general physics feature but it points to an intrinsic limitation of 1+1D studies: these models simply do not allow for the description of measurable quantities that are not forgotten in the evolution. Higher dimensional systems need to be studied to this end.

While most studies of hydrodynamization and thermalization are carried out in 1+1D models because of their technical simplicity, there have been studies in higher dimensions^{27,29,405,411,423–427}. Early numerical studies of radially symmetric colliding show waves mimicking small systems in strongly coupled field theory corroborated the importance of the time and length scale $O(1/T)$ for driving small systems toward fluid dynamic evolution^{428–430}. More generally, once radial symmetry is not imposed, one can study how efficiently initial conditions ϵ_n are remembered, and to what extent the response depends on the assumed dynamics.

For instance, evolving a system with initial spatial eccentricity ϵ_2 , first with kinetic theory up to a switching time τ_s and then with the corresponding Israel-Stewart dynamics to later times informs us about the sensitivity of collective response to the nature of non-fluid dynamic degrees of freedom. In such model studies, one third to one half of the elliptic flow signal seen in fully hydrodynamized systems can be built up in small collision systems that extend over only one mean free path and that do not hydrodynamize²⁶. Along a different line of investigation, there has been a significant computational effort to quantify in simple conformal kinetic theories the full opacity dependence of all relevant linear and non-linear response coefficients in the mapping $\{\epsilon_n\} \rightarrow \{v_n\}$ ^{27,29,424,425,427}. This opacity dependence interpolates smoothly between free-streaming and almost perfect fluid dynamics as a function of opacity. Despite their simplicity, these models have led to statements about the (in)applicability of hydrodynamics in pp, p-Pb and light nucleus collisions²⁸.

4.3. Model studies and data comparisons

Up to this point, our discussion has focused mainly on the description of basic physics concepts that may underlie the formulation of collectivity in small systems (section 4.1), and on the illustration of these concepts in highly simplified model studies whose conceptual transparency offers unique opportunities for understanding how and how efficiently collectivity may be built up in small systems. However, such simple models do not reflect the full complexity of ultra-relativistic hadronic and nuclear collisions. Here, we finally summarize data comparisons with phenomenologically more complete model frameworks.

4.3.1. Theory expectations prior to LHC data

Prior to the experimental observations of collectivity in small systems, different works had contemplated the possibility that azimuthal asymmetries may be seen in pp collisions at LHC as a consequence of various nuclear-like effects^{431,432}, as a consequence of fluid dynamic behavior^{433–436} or more generally as a consequence of a collective dynamical response to initial spatial eccentricities in the pp overlap^{437,438}. The very idea that pp collisions may develop fluid dynamic behavior is not new and had been considered early on, see e.g. Ref. 439. However, predictions of the size of v_2 in pp varied from zero⁴³³ to values of $O(0.1)$, depending on model assumptions, and mechanisms ranged from collective explosion³⁹⁵ to initial state effects in saturation physics⁴⁴⁰. In short, these early works formulated interesting expectations, but none of them constitutes a well-motivated *prediction* that can be regarded as having received detailed experimental support.

4.3.2. Small system collectivity in fluid models

Following the phenomenological success in ultra-relativistic nucleus–nucleus collisions, several works aimed at including small-system collectivity within the same

“fluid” modeling in small and large systems. This working hypothesis “one fluid to rule them all” has been supported by a viscous fluid dynamic description of high-multiplicity pp, p–Pb and Pb–Pb collisions at $\sqrt{s} = 5.02$ TeV^{441,442}. However, it also became clear that “one fluid might not rule them all”⁴⁴³. While the wordings cited here sound like contradicting each other, the scientific facts reported in these studies are consistent with each other. The main message is simply that “fluid” models are more than fluid models: they include additional physics. Additional physics found numerically relevant for small collision systems includes the physics of hadronization (recombination, see section 2.2 for details)⁴⁴⁴, the physics of hadronic^{445,446} non-fluid contributions to flow, and the physics of initial state fluctuations^{320,447–449}. These additional physical mechanisms appear to become numerically more relevant for smaller collision systems. In this sense, fluid dynamics does not become abruptly invalid below a certain system size, but it becomes gradually less and less relevant for the description of the system. The studies of “fluid” models cited above compare to a small subset of the measures of collectivity in Table 1 only (mainly measurements of $v_2(p_T)$ and $v_3(p_T)$). Where more detailed sets of data were included in the analysis, issues of fine-tuning and of a possibly limited range of validity of hydrodynamics became more important^{443,450}.

The EPOS event generator employs a core-corona model. The initial conditions are generated in a model of pomeron-type multiple scattering³²⁶. The corona of hadronic and nuclear collisions is modeled in a microscopic-dynamic picture that is assumed to be free of collective dynamics. The dynamics in the core (which becomes more important in large systems) is described by viscous fluid dynamics in recent versions of EPOS³²⁷. In this sense, EPOS is a particular variant of a viscous “fluid” model. Hadronic rescattering is simulated with UrQMD, but the fluid dynamic phase seems essential for the dynamical translation (1) from spatial to momentum anisotropies. Different versions of EPOS reproduce the ridge in pp collisions⁴⁵¹, anisotropic flow phenomena in p–Pb collisions⁴⁵², and radial flow phenomena in pp and p–Pb collisions including their mass hierarchy⁴⁵³. But EPOS also predicts a characteristic nuclear modification of heavy-flavor hadrons⁴⁵⁴ and a characteristic enhancement of thermal photon production⁴⁵⁵ in pp collisions which have not been observed, yet.

4.3.3. Small system collectivity in transport models

In ultra-relativistic heavy ion collisions, the modeling of the bulk of the collective evolution with partonic transport codes has a long history^{321,324,456–463}. For all these simulation packages, the code *is* the model in the sense that the code is more than a tool for solving an easily stated set of transport equations of motion. The interpretational question of why a transport code (that implement much more physics than transport physics) does or does not agree with data is as old as the comparison of transport codes to data and it can be difficult to address. Amongst the above-mentioned partonic transport codes, mainly A Multi Phase Transport

(AMPT) model^{321–323} and BAMPS^{324,325} have been compared recently to data from the LHC.

AMPT successfully reproduces elliptic and triangular flow in p–Pb, peripheral Pb–Pb^{464–466} and ³He–Au collisions⁴⁶⁷. It has also been shown to satisfactorily reproduce mass ordering of v_2 and v_3 in settings in which coalescence was enabled⁴⁶⁸. The question for why AMPT is successful has focused in particular on the problem that the AMPT code performs very differently from Molnar’s Parton Cascade MPC⁴⁶² although it uses nominally similarly small partonic cross sections. This links the discussion of AMPT to the time-honored problem of understanding the so-called “opacity puzzle”⁴⁶² at the beginning of the RHIC heavy-ion program. As Molnar had realized at the time, to account for the size of the elliptic flow at RHIC, MPC had to be initialized either with unphysically high parton densities per unit rapidity, or it had to be evolved with unphysically large partonic cross sections⁴⁶⁹. There is a detailed analysis in Ref. 401 of which model-dependent choices in AMPT may underlie its phenomenological success where other transport codes fail.

We mention in passing the role of hadronic transport in heavy-ion phenomenology. In simulations of nucleus–nucleus collisions that involve fluid dynamic modeling, the system is hadronized along Cooper-Frye⁵⁸ freeze-out hypersurfaces. The resulting hadron gas is sufficiently dilute to be evolved with Boltzmann transport codes. Interactions in this hadronic phase affect kinetic and hadrochemical distributions. RQMD³⁹⁸, URQMD³⁹⁹ and most recently SMASH⁴⁷⁰ are the main hadronic transport codes used to this end.

4.4. Model comparisons to hadrochemical measures of collectivity

In principle, any phenomenologically complete model of hadronic collisions should describe both hadrochemical and kinematic characteristics of multi-particle distributions. In practice, however, several microscopic mechanisms that affect kinematic contributions at best mildly are invoked to account for the observed hadrochemical distributions. These include statistical hadronization, recombination, string breaking, color reconnection, rope formation etc. Here, we comment on model comparisons invoking such hadronization models.

It is one profound consequence of the smooth evolution of strange particle production with event multiplicity that the hadronization mechanisms used in multi-purpose event generators need to be supplemented with qualitatively novel physics³⁷. Hadronization mechanisms where individual color degrees of freedom hadronize without seeing the nuclear environment cannot account for the observed multiplicity dependence. For instance, string breaking tuned to e^+e^- collisions cannot account for strangeness enhancement. Several mechanisms have been considered in the literature. These include color reconnections beyond leading color¹² as implemented in PYTHIA, color ropes where several strings hadronize together⁴⁷¹ or the explicit addition of collective phenomena as for instance in core/corona models like EPOS⁴⁷². Statistical models using a Grand Canonical ensemble including

a strangeness undersaturation factor γ_S (which is close to 1 in large systems and smaller than 1 in small collision systems) describe particle ratios in all systems within an accuracy of about 20%¹⁷¹.

While the above-mentioned models consider mechanisms of strangeness enhancement that are operational at the time of hadronization, there is also the question whether (some of) the observed strangeness enhancement could be generated dynamically by sufficiently efficient partonic interaction rates prior to hadronization, i.e., by turning an overdense gluon-rich system into a strangeness rich one via $gg \rightarrow s\bar{s}$. This motivates efforts to model the microscopic partonic (and hadronic) processes that can contribute to strangeness enhancement. Fermion production has been studied using perturbative reaction rates^{54,55}, classical real-time lattice simulations of nonequilibrium production⁴⁷³, rate equations^{474,475} and various partonic Boltzmann transport models^{456,461,476–478}. Inspired by the signs of collective behavior in the hadrochemical composition of small collision systems, there have been first studies of chemical equilibration in QCD effective kinetic theory⁴¹⁷, estimating that chemical equilibration can be reached for final state multiplicities $dN_{\text{ch}}/d\eta \gtrsim 100$. Measurements of the change of hadrochemical composition as a function of system size inform this discussion.

5. Concluding discussion and outlook

The experimental program reviewed here was not thought of or proposed prior to the start of LHC operation, but it emerged in response to a surprising discovery. Over the last decade, this led to a thorough and complete experimental exploration of the system-size dependence of all soft multi-particle phenomena including the traditional hallmarks of collectivity in flow observables, hadrochemical abundances and the study of heavy quarks. In line with the quote of T.D. Lee with which we have started this review, one may note that qualitatively novel collective phenomena had been thought to arise as a function of both, an increasing volume of the collision system and an increasing initial local energy density (which increases with \sqrt{s}). What we know now is that almost all collective phenomena observed in large A–A collisions can be identified also in small pp and p–Pb collisions. Collective phenomena are numerically larger in larger collision systems but they remain sizable across all hadronic collision systems and they evolve smoothly with the spatial extension of the colliding system, with event multiplicity and with \sqrt{s} without any experimental indication for a finite minimal scale required for collectivity.

Future experimental small-system runs at the LHC are foreseen to include proton–ion collisions, oxygen–oxygen collisions and possibly other light-ion collisions with increased integrated luminosity. In addition to increased experimental accuracy, this will substantially extend our experimental knowledge of collectivity into the heavy-quark sector in small systems and possibly identify the onset of jet quenching as a function of system size.

One decade into this program, what is the big picture that has emerged? Fig. 15

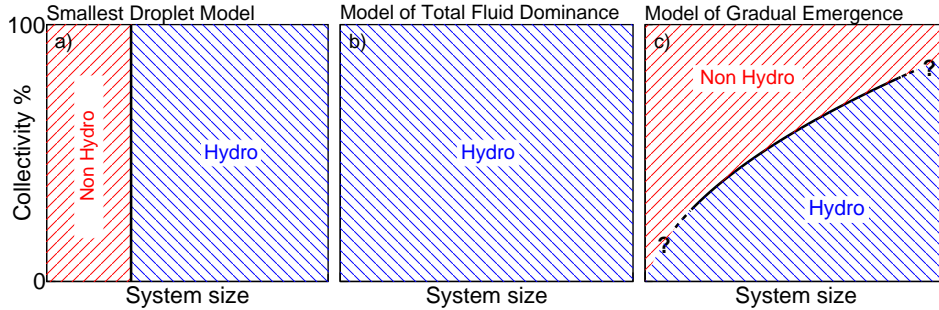


Fig. 15. Three simple sketches of the degree to which hydrodynamic and non-hydrodynamic mechanisms may contribute to the observed collectivity as a function of system size. There is strong support for the idea that the range of experimentally accessible system sizes allows one to vary significantly the relative importance of fluid- and non-fluid degrees of freedom in collective phenomena.

sketches three different ways to think about the onset of collectivity as a function of system size. According to the first picture (a), a mesoscopic system displays fluid dynamic behavior only above a finite minimal size. In this “minimal droplet” model, the HEP phenomenology of pp collisions (as embodied in standard multi-purpose event generators) and the HIP phenomenology of heavy ion collisions (based on the notion of an almost perfect fluid) could have lived side-by-side within limited, mutually exclusive regions of validity. This picture is falsified. Almost all collective phenomena observed in large A–A collisions have been identified by now also in small pp and p–Pb collisions. After a decade of small system physics, we know that the dependence of collective phenomena on system size does not show any clear onset of qualitatively novel physics above a minimal characteristic scale. Also, we do not have any evidence that the physical mechanisms responsible for that collectivity change abruptly or qualitatively as a function of system size. Second, there is the simple view (b) that if one observes collectivity in the smallest systems, then even the smallest systems flow. However, the identification of such observed “flow” with a signature of fluid dynamics is largely semantic and not tenable. A closer look at model studies reveals that there is no model in which fluid dynamics dominates collectivity for systems of all size. Rather, fluid dynamics is the universal long wavelength limit of any more complete and more microscopic description of collectivity. As the system size is reduced, this long wavelength limit becomes gradually less important and the non-fluid dynamic degrees of freedom play an increasingly important role in building up collectivity. The relative contribution of fluid dynamics to collectivity changes gradually with system size. The observed commonalities of collective phenomena in small and large systems thus give support to the idea that essentially the same microscopic mechanisms are at work in both pp and A–A, though their relative importance changes gradually with system size. This idea of a gradual emergence of fluid dynamics with system size is captured in the third

caricature (c) of Fig. 15. It is the experimentally and theoretically supported one.

How can this big picture guide future studies? What is surprising in hindsight is not so much that the picture of gradual emergence of fluid dynamics is the supported one. The fortunate surprise is rather that the transition from a collective dynamics dominated by non-fluid degrees of freedom to a collective dynamics dominated by fluid ones seems to occur exactly within the experimentally accessible range of system size. The picture of gradual emergence of fluid dynamics thus indicates that system size can be used as a tool to vary the relative importance of fluid- and non-fluid dynamic degrees of freedom in controlled experimentation. It also raises the question to what extent the impact of non-fluid dynamic degrees of freedom in large collision systems, even if subleading, could be quantified better. Small systems provide a natural inroad to understanding the QGP beyond its fluid dynamic manifestations.

Acknowledgments

We thank Katarina Krizkova Gajdosova, Aleksii Kurkela, Andreas Morsch, Krishna Rajagopal and Soeren Schlichting for constructive input and criticism at various stages of this work.

References

1. H. David Politzer. Reliable Perturbative Results for Strong Interactions? *Phys. Rev. Lett.*, 30:1346–1349, 1973. doi:10.1103/PhysRevLett.30.1346.
2. Gross, David J. and Wilczek, Frank. Ultraviolet Behavior of Nonabelian Gauge Theories. *Phys. Rev. Lett.*, 30:1343–1346, 1973. doi:10.1103/PhysRevLett.30.1343.
3. John C. Collins and M. J. Perry. Superdense Matter: Neutrons Or Asymptotically Free Quarks? *Phys. Rev. Lett.*, 34:1353, 1975. doi:10.1103/PhysRevLett.34.1353.
4. N. Cabibbo and G. Parisi. Exponential Hadronic Spectrum and Quark Liberation. *Phys. Lett. B*, 59:67–69, 1975. doi:10.1016/0370-2693(75)90158-6.
5. Edward V. Shuryak. Quark-Gluon Plasma and Hadronic Production of Leptons, Photons and Psions. *Phys. Lett. B*, 78:150, 1978. doi:10.1016/0370-2693(78)90370-2.
6. F. Karsch. Lattice QCD at Finite Temperature: A Status Report. *Z. Phys. C*, 38:147, 1988. doi:10.1007/BF01574529.
7. T. D. Lee. Abnormal Nuclear States and Vacuum Excitations. *Rev. Mod. Phys.*, 47:267–275, 1975. doi:10.1103/RevModPhys.47.267.
8. R. Keith Ellis, W. James Stirling, and B. R. Webber. *QCD and collider physics*, volume 8. Cambridge University Press, 2 2011. ISBN 978-0-511-82328-2, 978-0-521-54589-1. doi:10.1017/CBO9780511628788.
9. Torbjörn Sjöstrand, Stefan Ask, Jesper R. Christiansen, Richard Corke, Nishita Desai, Philip Ilten, Stephen Mrenna, Stefan Prestel, Christine O. Rasmussen, and Peter Z. Skands. An introduction to PYTHIA 8.2. *Comput. Phys. Commun.*, 191:159–177, 2015. doi:10.1016/j.cpc.2015.01.024.
10. Johannes Bellm et al. Herwig 7.0/Herwig++ 3.0 release note. *Eur. Phys. J. C*, 76(4):196, 2016. doi:10.1140/epjc/s10052-016-4018-8.
11. T. Gleisberg, Stefan Hoeche, F. Krauss, M. Schonherr, S. Schumann, F. Siegert, and J. Winter. Event generation with SHERPA 1.1. *JHEP*, 02:007, 2009. doi:10.1088/1126-6708/2009/02/007.
12. Jesper R. Christiansen and Peter Z. Skands. String Formation Beyond Leading Colour. *JHEP*, 08:003, 2015. doi:10.1007/JHEP08(2015)003.
13. John W. Harris and Berndt Muller. The Search for the quark - gluon plasma. *Ann. Rev. Nucl. Part. Sci.*, 46:71–107, 1996. doi:10.1146/annurev.nucl.46.1.71.
14. John W. Harris and Berndt Müller. “QGP Signatures” revisited. *Eur. Phys. J. C*, 84(3):247, 2024. doi:10.1140/epjc/s10052-024-12533-y.
15. Ulrich W. Heinz and Maurice Jacob. Evidence for a new state of matter: An Assessment of the results from the CERN lead beam program. 1 2000. doi:10.48550/arXiv.nucl-th/0002042.
16. G. Policastro, Dan T. Son, and Andrei O. Starinets. The Shear viscosity of strongly coupled N=4 supersymmetric Yang-Mills plasma. *Phys. Rev. Lett.*, 87:081601, 2001. doi:10.1103/PhysRevLett.87.081601.

17. Derek Teaney. The Effects of viscosity on spectra, elliptic flow, and HBT radii. *Phys. Rev. C*, 68:034913, 2003. doi:10.1103/PhysRevC.68.034913.
18. Rudolf Baier, Paul Romatschke, Dam Thanh Son, Andrei O. Starinets, and Mikhail A. Stephanov. Relativistic viscous hydrodynamics, conformal invariance, and holography. *JHEP*, 04:100, 2008. doi:10.1088/1126-6708/2008/04/100.
19. I. Arsene et al. Quark gluon plasma and color glass condensate at RHIC? The Perspective from the BRAHMS experiment. *Nucl. Phys. A*, 757:1–27, 2005. doi:10.1016/j.nuclphysa.2005.02.130.
20. K. Adcox et al. Formation of dense partonic matter in relativistic nucleus-nucleus collisions at RHIC: Experimental evaluation by the PHENIX collaboration. *Nucl. Phys. A*, 757:184–283, 2005. doi:10.1016/j.nuclphysa.2005.03.086.
21. B. B. Back et al. The PHOBOS perspective on discoveries at RHIC. *Nucl. Phys. A*, 757:28–101, 2005. doi:10.1016/j.nuclphysa.2005.03.084.
22. John Adams et al. Experimental and theoretical challenges in the search for the quark gluon plasma: The STAR Collaboration’s critical assessment of the evidence from RHIC collisions. *Nucl. Phys. A*, 757:102–183, 2005. doi:10.1016/j.nuclphysa.2005.03.085.
23. Paul Romatschke and Ulrike Romatschke. Viscosity Information from Relativistic Nuclear Collisions: How Perfect is the Fluid Observed at RHIC? *Phys. Rev. Lett.*, 99:172301, 2007. doi:10.1103/PhysRevLett.99.172301.
24. Huichao Song, Steffen A. Bass, Ulrich Heinz, Tetsufumi Hirano, and Chun Shen. 200 A GeV Au+Au collisions serve a nearly perfect quark-gluon liquid. *Phys. Rev. Lett.*, 106:192301, 2011. doi:10.1103/PhysRevLett.106.192301. [Erratum: *Phys.Rev.Lett.* 109, 139904 (2012)].
25. Jorge Casalderrey-Solana, Hong Liu, David Mateos, Krishna Rajagopal, and Urs Achim Wiedemann. *Gauge/String Duality, Hot QCD and Heavy Ion Collisions*. Cambridge University Press, 2014. ISBN 978-1-00-940350-4, 978-1-00-940349-8, 978-1-00-940352-8, 978-1-139-13674-7. doi:10.1017/9781009403504.
26. Aleksı Kurkela, Urs Achim Wiedemann, and Bin Wu. Opacity dependence of elliptic flow in kinetic theory. *Eur. Phys. J. C*, 79(9):759, 2019. doi:10.1140/epjc/s10052-019-7262-x.
27. Aleksı Kurkela, Urs Achim Wiedemann, and Bin Wu. Flow in AA and pA as an interplay of fluid-like and non-fluid like excitations. *Eur. Phys. J. C*, 79(11):965, 2019. doi:10.1140/epjc/s10052-019-7428-6.
28. Victor E. Ambrus, S. Schlichting, and C. Werthmann. Establishing the Range of Applicability of Hydrodynamics in High-Energy Collisions. *Phys. Rev. Lett.*, 130(15):152301, 2023. doi:10.1103/PhysRevLett.130.152301.
29. Victor E. Ambrus, S. Schlichting, and C. Werthmann. Opacity dependence of transverse flow, preequilibrium, and applicability of hydrodynamics in heavy-ion collisions. *Phys. Rev. D*, 107(9):094013, 2023. doi:10.1103/PhysRevD.107.094013.
30. M. Arslanđok et al. Hot QCD White Paper. 3 2023.

- doi:10.48550/arXiv.2303.17254.
31. Néstor Armesto. Small collision systems: Theory overview on cold nuclear matter effects. *EPJ Web Conf.*, 171:11001, 2018. doi:10.1051/epjconf/201817111001.
 32. C. A. Salgado et al. Proton-Nucleus Collisions at the LHC: Scientific Opportunities and Requirements. *J. Phys. G*, 39:015010, 2012. doi:10.1088/0954-3899/39/1/015010.
 33. Vardan Khachatryan et al. Observation of Long-Range Near-Side Angular Correlations in Proton-Proton Collisions at the LHC. *JHEP*, 09:091, 2010. doi:10.1007/JHEP09(2010)091.
 34. Georges Aad et al. Observation of associated near-side and away-side long-range correlations in $\sqrt{s_{\text{NN}}} = 5.02$ TeV p-Pb collisions with the ATLAS detector. *Phys. Rev. Lett.*, 110(18):182302, 2013. doi:10.1103/PhysRevLett.110.182302.
 35. Betty Abelev et al. Long-range angular correlations on the near and away side in p-Pb collisions at $\sqrt{s_{\text{NN}}} = 5.02$ TeV. *Phys. Lett.*, B719:29–41, 2013. doi:10.1016/j.physletb.2013.01.012.
 36. Serguei Chatrchyan et al. Observation of long-range near-side angular correlations in pPb collisions at the LHC. *Phys. Lett.*, B718:795–814, 2013. doi:10.1016/j.physletb.2012.11.025.
 37. Nadine Fischer and Torbjörn Sjöstrand. Thermodynamical String Fragmentation. *JHEP*, 01:140, 2017. doi:10.1007/JHEP01(2017)140.
 38. Kevin Dusling, Wei Li, and Björn Schenke. Novel collective phenomena in high-energy proton-proton and proton-nucleus collisions. *Int. J. Mod. Phys. E*, 25(01):1630002, 2016. doi:10.1142/S0218301316300022.
 39. Huichao Song, You Zhou, and Katarina Gajdosova. Collective flow and hydrodynamics in large and small systems at the LHC. *Nucl. Sci. Tech.*, 28(7):99, 2017. doi:10.1007/s41365-017-0245-4.
 40. James L. Nagle and William A. Zajc. Small System Collectivity in Relativistic Hadronic and Nuclear Collisions. *Ann. Rev. Nucl. Part. Sci.*, 68:211–235, 2018. doi:10.1146/annurev-nucl-101916-123209.
 41. Jorge Noronha, Björn Schenke, Chun Shen, and Wenbin Zhao. Progress and Challenges in Small Systems. 1 2024. doi:10.48550/arXiv.2401.09208.
 42. P. W. Anderson. More Is Different. *Science*, 177(4047):393–396, 1972. doi:10.1126/science.177.4047.393.
 43. Jurgen Schukraft, Anthony Timmins, and Sergei A. Voloshin. Ultra-relativistic nuclear collisions: event shape engineering. *Phys. Lett. B*, 719:394–398, 2013. doi:10.1016/j.physletb.2013.01.045.
 44. S. Voloshin and Y. Zhang. Flow study in relativistic nuclear collisions by Fourier expansion of Azimuthal particle distributions. *Z. Phys. C*, 70:665–672, 1996. doi:10.1007/s002880050141.
 45. S. Wang, Y. Z. Jiang, Y. M. Liu, D. Keane, D. Beavis, S. Y. Chu, S. Y. Fung, M. Vient, C. Hartnack, and Horst Stoecker. Measurement of collective

- flow in heavy ion collisions using particle pair correlations. *Phys. Rev. C*, 44: 1091–1095, 1991. doi:10.1103/PhysRevC.44.1091.
46. Georges Aad et al. Observation of Long-Range Elliptic Azimuthal Anisotropies in $\sqrt{s} = 13$ and 2.76 TeV pp Collisions with the ATLAS Detector. *Phys. Rev. Lett.*, 116(17):172301, 2016. doi:10.1103/PhysRevLett.116.172301.
 47. Nicolas Borghini, Phuong Mai Dinh, and Jean-Yves Ollitrault. A New method for measuring azimuthal distributions in nucleus-nucleus collisions. *Phys. Rev. C*, 63:054906, 2001. doi:10.1103/PhysRevC.63.054906.
 48. Nicolas Borghini, Phuong Mai Dinh, and Jean-Yves Ollitrault. Flow analysis from multiparticle azimuthal correlations. *Phys. Rev. C*, 64:054901, 2001. doi:10.1103/PhysRevC.64.054901.
 49. R. S. Bhalerao, N. Borghini, and J. Y. Ollitrault. Analysis of anisotropic flow with Lee-Yang zeroes. *Nucl. Phys. A*, 727:373–426, 2003. doi:10.1016/j.nuclphysa.2003.08.007.
 50. Ante Bilandzic, Raimond Snellings, and Sergei Voloshin. Flow analysis with cumulants: Direct calculations. *Phys. Rev. C*, 83:044913, 2011. doi:10.1103/PhysRevC.83.044913.
 51. Jiangyong Jia, Mingliang Zhou, and Adam Trzupek. Revealing long-range multiparticle collectivity in small collision systems via subevent cumulants. *Phys. Rev. C*, 96(3):034906, 2017. doi:10.1103/PhysRevC.96.034906.
 52. Shreyasi Acharya et al. Multiplicity dependence of light-flavor hadron production in pp collisions at $\sqrt{s} = 7$ TeV. *Phys. Rev.*, C99(2):024906, 2019. doi:10.1103/PhysRevC.99.024906.
 53. Anton Andronic, Peter Braun-Munzinger, Krzysztof Redlich, and Johanna Stachel. Decoding the phase structure of QCD via particle production at high energy. *Nature*, 561(7723):321–330, 2018. doi:10.1038/s41586-018-0491-6.
 54. Johann Rafelski and Berndt Muller. Strangeness Production in the Quark - Gluon Plasma. *Phys. Rev. Lett.*, 48:1066, 1982. doi:10.1103/PhysRevLett.48.1066. [Erratum: *Phys. Rev. Lett.* 56, 2334 (1986)].
 55. P. Koch, Berndt Muller, and Johann Rafelski. Strangeness in Relativistic Heavy Ion Collisions. *Phys. Rept.*, 142:167–262, 1986. doi:10.1016/0370-1573(86)90096-7.
 56. Peter Braun-Munzinger, Krzysztof Redlich, and Johanna Stachel. Particle production in heavy ion collisions. pages 491–599, 4 2003. doi:10.1142/9789812795533_0008.
 57. Anton Andronic, Peter Braun-Munzinger, Markus K. Köhler, Aleksas Mazeliauskas, Krzysztof Redlich, Johanna Stachel, and Vytautas Vislavicius. The multiple-charm hierarchy in the statistical hadronization model. *JHEP*, 07: 035, 2021. doi:10.1007/JHEP07(2021)035.
 58. Fred Cooper and Graham Frye. Comment on the Single Particle Distribution in the Hydrodynamic and Statistical Thermodynamic Models of Multiparticle Production. *Phys. Rev. D*, 10:186, 1974. doi:10.1103/PhysRevD.10.186.

59. Fabrice Retiere and Michael Annan Lisa. Observable implications of geometrical and dynamical aspects of freeze out in heavy ion collisions. *Phys. Rev. C*, 70:044907, 2004. doi:10.1103/PhysRevC.70.044907.
60. Bo Andersson. *The Lund Model*, volume 7 of *Cambridge Monographs on Particle Physics, Nuclear Physics and Cosmology*. Cambridge University Press, 7 2023. ISBN 978-1-00-940129-6, 978-1-00-940125-8, 978-1-00-940128-9, 978-0-521-01734-3, 978-0-521-42094-5, 978-0-511-88149-7. doi:10.1017/9781009401296.
61. R. J. Fries, Berndt Muller, C. Nonaka, and S. A. Bass. Hadron production in heavy ion collisions: Fragmentation and recombination from a dense parton phase. *Phys. Rev. C*, 68:044902, 2003. doi:10.1103/PhysRevC.68.044902.
62. R. J. Fries, Berndt Muller, C. Nonaka, and S. A. Bass. Hadronization in heavy ion collisions: Recombination and fragmentation of partons. *Phys. Rev. Lett.*, 90:202303, 2003. doi:10.1103/PhysRevLett.90.202303.
63. Megan Connors, Christine Nattrass, Rosi Reed, and Sevil Salur. Jet measurements in heavy ion physics. *Rev. Mod. Phys.*, 90:025005, 2018. doi:10.1103/RevModPhys.90.025005.
64. Michael L. Miller, Klaus Reygers, Stephen J. Sanders, and Peter Steinberg. Glauber modeling in high energy nuclear collisions. *Ann. Rev. Nucl. Part. Sci.*, 57:205–243, 2007. doi:10.1146/annurev.nucl.57.090506.123020.
65. Vardan Khachatryan et al. Charged-particle nuclear modification factors in PbPb and pPb collisions at $\sqrt{s_{NN}} = 5.02$ TeV. *JHEP*, 04:039, 2017. doi:10.1007/JHEP04(2017)039.
66. Constantin Loizides and Andreas Morsch. Absence of jet quenching in peripheral nucleus–nucleus collisions. *Phys. Lett. B*, 773:408–411, 2017. doi:10.1016/j.physletb.2017.09.002.
67. Shreyasi Acharya et al. Analysis of the apparent nuclear modification in peripheral Pb–Pb collisions at 5.02 TeV. *Phys. Lett. B*, 793:420–432, 2019. doi:10.1016/j.physletb.2019.04.047.
68. Jaroslav Adam et al. Centrality dependence of particle production in p-Pb collisions at $\sqrt{s_{NN}} = 5.02$ TeV. *Phys. Rev.*, C91(6):064905, 2015. doi:10.1103/PhysRevC.91.064905.
69. Nestor Armesto, Doga Can Gülhan, and Jose Guilherme Milhano. Kinematic bias on centrality selection of jet events in pPb collisions at the LHC. *Phys. Lett. B*, 747:441–445, 2015. doi:10.1016/j.physletb.2015.06.032.
70. Alexander Huss, Aleks Kurkela, Aleksas Mazeliauskas, Risto Paatelainen, Wilke van der Schee, and Urs Achim Wiedemann. Discovering Partonic Rescattering in Light Nucleus Collisions. *Phys. Rev. Lett.*, 126(19):192301, 2021. doi:10.1103/PhysRevLett.126.192301.
71. Alexander Huss, Aleks Kurkela, Aleksas Mazeliauskas, Risto Paatelainen, Wilke van der Schee, and Urs Achim Wiedemann. Predicting parton energy loss in small collision systems. *Phys. Rev. C*, 103(5):054903, 2021. doi:10.1103/PhysRevC.103.054903.

72. J. D. Bjorken. Energy Loss of Energetic Partons in Quark - Gluon Plasma: Possible Extinction of High $p(t)$ Jets in Hadron - Hadron Collisions. 8 1982.
73. K. Aamodt et al. Harmonic decomposition of two-particle angular correlations in Pb-Pb collisions at $\sqrt{s_{NN}} = 2.76$ TeV. *Phys. Lett.*, B708:249–264, 2012. doi:10.1016/j.physletb.2012.01.060.
74. Serguei Chatrchyan et al. Long-range and short-range dihadron angular correlations in central Pb-Pb collisions at a nucleon-nucleon center of mass energy of 2.76 TeV. *JHEP*, 07:076, 2011. doi:10.1007/JHEP07(2011)076.
75. Georges Aad et al. Measurement of the azimuthal anisotropy for charged particle production in $\sqrt{s_{NN}} = 2.76$ TeV lead-lead collisions with the ATLAS detector. *Phys. Rev.*, C86:014907, 2012. doi:10.1103/PhysRevC.86.014907.
76. Serguei Chatrchyan et al. Centrality dependence of dihadron correlations and azimuthal anisotropy harmonics in Pb-Pb collisions at $\sqrt{s_{NN}} = 2.76$ TeV. *Eur. Phys. J.*, C72:2012, 2012. doi:10.1140/epjc/s10052-012-2012-3.
77. Georges Aad et al. Measurement of long-range pseudorapidity correlations and azimuthal harmonics in $\sqrt{s_{NN}} = 5.02$ TeV proton-lead collisions with the ATLAS detector. *Phys. Rev.*, C90(4):044906, 2014. doi:10.1103/PhysRevC.90.044906.
78. A. Adare et al. Measurement of long-range angular correlation and quadrupole anisotropy of pions and (anti)protons in central d +Au collisions at $\sqrt{s_{NN}}=200$ GeV. *Phys. Rev. Lett.*, 114(19):192301, 2015. doi:10.1103/PhysRevLett.114.192301.
79. Vardan Khachatryan et al. Measurement of long-range near-side two-particle angular correlations in pp collisions at $\sqrt{s} = 13$ TeV. *Phys. Rev. Lett.*, 116(17):172302, 2016. doi:10.1103/PhysRevLett.116.172302.
80. L. Adamczyk et al. Long-range pseudorapidity dihadron correlations in d +Au collisions at $\sqrt{s_{NN}} = 200$ GeV. *Phys. Lett. B*, 747:265–271, 2015. doi:10.1016/j.physletb.2015.05.075.
81. Jaroslav Adam et al. Higher harmonic flow coefficients of identified hadrons in Pb-Pb collisions at $\sqrt{s_{NN}} = 2.76$ TeV. *JHEP*, 09:164, 2016. doi:10.1007/JHEP09(2016)164.
82. Jaroslav Adam et al. Pseudorapidity dependence of the anisotropic flow of charged particles in Pb-Pb collisions at $\sqrt{s_{NN}} = 2.76$ TeV. *Phys. Lett.*, B762:376–388, 2016. doi:10.1016/j.physletb.2016.07.017.
83. Vardan Khachatryan et al. Evidence for collectivity in pp collisions at the LHC. *Phys. Lett.*, B765:193–220, 2017. doi:10.1016/j.physletb.2016.12.009.
84. Morad Aaboud et al. Measurement of multi-particle azimuthal correlations in pp , p +Pb and low-multiplicity Pb+Pb collisions with the ATLAS detector. *Eur. Phys. J.*, C77(6):428, 2017. doi:10.1140/epjc/s10052-017-4988-1.
85. Shreyasi Acharya et al. Searches for transverse momentum dependent flow vector fluctuations in Pb-Pb and p-Pb collisions at the LHC. *JHEP*, 09:032, 2017. doi:10.1007/JHEP09(2017)032.
86. Albert M Sirunyan et al. Observation of Correlated Azimuthal Anisotropy

- Fourier Harmonics in pp and $p + Pb$ Collisions at the LHC. *Phys. Rev. Lett.*, 120(9):092301, 2018. doi:10.1103/PhysRevLett.120.092301.
87. S. Acharya et al. Anisotropic flow of identified particles in Pb-Pb collisions at $\sqrt{s_{NN}} = 5.02$ TeV. *JHEP*, 09:006, 2018. doi:10.1007/JHEP09(2018)006.
 88. Shreyasi Acharya et al. Investigations of Anisotropic Flow Using Multiparticle Azimuthal Correlations in pp , p -Pb, Xe-Xe, and Pb-Pb Collisions at the LHC. *Phys. Rev. Lett.*, 123(14):142301, 2019. doi:10.1103/PhysRevLett.123.142301.
 89. Shreyasi Acharya et al. Higher harmonic non-linear flow modes of charged hadrons in Pb-Pb collisions at $\sqrt{s_{NN}} = 5.02$ TeV. *JHEP*, 05:085, 2020. doi:10.1007/JHEP05(2020)085.
 90. Georges Aad et al. Measurement of the pseudorapidity and transverse momentum dependence of the elliptic flow of charged particles in lead-lead collisions at $\sqrt{s_{NN}} = 2.76$ TeV with the ATLAS detector. *Phys. Lett.*, B707:330–348, 2012. doi:10.1016/j.physletb.2011.12.056.
 91. Georges Aad et al. Measurement of the centrality and pseudorapidity dependence of the integrated elliptic flow in lead-lead collisions at $\sqrt{s_{NN}} = 2.76$ TeV with the ATLAS detector. *Eur. Phys. J.*, C74(8):2982, 2014. doi:10.1140/epjc/s10052-014-2982-4.
 92. Roel Aaij et al. Measurements of long-range near-side angular correlations in $\sqrt{s_{NN}} = 5$ TeV proton-lead collisions in the forward region. *Phys. Lett.*, B762:473–483, 2016. doi:10.1016/j.physletb.2016.09.064.
 93. Jaroslav Adam et al. Forward-central two-particle correlations in pPb collisions at $\sqrt{s_{NN}} = 5.02$ TeV. *Phys. Lett.*, B753:126–139, 2016. doi:10.1016/j.physletb.2015.12.010.
 94. Morad Aaboud et al. Measurement of forward-backward multiplicity correlations in lead-lead, proton-lead, and proton-proton collisions with the ATLAS detector. *Phys. Rev.*, C95(6):064914, 2017. doi:10.1103/PhysRevC.95.064914.
 95. Vardan Khachatryan et al. Pseudorapidity dependence of long-range two-particle correlations in pPb collisions at $\sqrt{s_{NN}} = 5.02$ TeV. *Phys. Rev.*, C96(1):014915, 2017. doi:10.1103/PhysRevC.96.014915.
 96. Albert M Sirunyan et al. Pseudorapidity and transverse momentum dependence of flow harmonics in pPb and PbPb collisions. *Phys. Rev.*, C98(4):044902, 2018. doi:10.1103/PhysRevC.98.044902.
 97. Georges Aad et al. Measurements of longitudinal flow decorrelations in pp and Xe+Xe collisions with the ATLAS detector. 8 2023. doi:10.48550/arXiv.2308.16745.
 98. Shreyasi Acharya et al. Measurements of long-range two-particle correlation over a wide pseudorapidity range in p -Pb collisions at $\sqrt{s_{NN}} = 5.0$ TeV. *JHEP*, 01:199, 2024. doi:10.1007/JHEP01(2024)199.
 99. Z. Citron et al. Report from Working Group 5: Future physics opportunities for high-density QCD at the LHC with heavy-ion and proton beams. *CERN Yellow Rep. Monogr.*, 7:1159–1410, 2019. doi:10.23731/CYRM-2019-007.1159.
 100. Shreyasi Acharya et al. Emergence of Long-Range Angular Correlations in

- Low-Multiplicity Proton-Proton Collisions. *Phys. Rev. Lett.*, 132(17):172302, 2024. doi:10.1103/PhysRevLett.132.172302.
101. C. Aidala et al. Creation of quark–gluon plasma droplets with three distinct geometries. *Nature Phys.*, 15(3):214–220, 2019. doi:10.1038/s41567-018-0360-0.
 102. M. I. Abdulhamid et al. Measurements of the Elliptic and Triangular Azimuthal Anisotropies in Central He3+Au, d+Au and p+Au Collisions at $\sqrt{s_{NN}} = 200$ GeV. *Phys. Rev. Lett.*, 130(24):242301, 2023. doi:10.1103/PhysRevLett.130.242301.
 103. Betty Abelev et al. Anisotropic flow of charged hadrons, pions and (anti-)protons measured at high transverse momentum in Pb–Pb collisions at $\sqrt{s_{NN}} = 2.76$ TeV. *Phys. Lett.*, B719:18–28, 2013. doi:10.1016/j.physletb.2012.12.066.
 104. Betty Abelev et al. Long-range angular correlations of π , K and p in p–Pb collisions at $\sqrt{s_{NN}} = 5.02$ TeV. *Phys. Lett.*, B726:164–177, 2013. doi:10.1016/j.physletb.2013.08.024.
 105. Betty Abelev et al. Elliptic flow of identified hadrons in Pb–Pb collisions at $\sqrt{s_{NN}} = 2.76$ TeV. *JHEP*, 06:190, 2015. doi:10.1007/JHEP06(2015)190.
 106. Vardan Khachatryan et al. Long-range two-particle correlations of strange hadrons with charged particles in p–Pb and Pb–Pb collisions at LHC energies. *Phys. Lett.*, B742:200–224, 2015. doi:10.1016/j.physletb.2015.01.034.
 107. A. Adare et al. Measurements of mass-dependent azimuthal anisotropy in central p+Au, d+Au, and $^3\text{He}+\text{Au}$ collisions at $\sqrt{s_{NN}} = 200$ GeV. *Phys. Rev. C*, 97:064904, 2018. doi:10.1103/PhysRevC.97.064904.
 108. A. M. Sirunyan et al. Elliptic flow of charm and strange hadrons in high-multiplicity pPb collisions at $\sqrt{s_{NN}} = 8.16$ TeV. *Phys. Rev. Lett.*, 121(8):082301, 2018. doi:10.1103/PhysRevLett.121.082301.
 109. Shreyasi Acharya et al. Anisotropic flow and flow fluctuations of identified hadrons in Pb–Pb collisions at $\sqrt{s_{NN}} = 5.02$ TeV. *JHEP*, 05:243, 2023. doi:10.1007/JHEP05(2023)243.
 110. Armen Tumasyan et al. Strange hadron collectivity in pPb and PbPb collisions. *JHEP*, 05:007, 2023. doi:10.1007/JHEP05(2023)007.
 111. K. Aamodt et al. Elliptic flow of charged particles in Pb–Pb collisions at 2.76 TeV. *Phys. Rev. Lett.*, 105:252302, 2010. doi:10.1103/PhysRevLett.105.252302.
 112. K. Aamodt et al. Higher harmonic anisotropic flow measurements of charged particles in Pb–Pb collisions at $\sqrt{s_{NN}} = 2.76$ TeV. *Phys. Rev. Lett.*, 107:032301, 2011. doi:10.1103/PhysRevLett.107.032301.
 113. Serguei Chatrchyan et al. Measurement of the elliptic anisotropy of charged particles produced in Pb–Pb collisions at $\sqrt{s_{NN}} = 2.76$ TeV. *Phys. Rev.*, C87(1):014902, 2013. doi:10.1103/PhysRevC.87.014902.
 114. Georges Aad et al. Measurement with the ATLAS detector of multi-particle azimuthal correlations in p–Pb collisions at $\sqrt{s_{NN}} = 5.02$ TeV. *Phys. Lett.*,

- B725:60–78, 2013. doi:10.1016/j.physletb.2013.06.057.
115. Serguei Chatrchyan et al. Measurement of higher-order harmonic azimuthal anisotropy in Pb–Pb collisions at $\sqrt{s_{\text{NN}}} = 2.76$ TeV. *Phys. Rev.*, C89(4):044906, 2014. doi:10.1103/PhysRevC.89.044906.
116. Serguei Chatrchyan et al. Multiplicity and transverse momentum dependence of two- and four-particle correlations in p–Pb and Pb–Pb collisions. *Phys. Lett.*, B724:213–240, 2013. doi:10.1016/j.physletb.2013.06.028.
117. Georges Aad et al. Measurement of flow harmonics with multi-particle cumulants in Pb–Pb collisions at $\sqrt{s_{\text{NN}}} = 2.76$ TeV with the ATLAS detector. *Eur. Phys. J.*, C74(11):3157, 2014. doi:10.1140/epjc/s10052-014-3157-z.
118. Betty Abelev et al. Multiparticle azimuthal correlations in p–Pb and Pb–Pb collisions at the CERN Large Hadron Collider. *Phys. Rev.*, C90(5):054901, 2014. doi:10.1103/PhysRevC.90.054901.
119. Vardan Khachatryan et al. Evidence for collective multiparticle correlations in p–Pb collisions. *Phys. Rev. Lett.*, 115(1):012301, 2015. doi:10.1103/PhysRevLett.115.012301.
120. Jaroslav Adam et al. Anisotropic flow of charged particles in Pb–Pb collisions at $\sqrt{s_{\text{NN}}} = 5.02$ TeV. *Phys. Rev. Lett.*, 116(13):132302, 2016. doi:10.1103/PhysRevLett.116.132302.
121. Morad Aaboud et al. Measurement of long-range multiparticle azimuthal correlations with the subevent cumulant method in pp and $p + Pb$ collisions with the ATLAS detector at the CERN Large Hadron Collider. *Phys. Rev.*, C97(2):024904, 2018. doi:10.1103/PhysRevC.97.024904.
122. A. M. Sirunyan et al. Azimuthal anisotropy of charged particles with transverse momentum up to 100 GeV/ c in PbPb collisions at $\sqrt{s_{\text{NN}}}=5.02$ TeV. *Phys. Lett.*, B776:195–216, 2018. doi:10.1016/j.physletb.2017.11.041.
123. Albert M Sirunyan et al. Multiparticle correlation studies in pPb collisions at $\sqrt{s_{\text{NN}}} = 8.16$ TeV. *Phys. Rev. C*, 101(1):014912, 2020. doi:10.1103/PhysRevC.101.014912.
124. Georges Aad et al. Measurement of event-plane correlations in $\sqrt{s_{\text{NN}}} = 2.76$ TeV lead-lead collisions with the ATLAS detector. *Phys. Rev.*, C90(2):024905, 2014. doi:10.1103/PhysRevC.90.024905.
125. Georges Aad et al. Measurement of the correlation between flow harmonics of different order in lead-lead collisions at $\sqrt{s_{\text{NN}}} = 2.76$ TeV with the ATLAS detector. *Phys. Rev.*, C92(3):034903, 2015. doi:10.1103/PhysRevC.92.034903.
126. Jaroslav Adam et al. Correlated event-by-event fluctuations of flow harmonics in Pb–Pb collisions at $\sqrt{s_{\text{NN}}} = 2.76$ TeV. *Phys. Rev. Lett.*, 117:182301, 2016. doi:10.1103/PhysRevLett.117.182301.
127. Shreyasi Acharya et al. Systematic studies of correlations between different order flow harmonics in Pb–Pb collisions at $\sqrt{s_{\text{NN}}} = 2.76$ TeV. *Phys. Rev.*, C97(2):024906, 2018. doi:10.1103/PhysRevC.97.024906.
128. Morad Aaboud et al. Correlated long-range mixed-harmonic fluctuations measured in pp , $p+Pb$ and low-multiplicity Pb+Pb collisions with the ATLAS de-

- tector. *Phys. Lett.*, B789:444–471, 2019. doi:10.1016/j.physletb.2018.11.065.
129. Albert M Sirunyan et al. Correlations of azimuthal anisotropy Fourier harmonics with subevent cumulants in pPb collisions at $\sqrt{s_{NN}}=8.16\text{TeV}$. *Phys. Rev. C*, 103(1):014902, 2021. doi:10.1103/PhysRevC.103.014902.
 130. Bassam Aboona et al. Beam energy dependence of the linear and mode-coupled flow harmonics in Au+Au collisions. *Phys. Lett. B*, 839:137755, 2023. doi:10.1016/j.physletb.2023.137755.
 131. Shreyasi Acharya et al. Linear and non-linear flow modes in Pb-Pb collisions at $\sqrt{s_{NN}} = 2.76$ TeV. *Phys. Lett.*, B773:68–80, 2017. doi:10.1016/j.physletb.2017.07.060.
 132. Albert M Sirunyan et al. Mixed higher-order anisotropic flow and nonlinear response coefficients of charged particles in PbPb collisions at $\sqrt{s_{NN}} = 2.76$ and 5.02 TeV. *Eur. Phys. J. C*, 80(6):534, 2020. doi:10.1140/epjc/s10052-020-7834-9.
 133. Vardan Khachatryan et al. Evidence for transverse momentum and pseudorapidity dependent event plane fluctuations in Pb–Pb and p–Pb collisions. *Phys. Rev.*, C92(3):034911, 2015. doi:10.1103/PhysRevC.92.034911.
 134. Morad Aaboud et al. Measurement of longitudinal flow decorrelations in Pb+Pb collisions at $\sqrt{s_{NN}} = 2.76$ and 5.02 TeV with the ATLAS detector. *Eur. Phys. J.*, C78(2):142, 2018. doi:10.1140/epjc/s10052-018-5605-7.
 135. A. M. Sirunyan et al. Principal-component analysis of two-particle azimuthal correlations in PbPb and pPb collisions at CMS. *Phys. Rev.*, C96(6):064902, 2017. doi:10.1103/PhysRevC.96.064902.
 136. Georges Aad et al. Longitudinal Flow Decorrelations in Xe+Xe Collisions at $\sqrt{s_{NN}} = 5.44$ TeV with the ATLAS Detector. *Phys. Rev. Lett.*, 126(12):122301, 2021. doi:10.1103/PhysRevLett.126.122301.
 137. Shreyasi Acharya et al. Observation of flow angle and flow magnitude fluctuations in Pb-Pb collisions at $\sqrt{s_{NN}} = 5.02$ TeV at the CERN Large Hadron Collider. *Phys. Rev. C*, 107(5):L051901, 2023. doi:10.1103/PhysRevC.107.L051901.
 138. Georges Aad et al. Measurement of the distributions of event-by-event flow harmonics in lead-lead collisions at $\sqrt{s_{NN}} = 2.76$ TeV with the ATLAS detector at the LHC. *JHEP*, 11:183, 2013. doi:10.1007/JHEP11(2013)183.
 139. Albert M Sirunyan et al. Non-Gaussian elliptic-flow fluctuations in PbPb collisions at $\sqrt{s_{NN}} = 5.02$ TeV. *Phys. Lett.*, B789:643–665, 2019. doi:10.1016/j.physletb.2018.11.063.
 140. S. Acharya et al. Energy dependence and fluctuations of anisotropic flow in Pb-Pb collisions at $\sqrt{s_{NN}} = 5.02$ and 2.76 TeV. *JHEP*, 07:103, 2018. doi:10.1007/JHEP07(2018)103.
 141. Georges Aad et al. Measurement of flow harmonics correlations with mean transverse momentum in lead-lead and proton-lead collisions at $\sqrt{s_{NN}} = 5.02$ TeV with the ATLAS detector. *Eur. Phys. J. C*, 79(12):985, 2019. doi:10.1140/epjc/s10052-019-7489-6.

142. Shreyasi Acharya et al. Characterizing the initial conditions of heavy-ion collisions at the LHC with mean transverse momentum and anisotropic flow correlations. *Phys. Lett. B*, 834:137393, 2022. doi:10.1016/j.physletb.2022.137393.
143. Betty Abelev et al. Directed flow of charged particles at midrapidity relative to the spectator plane in Pb–Pb collisions at $\sqrt{s_{NN}} = 2.76$ TeV. *Phys. Rev. Lett.*, 111(23):232302, 2013. doi:10.1103/PhysRevLett.111.232302.
144. Betty Abelev et al. Charge correlations using the balance function in Pb-Pb collisions at $\sqrt{s_{NN}} = 2.76$ TeV. *Phys. Lett.*, B723:267–279, 2013. doi:10.1016/j.physletb.2013.05.039.
145. Jaroslav Adam et al. Multiplicity and transverse momentum evolution of charge-dependent correlations in pp, p-Pb, and Pb-Pb collisions at the LHC. *Eur. Phys. J.*, C76(2):86, 2016. doi:10.1140/epjc/s10052-016-3915-1.
146. Jaroslav Adam et al. Charge-dependent flow and the search for the chiral magnetic wave in Pb-Pb collisions at $\sqrt{s_{NN}} = 2.76$ TeV. *Phys. Rev.*, C93(4):044903, 2016. doi:10.1103/PhysRevC.93.044903.
147. Vardan Khachatryan et al. Observation of charge-dependent azimuthal correlations in p -Pb collisions and its implication for the search for the chiral magnetic effect. *Phys. Rev. Lett.*, 118(12):122301, 2017. doi:10.1103/PhysRevLett.118.122301.
148. Shreyasi Acharya et al. Constraining the magnitude of the Chiral Magnetic Effect with Event Shape Engineering in Pb-Pb collisions at $\sqrt{s_{NN}} = 2.76$ TeV. *Phys. Lett.*, B777:151–162, 2018. doi:10.1016/j.physletb.2017.12.021.
149. Albert M Sirunyan et al. Probing the chiral magnetic wave in pPb and PbPb collisions at $\sqrt{s_{NN}} = 5.02$ TeV using charge-dependent azimuthal anisotropies. *Phys. Rev. C*, 100(6):064908, 2019. doi:10.1103/PhysRevC.100.064908.
150. Albert M Sirunyan et al. Constraints on the chiral magnetic effect using charge-dependent azimuthal correlations in pPb and PbPb collisions at the CERN Large Hadron Collider. *Phys. Rev.*, C97(4):044912, 2018. doi:10.1103/PhysRevC.97.044912.
151. Betty Abelev et al. Pion, kaon, and proton production in central PbPb collisions at $\sqrt{s_{NN}} = 2.76$ TeV. *Phys. Rev. Lett.*, 109:252301, 2012. doi:10.1103/PhysRevLett.109.252301.
152. Serguei Chatrchyan et al. Study of the inclusive production of charged pions, kaons, and protons in pp collisions at $\sqrt{s} = 0.9, 2.76,$ and 7 TeV. *Eur. Phys. J.*, C72:2164, 2012. doi:10.1140/epjc/s10052-012-2164-1.
153. Betty Abelev et al. Multiplicity dependence of pion, kaon, proton and Λ production in pPb collisions at $\sqrt{s_{NN}} = 5.02$ TeV. *Phys. Lett.*, B728:25–38, 2014. doi:10.1016/j.physletb.2013.11.020.
154. Betty Abelev et al. Centrality dependence of π, K, p production in PbPb collisions at $\sqrt{s_{NN}} = 2.76$ TeV. *Phys. Rev.*, C88:044910, 2013. doi:10.1103/PhysRevC.88.044910.
155. Serguei Chatrchyan et al. Study of the production of charged pions, kaons, and protons in pPb collisions at $\sqrt{s_{NN}} = 5.02$ TeV. *Eur. Phys. J.*, C74(6):

- 2847, 2014. doi:10.1140/epjc/s10052-014-2847-x.
156. C. Andrei. Light flavor hadron spectra at low p_T and search for collective phenomena in high multiplicity pp, p-Pb and Pb-Pb collisions measured with the ALICE experiment. *Nucl. Phys.*, A931:888–892, 2014. doi:10.1016/j.nuclphysa.2014.08.002.
 157. Jaroslav Adam et al. Multi-strange baryon production in p-Pb collisions at $\sqrt{s_{NN}} = 5.02$ TeV. *Phys. Lett.*, B758:389–401, 2016. doi:10.1016/j.physletb.2016.05.027.
 158. Jaroslav Adam et al. Production of $K^*(892)^0$ and $\phi(1020)$ in pPb collisions at $\sqrt{s_{NN}} = 5.02$ TeV. *Eur. Phys. J.*, C76(5):245, 2016. doi:10.1140/epjc/s10052-016-4088-7.
 159. Shreyasi Acharya et al. Measurement of deuteron spectra and elliptic flow in PbPb collisions at $\sqrt{s_{NN}} = 2.76$ TeV at the LHC. *Eur. Phys. J.*, C77(10):658, 2017. doi:10.1140/epjc/s10052-017-5222-x.
 160. Jaroslav Adam et al. $K^*(892)^0$ and $\phi(1020)$ meson production at high transverse momentum in pp and Pb-Pb collisions at $\sqrt{s_{NN}} = 2.76$ TeV. *Phys. Rev.*, C95(6):064606, 2017. doi:10.1103/PhysRevC.95.064606.
 161. Shreyasi Acharya et al. Production of charged pions, kaons, and (anti-)protons in Pb-Pb and inelastic pp collisions at $\sqrt{s_{NN}} = 5.02$ TeV. *Phys. Rev. C*, 101(4):044907, 2020. doi:10.1103/PhysRevC.101.044907.
 162. Betty Abelev et al. K_S^0 and Λ production in PbPb collisions at $\sqrt{s_{NN}} = 2.76$ TeV. *Phys. Rev. Lett.*, 111:222301, 2013. doi:10.1103/PhysRevLett.111.222301.
 163. Betty Bezverkhny Abelev et al. $K^*(892)^0$ and $\phi(1020)$ production in PbPb collisions at $\sqrt{s_{NN}} = 2.76$ TeV. *Phys. Rev.*, C91:024609, 2015. doi:10.1103/PhysRevC.91.024609.
 164. Jaroslav Adam et al. ϕ -meson production at forward rapidity in p-Pb collisions at $\sqrt{s_{NN}} = 5.02$ TeV and in pp collisions at $\sqrt{s} = 2.76$ TeV. *Phys. Lett.*, B768:203–217, 2017. doi:10.1016/j.physletb.2017.01.074.
 165. Jaroslav Adam et al. Multiplicity dependence of charged pion, kaon, and (anti)proton production at large transverse momentum in p-Pb collisions at $\sqrt{s_{NN}} = 5.02$ TeV. *Phys. Lett.*, B760:720–735, 2016. doi:10.1016/j.physletb.2016.07.050.
 166. Vardan Khachatryan et al. Multiplicity and rapidity dependence of strange hadron production in pp, pPb, and PbPb collisions at the LHC. *Phys. Lett.*, B768:103–129, 2017. doi:10.1016/j.physletb.2017.01.075.
 167. Betty Bezverkhny Abelev et al. Multi-strange baryon production at mid-rapidity in PbPb collisions at $\sqrt{s_{NN}} = 2.76$ TeV. *Phys. Lett.*, B728:216–227, 2014. doi:10.1016/j.physletb.2014.05.052, 10.1016/j.physletb.2013.11.048.
 168. Jaroslav Adam et al. Enhanced production of multi-strange hadrons in high-multiplicity proton-proton collisions. *Nature Phys.*, 13:535–539, 2017. doi:10.1038/nphys4111.
 169. Shreyasi Acharya et al. Multiplicity dependence of π , K, and p produc-

- tion in pp collisions at $\sqrt{s} = 13$ TeV. *Eur. Phys. J. C*, 80(8):693, 2020. doi:10.1140/epjc/s10052-020-8125-1.
170. Shreyasi Acharya et al. Production of pions, kaons, (anti-)protons and ϕ mesons in Xe–Xe collisions at $\sqrt{s_{NN}} = 5.44$ TeV. *Eur. Phys. J. C*, 81(7):584, 2021. doi:10.1140/epjc/s10052-021-09304-4.
171. Shreyasi Acharya et al. The ALICE experiment – A journey through QCD. 11 2022. doi:10.48550/arXiv.2211.04384.
172. K. Aamodt et al. Femtoscopy of pp collisions at $\sqrt{s} = 0.9$ and 7 TeV at the LHC with two-pion Bose-Einstein correlations. *Phys. Rev.*, D84:112004, 2011. doi:10.1103/PhysRevD.84.112004.
173. Betty Abelev et al. Freeze-out radii extracted from three-pion cumulants in pp, pPb and PbPb collisions at the LHC. *Phys. Lett.*, B739:139–151, 2014. doi:10.1016/j.physletb.2014.10.034.
174. J. Adam et al. Two-pion femtoscopy in pPb collisions at $\sqrt{s_{NN}} = 5.02$ TeV. *Phys. Rev.*, C91:034906, 2015. doi:10.1103/PhysRevC.91.034906.
175. Jaroslav Adam et al. One-dimensional pion, kaon, and proton femtoscopy in PbPb collisions at $\sqrt{s_{NN}} = 2.76$ TeV. *Phys. Rev.*, C92(5):054908, 2015. doi:10.1103/PhysRevC.92.054908.
176. Jaroslav Adam et al. Centrality dependence of pion freeze-out radii in Pb-Pb collisions at $\sqrt{s_{NN}} = 2.76$ TeV. *Phys. Rev.*, C93(2):024905, 2016. doi:10.1103/PhysRevC.93.024905.
177. Morad Aaboud et al. Femtoscopy with identified charged pions in proton-lead collisions at $\sqrt{s_{NN}} = 5.02$ TeV with ATLAS. *Phys. Rev.*, C96(6):064908, 2017. doi:10.1103/PhysRevC.96.064908.
178. Shreyasi Acharya et al. Kaon femtoscopy in Pb-Pb collisions at $\sqrt{s_{NN}} = 2.76$ TeV. *Phys. Rev.*, C96(6):064613, 2017. doi:10.1103/PhysRevC.96.064613.
179. K_S^0 and $\Lambda(\bar{\Lambda})$ two-particle femtoscopic correlations in PbPb collisions at $\sqrt{s_{NN}} = 5.02$ TeV. 1 2023. doi:10.48550/arXiv.2301.05290.
180. Armen Tumasyan et al. Two-particle Bose-Einstein correlations and their Lévy parameters in PbPb collisions at $\sqrt{s_{NN}} = 5.02$ TeV. *Phys. Rev. C*, 109(2):024914, 2024. doi:10.1103/PhysRevC.109.024914.
181. Jaroslav Adam et al. Direct photon production in Pb-Pb collisions at $\sqrt{s_{NN}} = 2.76$ TeV. *Phys. Lett.*, B754:235–248, 2016. doi:10.1016/j.physletb.2016.01.020.
182. Shreyasi Acharya et al. Direct photon production at low transverse momentum in proton-proton collisions at $\sqrt{s} = 2.76$ and 8 TeV. *Phys. Rev.*, C99(2):024912, 2019. doi:10.1103/PhysRevC.99.024912.
183. Shreyasi Acharya et al. Dielectron production in central Pb–Pb collisions at $\sqrt{s_{NN}} = 5.02$ TeV. 8 2023. doi:10.48550/arXiv.2308.16704.
184. Georges Aad et al. Transverse momentum and process dependent azimuthal anisotropies in $\sqrt{s_{NN}} = 8.16$ TeV p+Pb collisions with the ATLAS detector. *Eur. Phys. J. C*, 80(1):73, 2020. doi:10.1140/epjc/s10052-020-7624-4.
185. Morad Aaboud et al. Measurement of long-range two-particle azimuthal correlations in Z-boson tagged pp collisions at $\sqrt{s}=8$ and 13 TeV. *Eur. Phys. J.*

- C*, 80(1):64, 2020. doi:10.1140/epjc/s10052-020-7606-6.
186. Georges Aad et al. Measurement of the Sensitivity of Two-Particle Correlations in pp Collisions to the Presence of Hard Scatterings. *Phys. Rev. Lett.*, 131(16): 162301, 2023. doi:10.1103/PhysRevLett.131.162301.
 187. Shreyasi Acharya et al. Azimuthal anisotropy of jet particles in p-Pb and Pb-Pb collisions at $\sqrt{s_{\text{NN}}} = 5.02$ TeV. 12 2022. doi:10.48550/arXiv.2212.12609.
 188. Aram Hayrapetyan et al. Observation of enhanced long-range elliptic anisotropies inside high-multiplicity jets in pp collisions at $\sqrt{s} = 13$ TeV. 12 2023. doi:10.48550/arXiv.2312.17103.
 189. K. Aamodt et al. Suppression of charged particle production at large transverse momentum in central Pb–Pb collisions at $\sqrt{s_{\text{NN}}} = 2.76$ TeV. *Phys. Lett.*, B696: 30–39, 2011. doi:10.1016/j.physletb.2010.12.020.
 190. Betty Abelev et al. Suppression of high transverse momentum D mesons in central Pb–Pb collisions at $\sqrt{s_{\text{NN}}} = 2.76$ TeV. *JHEP*, 09:112, 2012. doi:10.1007/JHEP09(2012)112.
 191. Betty Abelev et al. Centrality dependence of charged particle production at large transverse momentum in Pb–Pb collisions at $\sqrt{s_{\text{NN}}} = 2.76$ TeV. *Phys. Lett.*, B720:52–62, 2013. doi:10.1016/j.physletb.2013.01.051.
 192. Serguei Chatrchyan et al. Study of high- p_{T} charged particle suppression in Pb–Pb compared to pp collisions at $\sqrt{s_{\text{NN}}} = 2.76$ TeV. *Eur. Phys. J.*, C72: 1945, 2012. doi:10.1140/epjc/s10052-012-1945-x.
 193. Georges Aad et al. Centrality and rapidity dependence of inclusive jet production in $\sqrt{s_{\text{NN}}} = 5.02$ TeV proton-lead collisions with the ATLAS detector. *Phys. Lett.*, B748:392–413, 2015. doi:10.1016/j.physletb.2015.07.023.
 194. Georges Aad et al. Measurements of the nuclear modification factor for jets in Pb–Pb collisions at $\sqrt{s_{\text{NN}}} = 2.76$ TeV with the ATLAS Detector. *Phys. Rev. Lett.*, 114(7):072302, 2015. doi:10.1103/PhysRevLett.114.072302.
 195. Georges Aad et al. Measurement of charged-particle spectra in Pb–Pb collisions at $\sqrt{s_{\text{NN}}} = 2.76$ TeV with the ATLAS detector at the LHC. *JHEP*, 09: 050, 2015. doi:10.1007/JHEP09(2015)050.
 196. Jaroslav Adam et al. Measurement of jet suppression in central Pb–Pb collisions at $\sqrt{s_{\text{NN}}} = 2.76$ TeV. *Phys. Lett.*, B746:1–14, 2015. doi:10.1016/j.physletb.2015.04.039.
 197. Vardan Khachatryan et al. Nuclear Effects on the Transverse Momentum Spectra of Charged Particles in pPb Collisions at $\sqrt{s_{\text{NN}}} = 5.02$ TeV. *Eur. Phys. J.*, C75(5):237, 2015. doi:10.1140/epjc/s10052-015-3435-4.
 198. Jaroslav Adam et al. Centrality dependence of charged jet production in p-Pb collisions at $\sqrt{s_{\text{NN}}} = 5.02$ TeV. *Eur. Phys. J.*, C76(5):271, 2016. doi:10.1140/epjc/s10052-016-4107-8.
 199. Albert M Sirunyan et al. Measurements of the charm jet cross section and nuclear modification factor in pPb collisions at $\sqrt{s_{\text{NN}}} = 5.02$ TeV. *Phys. Lett.*, B772:306–329, 2017. doi:10.1016/j.physletb.2017.06.053.
 200. Shreyasi Acharya et al. Transverse momentum spectra and nuclear modifi-

- cation factors of charged particles in Xe-Xe collisions at $\sqrt{s_{\text{NN}}} = 5.44$ TeV. *Phys. Lett. B*, 788:166–179, 2019. doi:10.1016/j.physletb.2018.10.052.
201. S. Acharya et al. Transverse momentum spectra and nuclear modification factors of charged particles in pp, p-Pb and Pb-Pb collisions at the LHC. *JHEP*, 11:013, 2018. doi:10.1007/JHEP11(2018)013.
202. Albert M Sirunyan et al. Charged-particle nuclear modification factors in XeXe collisions at $\sqrt{s_{\text{NN}}} = 5.44$ TeV. *JHEP*, 10:138, 2018. doi:10.1007/JHEP10(2018)138.
203. Georges Aad et al. Charged-hadron production in pp , $p+\text{Pb}$, $\text{Pb}+\text{Pb}$, and $\text{Xe}+\text{Xe}$ collisions at $\sqrt{s_{\text{NN}}} = 5$ TeV with the ATLAS detector at the LHC. *JHEP*, 07:074, 2023. doi:10.1007/JHEP07(2023)074.
204. Georges Aad et al. Comparison of inclusive and photon-tagged jet suppression in 5.02 TeV $\text{Pb}+\text{Pb}$ collisions with ATLAS. *Phys. Lett. B*, 846:138154, 2023. doi:10.1016/j.physletb.2023.138154.
205. Georges Aad et al. Observation of a centrality-dependent dijet asymmetry in lead-lead collisions at $\sqrt{s_{\text{NN}}} = 2.76$ TeV with the ATLAS Detector at the LHC. *Phys. Rev. Lett.*, 105:252303, 2010. doi:10.1103/PhysRevLett.105.252303.
206. Serguei Chatrchyan et al. Observation and studies of jet quenching in $\text{Pb}-\text{Pb}$ collisions at nucleon-nucleon center-of-mass energy = 2.76 TeV. *Phys. Rev.*, C84:024906, 2011. doi:10.1103/PhysRevC.84.024906.
207. Serguei Chatrchyan et al. Studies of dijet transverse momentum balance and pseudorapidity distributions in pPb collisions at $\sqrt{s_{\text{NN}}} = 5.02$ TeV. *Eur. Phys. J.*, C74(7):2951, 2014. doi:10.1140/epjc/s10052-014-2951-y.
208. Vardan Khachatryan et al. Decomposing transverse momentum balance contributions for quenched jets in PbPb collisions at $\sqrt{s_{\text{NN}}} = 2.76$ TeV. *JHEP*, 11:055, 2016. doi:10.1007/JHEP11(2016)055.
209. Albert M Sirunyan et al. Measurement of the Splitting Function in pp and $\text{Pb}-\text{Pb}$ Collisions at $\sqrt{s_{\text{NN}}} = 5.02$ TeV. *Phys. Rev. Lett.*, 120(14):142302, 2018. doi:10.1103/PhysRevLett.120.142302.
210. Albert M Sirunyan et al. Comparing transverse momentum balance of b jet pairs in pp and PbPb collisions at $\sqrt{s_{\text{NN}}} = 5.02$ TeV. *JHEP*, 03:181, 2018. doi:10.1007/JHEP03(2018)181.
211. Albert M Sirunyan et al. In-medium modification of dijets in PbPb collisions at $\sqrt{s_{\text{NN}}} = 5.02$ TeV. *JHEP*, 05:116, 2021. doi:10.1007/JHEP05(2021)116.
212. G. Aad et al. Measurements of the suppression and correlations of dijets in $\text{Xe}+\text{Xe}$ collisions at $\sqrt{s_{\text{NN}}} = 5.44$ TeV. *Phys. Rev. C*, 108(2):024906, 2023. doi:10.1103/PhysRevC.108.024906.
213. Jaroslav Adam et al. Measurement of jet quenching with semi-inclusive hadron-jet distributions in central $\text{Pb}-\text{Pb}$ collisions at $\sqrt{s_{\text{NN}}} = 2.76$ TeV. *JHEP*, 09:170, 2015. doi:10.1007/JHEP09(2015)170.
214. Jaroslav Adam et al. Jet-like correlations with neutral pion triggers in pp and central $\text{Pb}+\text{Pb}$ collisions at 2.76 TeV. *Phys. Lett.*, B763:238–250, 2016. doi:10.1016/j.physletb.2016.10.048.

215. Morad Aaboud et al. Measurement of jet p_T correlations in Pb+Pb and pp collisions at $\sqrt{s_{NN}} = 2.76$ TeV with the ATLAS detector. *Phys. Lett.*, B774: 379–402, 2017. doi:10.1016/j.physletb.2017.09.078.
216. Shreyasi Acharya et al. Constraints on jet quenching in p-Pb collisions at $\sqrt{s_{NN}} = 5.02$ TeV measured by the event-activity dependence of semi-inclusive hadron-jet distributions. *Phys. Lett.*, B783:95–113, 2018. doi:10.1016/j.physletb.2018.05.059.
217. Albert M Sirunyan et al. Study of jet quenching with isolated-photon+jet correlations in PbPb and pp collisions at $\sqrt{s_{NN}} = 5.02$ TeV. *Phys. Lett. B*, 785:14–39, 2018. doi:10.1016/j.physletb.2018.07.061.
218. Albert M Sirunyan et al. Study of Jet Quenching with Z + jet Correlations in Pb-Pb and pp Collisions at $\sqrt{s_{NN}} = 5.02$ TeV. *Phys. Rev. Lett.*, 119(8): 082301, 2017. doi:10.1103/PhysRevLett.119.082301.
219. Albert M Sirunyan et al. Jet properties in PbPb and pp collisions at $\sqrt{s_{NN}} = 5.02$ TeV. *JHEP*, 05:006, 2018. doi:10.1007/JHEP05(2018)006.
220. Albert M Sirunyan et al. Observation of medium induced modifications of jet fragmentation in PbPb collisions using isolated-photon-tagged jets. *Phys. Rev. Lett.*, 121:242301, 2018. doi:10.1103/PhysRevLett.121.242301.
221. Georges Aad et al. Strong Constraints on Jet Quenching in Centrality-Dependent p+Pb Collisions at 5.02 TeV from ATLAS. *Phys. Rev. Lett.*, 131(7):072301, 2023. doi:10.1103/PhysRevLett.131.072301.
222. Georges Aad et al. Measurements of the suppression and correlations of dijets in Pb+Pb collisions at $\sqrt{s_{NN}} = 5.02$ TeV. *Phys. Rev. C*, 107(5):054908, 2023. doi:10.1103/PhysRevC.107.054908.
223. Serguei Chatrchyan et al. Azimuthal Anisotropy of Charged Particles at High Transverse Momenta in PbPb Collisions at $\sqrt{s_{NN}} = 2.76$ TeV. *Phys. Rev. Lett.*, 109:022301, 2012. doi:10.1103/PhysRevLett.109.022301.
224. Georges Aad et al. Measurements of azimuthal anisotropies of jet production in Pb+Pb collisions at $\sqrt{s_{NN}} = 5.02$ TeV with the ATLAS detector. *Phys. Rev. C*, 105(6):064903, 2022. doi:10.1103/PhysRevC.105.064903.
225. Armen Tumasyan et al. Azimuthal anisotropy of dijet events in PbPb collisions at $\sqrt{s_{NN}} = 5.02$ TeV. *JHEP*, 07:139, 2023. doi:10.1007/JHEP07(2023)139.
226. Ehab Abbas et al. J/ψ elliptic flow in Pb–Pb collisions at $\sqrt{s_{NN}} = 2.76$ TeV. *Phys. Rev. Lett.*, 111:162301, 2013. doi:10.1103/PhysRevLett.111.162301.
227. B. Abelev et al. D meson elliptic flow in non-central Pb–Pb collisions at $\sqrt{s_{NN}} = 2.76$ TeV. *Phys. Rev. Lett.*, 111:102301, 2013. doi:10.1103/PhysRevLett.111.102301.
228. Betty Bezverkhny Abelev et al. Azimuthal anisotropy of D meson production in Pb–Pb collisions at $\sqrt{s_{NN}} = 2.76$ TeV. *Phys. Rev.*, C90(3):034904, 2014. doi:10.1103/PhysRevC.90.034904.
229. Jaroslav Adam et al. Elliptic flow of muons from heavy-flavour hadron decays at forward rapidity in Pb–Pb collisions at $\sqrt{s_{NN}} = 2.76$ TeV. *Phys. Lett.*, B753:41–56, 2016. doi:10.1016/j.physletb.2015.11.059.

230. Jaroslav Adam et al. Measurement of azimuthal correlations of D mesons and charged particles in pp collisions at $\sqrt{s} = 7$ TeV and p-Pb collisions at $\sqrt{s_{NN}} = 5.02$ TeV. *Eur. Phys. J.*, C77(4):245, 2017. doi:10.1140/epjc/s10052-017-4779-8.
231. Jaroslav Adam et al. Elliptic flow of electrons from heavy-flavour hadron decays at mid-rapidity in Pb-Pb collisions at $\sqrt{s_{NN}} = 2.76$ TeV. *JHEP*, 09:028, 2016. doi:10.1007/JHEP09(2016)028.
232. Vardan Khachatryan et al. Suppression and azimuthal anisotropy of prompt and nonprompt J/ψ production in PbPb collisions at $\sqrt{s_{NN}} = 2.76$ TeV. *Eur. Phys. J.*, C77(4):252, 2017. doi:10.1140/epjc/s10052-017-4781-1.
233. Shreyasi Acharya et al. D -meson azimuthal anisotropy in midcentral Pb-Pb collisions at $\sqrt{s_{NN}} = 5.02$ TeV. *Phys. Rev. Lett.*, 120(10):102301, 2018. doi:10.1103/PhysRevLett.120.102301.
234. S. Acharya et al. Search for collectivity with azimuthal J/ψ -hadron correlations in high multiplicity p-Pb collisions at $\sqrt{s_{NN}} = 5.02$ and 8.16 TeV. *Phys. Lett.*, B780:7–20, 2018. doi:10.1016/j.physletb.2018.02.039.
235. Shreyasi Acharya et al. J/ψ elliptic flow in Pb-Pb collisions at $\sqrt{s_{NN}} = 5.02$ TeV. *Phys. Rev. Lett.*, 119(24):242301, 2017. doi:10.1103/PhysRevLett.119.242301.
236. Albert M Sirunyan et al. Measurement of prompt D^0 meson azimuthal anisotropy in Pb-Pb collisions at $\sqrt{s_{NN}} = 5.02$ TeV. *Phys. Rev. Lett.*, 120(20):202301, 2018. doi:10.1103/PhysRevLett.120.202301.
237. Shreyasi Acharya et al. Azimuthal Anisotropy of Heavy-Flavor Decay Electrons in p-Pb Collisions at $\sqrt{s_{NN}} = 5.02$ TeV. *Phys. Rev. Lett.*, 122(7):072301, 2019. doi:10.1103/PhysRevLett.122.072301.
238. Shreyasi Acharya et al. J/ψ elliptic and triangular flow in Pb-Pb collisions at $\sqrt{s_{NN}} = 5.02$ TeV. *JHEP*, 10:141, 2020. doi:10.1007/JHEP10(2020)141.
239. Georges Aad et al. Measurement of azimuthal anisotropy of muons from charm and bottom hadrons in Pb+Pb collisions at $\sqrt{s_{NN}} = 5.02$ TeV with the ATLAS detector. *Phys. Lett. B*, 807:135595, 2020. doi:10.1016/j.physletb.2020.135595.
240. Albert M Sirunyan et al. Studies of charm and beauty hadron long-range correlations in pp and pPb collisions at LHC energies. *Phys. Lett. B*, 813:136036, 2021. doi:10.1016/j.physletb.2020.136036.
241. Armen Tumasyan et al. Probing Charm Quark Dynamics via Multiparticle Correlations in Pb-Pb Collisions at $\sqrt{s_{NN}} = 5.02$ TeV. *Phys. Rev. Lett.*, 129(2):022001, 2022. doi:10.1103/PhysRevLett.129.022001.
242. Shreyasi Acharya et al. Measurements of azimuthal anisotropies at forward and backward rapidity with muons in high-multiplicity p-Pb collisions at $\sqrt{s_{NN}} = 8.16$ TeV. *Phys. Lett. B*, 846:137782, 2023. doi:10.1016/j.physletb.2023.137782.
243. Armen Tumasyan et al. Measurements of azimuthal anisotropy of nonprompt D^0 mesons in PbPb collisions at $\sqrt{s_{NN}} = 5.02$ TeV. *Phys. Lett. B*, 850:138389, 2024. doi:10.1016/j.physletb.2023.138389.

244. Armen Tumasyan et al. Measurements of the azimuthal anisotropy of prompt and nonprompt charmonia in PbPb collisions at $\sqrt{s_{\text{NN}}} = 5.02$ TeV. *JHEP*, 10:115, 2023. doi:10.1007/JHEP10(2023)115.
245. Armen Tumasyan et al. Study of azimuthal anisotropy of $\Upsilon(1S)$ mesons in pPb collisions at $\sqrt{s_{\text{NN}}} = 8.16$ TeV. *Phys. Lett. B*, 850:138518, 2024. doi:10.1016/j.physletb.2024.138518.
246. Shreyasi Acharya et al. Measurement of $\Upsilon(1S)$ elliptic flow at forward rapidity in Pb-Pb collisions at $\sqrt{s_{\text{NN}}} = 5.02$ TeV. *Phys. Rev. Lett.*, 123(19):192301, 2019. doi:10.1103/PhysRevLett.123.192301.
247. Georges Aad et al. Measurement of azimuthal anisotropy of muons from charm and bottom hadrons in pp collisions at $\sqrt{s} = 13$ TeV with the ATLAS detector. *Phys. Rev. Lett.*, 124(8):082301, 2020. doi:10.1103/PhysRevLett.124.082301.
248. Albert M Sirunyan et al. Measurement of the azimuthal anisotropy of $\Upsilon(1S)$ and $\Upsilon(2S)$ mesons in PbPb collisions at $\sqrt{s_{\text{NN}}} = 5.02$ TeV. *Phys. Lett. B*, 819:136385, 2021. doi:10.1016/j.physletb.2021.136385.
249. Betty Abelev et al. J/ψ suppression at forward rapidity in PbPb collisions at $\sqrt{s_{\text{NN}}} = 2.76$ TeV. *Phys. Rev. Lett.*, 109:072301, 2012. doi:10.1103/PhysRevLett.109.072301.
250. Serguei Chatrchyan et al. Suppression of Non-Prompt J/ψ , Prompt J/ψ , and $Y(1S)$ in PbPb Collisions at $\sqrt{s_{\text{NN}}} = 2.76$ TeV. *JHEP*, 05:063, 2012. doi:10.1007/JHEP05(2012)063.
251. Serguei Chatrchyan et al. Observation of sequential Upsilon suppression in PbPb collisions. *Phys. Rev. Lett.*, 109:222301, 2012. doi:10.1103/PhysRevLett.109.222301.
252. Betty Bezverkhny Abelev et al. J/ψ production and nuclear effects in p-Pb collisions at $\sqrt{s_{\text{NN}}} = 5.02$ TeV. *JHEP*, 02:073, 2014. doi:10.1007/JHEP02(2014)073.
253. Serguei Chatrchyan et al. Event activity dependence of $Y(nS)$ production in $\sqrt{s_{\text{NN}}} = 5.02$ TeV pPb and $\sqrt{s} = 2.76$ TeV pp collisions. *JHEP*, 04:103, 2014. doi:10.1007/JHEP04(2014)103.
254. Betty Bezverkhny Abelev et al. Production of inclusive $\Upsilon(1S)$ and $\Upsilon(2S)$ in p-Pb collisions at $\sqrt{s_{\text{NN}}} = 5.02$ TeV. *Phys. Lett. B*, 740:105–117, 2015. doi:10.1016/j.physletb.2014.11.041.
255. Betty Bezverkhny Abelev et al. Suppression of $\psi(2S)$ production in pPb collisions at $\sqrt{s_{\text{NN}}} = 5.02$ TeV. *JHEP*, 12:073, 2014. doi:10.1007/JHEP12(2014)073.
256. Jaroslav Adam et al. Rapidity and transverse-momentum dependence of the inclusive J/ψ nuclear modification factor in p-Pb collisions at $\sqrt{s_{\text{NN}}} = 5.02$ TeV. *JHEP*, 06:055, 2015. doi:10.1007/JHEP06(2015)055.
257. Jaroslav Adam et al. Differential studies of inclusive J/Ψ and $\Psi(2S)$ production at forward rapidity in Pb-Pb collisions at $\sqrt{s_{\text{NN}}} = 2.76$ TeV. *JHEP*, 05:179, 2016. doi:10.1007/JHEP05(2016)179.
258. Jaroslav Adam et al. Centrality dependence of inclusive J/ψ produc-

- tion in pPb collisions at $\sqrt{s_{\text{NN}}} = 5.02$ TeV. *JHEP*, 11:127, 2015. doi:10.1007/JHEP11(2015)127.
259. Jaroslav Adam et al. Inclusive, prompt and non-prompt J/ψ production at mid-rapidity in PbPb collisions at $\sqrt{s_{\text{NN}}} = 2.76$ TeV. *JHEP*, 07:051, 2015. doi:10.1007/JHEP07(2015)051.
260. Jaroslav Adam et al. Centrality dependence of $\psi(2S)$ suppression in p-Pb collisions at $\sqrt{s_{\text{NN}}} = 5.02$ TeV. *JHEP*, 06:050, 2016. doi:10.1007/JHEP06(2016)050.
261. Jaroslav Adam et al. J/ψ suppression at forward rapidity in Pb-Pb collisions at $\sqrt{s_{\text{NN}}} = 5.02$ TeV. *Phys. Lett.*, B766:212–224, 2017. doi:10.1016/j.physletb.2016.12.064.
262. Vardan Khachatryan et al. Suppression of $\Upsilon(1S)$, $\Upsilon(2S)$ and $\Upsilon(3S)$ production in PbPb collisions at $\sqrt{s_{\text{NN}}} = 2.76$ TeV. *Phys. Lett.*, B770:357–379, 2017. doi:10.1016/j.physletb.2017.04.031.
263. Albert M Sirunyan et al. Relative Modification of Prompt $\psi(2S)$ and J/ψ Yields from pp to PbPb Collisions at $\sqrt{s_{\text{NN}}} = 5.02$ TeV. *Phys. Rev. Lett.*, 118(16):162301, 2017. doi:10.1103/PhysRevLett.118.162301.
264. Morad Aaboud et al. Measurement of quarkonium production in proton-lead and proton-proton collisions at 5.02 TeV with the ATLAS detector. *Eur. Phys. J.*, C78(3):171, 2018. doi:10.1140/epjc/s10052-018-5624-4.
265. R. Aaij et al. Prompt and nonprompt J/ψ production and nuclear modification in pPb collisions at $\sqrt{s_{\text{NN}}} = 8.16$ TeV. *Phys. Lett.*, B774:159–178, 2017. doi:10.1016/j.physletb.2017.09.058.
266. D. Adamová et al. J/ψ production as a function of charged-particle pseudorapidity density in p-Pb collisions at $\sqrt{s_{\text{NN}}} = 5.02$ TeV. *Phys. Lett.*, B776:91–104, 2018. doi:10.1016/j.physletb.2017.11.008.
267. Albert M. Sirunyan et al. Measurement of prompt and nonprompt charmonium suppression in PbPb collisions at 5.02 TeV. *Eur. Phys. J. C*, 78(6):509, 2018. doi:10.1140/epjc/s10052-018-5950-6.
268. Albert M Sirunyan et al. Suppression of Excited Υ States Relative to the Ground State in Pb-Pb Collisions at $\sqrt{s_{\text{NN}}}=5.02$ TeV. *Phys. Rev. Lett.*, 120(14):142301, 2018. doi:10.1103/PhysRevLett.120.142301.
269. Albert M Sirunyan et al. Measurement of prompt and nonprompt J/ψ production in pp and pPb collisions at $\sqrt{s_{\text{NN}}} = 5.02$ TeV. *Eur. Phys. J.*, C77(4):269, 2017. doi:10.1140/epjc/s10052-017-4828-3.
270. Shreyasi Acharya et al. Inclusive J/ψ production at forward and backward rapidity in p-Pb collisions at $\sqrt{s_{\text{NN}}} = 8.16$ TeV. *JHEP*, 07:160, 2018. doi:10.1007/JHEP07(2018)160.
271. Shreyasi Acharya et al. Prompt and non-prompt J/ψ production and nuclear modification at mid-rapidity in p-Pb collisions at $\sqrt{s_{\text{NN}}} = 5.02$ TeV. *Eur. Phys. J. C*, 78(6):466, 2018. doi:10.1140/epjc/s10052-018-5881-2.
272. Shreyasi Acharya et al. Υ suppression at forward rapidity in Pb-Pb collisions at $\sqrt{s_{\text{NN}}} = 5.02$ TeV. *Phys. Lett. B*, 790:89–101, 2019.

- doi:10.1016/j.physletb.2018.11.067.
273. Morad Aaboud et al. Prompt and non-prompt J/ψ and $\psi(2S)$ suppression at high transverse momentum in 5.02 TeV Pb+Pb collisions with the ATLAS experiment. *Eur. Phys. J. C*, 78(9):762, 2018. doi:10.1140/epjc/s10052-018-6219-9.
274. Albert M Sirunyan et al. Measurement of nuclear modification factors of $\Upsilon(1S)$, $\Upsilon(2S)$, and $\Upsilon(3S)$ mesons in PbPb collisions at $\sqrt{s_{NN}} = 5.02$ TeV. *Phys. Lett. B*, 790:270–293, 2019. doi:10.1016/j.physletb.2019.01.006.
275. Shreyasi Acharya et al. Υ production in p–Pb collisions at $\sqrt{s_{NN}}=8.16$ TeV. *Phys. Lett. B*, 806:135486, 2020. doi:10.1016/j.physletb.2020.135486.
276. Jaroslav Adam et al. Measurement of inclusive J/ψ suppression in Au+Au collisions at $\sqrt{s_{NN}} = 200$ GeV through the dimuon channel at STAR. *Phys. Lett. B*, 797:134917, 2019. doi:10.1016/j.physletb.2019.134917.
277. Shreyasi Acharya et al. Υ production and nuclear modification at forward rapidity in Pb–Pb collisions at $\sqrt{s_{NN}} = 5.02$ TeV. *Phys. Lett. B*, 822:136579, 2021. doi:10.1016/j.physletb.2021.136579.
278. Shreyasi Acharya et al. $\psi(2S)$ Suppression in Pb-Pb Collisions at the LHC. *Phys. Rev. Lett.*, 132(4):042301, 2024. doi:10.1103/PhysRevLett.132.042301.
279. Shreyasi Acharya et al. J/ψ production at midrapidity in p–Pb collisions at $\sqrt{s_{NN}} = 8.16$ TeV. *JHEP*, 07:137, 2023. doi:10.1007/JHEP07(2023)137.
280. Georges Aad et al. Production of $\Upsilon(nS)$ mesons in Pb+Pb and pp collisions at 5.02 TeV. *Phys. Rev. C*, 107(5):054912, 2023. doi:10.1103/PhysRevC.107.054912.
281. Armen Tumasyan et al. Nuclear modification of Υ states in pPb collisions at $\sqrt{s_{NN}} = 5.02$ TeV. *Phys. Lett. B*, 835:137397, 2022. doi:10.1016/j.physletb.2022.137397.
282. Shreyasi Acharya et al. Measurements of inclusive J/ψ production at midrapidity and forward rapidity in Pb–Pb collisions at $\sqrt{s_{NN}} = 5.02$ TeV. *Phys. Lett. B*, 849:138451, 2024. doi:10.1016/j.physletb.2024.138451.
283. Shreyasi Acharya et al. Prompt and non-prompt J/ψ production at midrapidity in Pb–Pb collisions at $\sqrt{s_{NN}} = 5.02$ TeV. *JHEP*, 02:066, 2024. doi:10.1007/JHEP02(2024)066.
284. Armen Tumasyan et al. Observation of the $\Upsilon(3S)$ meson and suppression of Υ states in PbPb collisions at $\sqrt{s_{NN}} = 5.02$ TeV. 3 2023. doi:10.48550/arXiv.2303.17026.
285. Wenbin Zhao, Sangwook Ryu, Chun Shen, and Björn Schenke. 3D structure of anisotropic flow in small collision systems at energies available at the BNL Relativistic Heavy Ion Collider. *Phys. Rev. C*, 107(1):014904, 2023. doi:10.1103/PhysRevC.107.014904.
286. Derek Teaney and Li Yan. Triangularity and Dipole Asymmetry in Heavy Ion Collisions. *Phys. Rev. C*, 83:064904, 2011. doi:10.1103/PhysRevC.83.064904.
287. Derek Teaney and Li Yan. Non linearities in the harmonic spectrum of heavy ion collisions with ideal and viscous hydrodynamics. *Phys. Rev. C*, 86:044908,

2012. doi:10.1103/PhysRevC.86.044908.
288. Stefan Floerchinger, Urs Achim Wiedemann, Andrea Beraudo, Luca Del Zanna, Gabriele Inghirami, and Valentina Rolando. How (non-)linear is the hydrodynamics of heavy ion collisions? *Phys. Lett. B*, 735:305–310, 2014. doi:10.1016/j.physletb.2014.06.049.
289. Jacquelyn Noronha-Hostler, Li Yan, Fernando G. Gardim, and Jean-Yves Ollitrault. Linear and cubic response to the initial eccentricity in heavy-ion collisions. *Phys. Rev. C*, 93(1):014909, 2016. doi:10.1103/PhysRevC.93.014909.
290. Nicolas Borghini, Steffen Feld, and Nina Kersting. Scaling behavior of anisotropic flow harmonics in the far from equilibrium regime. *Eur. Phys. J. C*, 78(10):832, 2018. doi:10.1140/epjc/s10052-018-6313-z.
291. Aleksi Kurkela, Urs Achim Wiedemann, and Bin Wu. Nearly isentropic flow at sizeable η/s . *Phys. Lett. B*, 783:274–279, 2018. doi:10.1016/j.physletb.2018.06.064.
292. E. Andersen et al. Strangeness enhancement at mid-rapidity in Pb Pb collisions at 158-A-GeV/c. *Phys. Lett. B*, 449:401–406, 1999. doi:10.1016/S0370-2693(99)00140-9.
293. Michael Annan Lisa, Scott Pratt, Ron Soltz, and Urs Wiedemann. Femtoscopy in relativistic heavy ion collisions. *Ann. Rev. Nucl. Part. Sci.*, 55:357–402, 2005. doi:10.1146/annurev.nucl.55.090704.151533.
294. Shreyasi Acharya et al. Study of charged particle production at high pT using event topology in pp, p–Pb and Pb–Pb collisions at $\sqrt{s_{NN}}=5.02$ TeV. *Phys. Lett. B*, 843:137649, 2023. doi:10.1016/j.physletb.2022.137649.
295. Anthony Badea, Austin Baty, Paoti Chang, Gian Michele Innocenti, Marcello Maggi, Christopher McGinn, Michael Peters, Tzu-An Sheng, Jesse Thaler, and Yen-Jie Lee. Measurements of two-particle correlations in e^+e^- collisions at 91 GeV with ALEPH archived data. *Phys. Rev. Lett.*, 123(21):212002, 2019. doi:10.1103/PhysRevLett.123.212002.
296. Y. C. Chen et al. Two-particle angular correlations in e^+e^- collisions to hadronic final states in two reference coordinates at Belle. *JHEP*, 03:171, 2023. doi:10.1007/JHEP03(2023)171.
297. Y. C. Chen et al. Measurement of Two-Particle Correlations of Hadrons in $e+e-$ Collisions at Belle. *Phys. Rev. Lett.*, 128(14):142005, 2022. doi:10.1103/PhysRevLett.128.142005.
298. Armen Tumasyan et al. Two-particle azimuthal correlations in γp interactions using pPb collisions at $\sqrt{s_{NN}}=8.16$ TeV. *Phys. Lett. B*, 844:137905, 2023. doi:10.1016/j.physletb.2023.137905.
299. Yu-Chen Chen et al. Long-range near-side correlation in e^+e^- Collisions at 183-209 GeV with ALEPH Archived Data. 12 2023. doi:10.48550/arXiv.2312.05084.
300. I. Abt et al. Two-particle azimuthal correlations as a probe of collective behaviour in deep inelastic ep scattering at HERA. *JHEP*, 04:070, 2020. doi:10.1007/JHEP04(2020)070.

301. I. Abt et al. Azimuthal correlations in photoproduction and deep inelastic ep scattering at HERA. *JHEP*, 12:102, 2021. doi:10.1007/JHEP12(2021)102.
302. Georges Aad et al. Two-particle azimuthal correlations in photonuclear ultra-peripheral Pb+Pb collisions at 5.02 TeV with ATLAS. *Phys. Rev. C*, 104(1):014903, 2021. doi:10.1103/PhysRevC.104.014903.
303. Ulrich Heinz and Raimond Snellings. Collective flow and viscosity in relativistic heavy-ion collisions. *Ann. Rev. Nucl. Part. Sci.*, 63:123–151, 2013. doi:10.1146/annurev-nucl-102212-170540.
304. Chun Shen, Zhi Qiu, Huichao Song, Jonah Bernhard, Steffen Bass, and Ulrich Heinz. The iEBE-VISHNU code package for relativistic heavy-ion collisions. *Comput. Phys. Commun.*, 199:61–85, 2016. doi:10.1016/j.cpc.2015.08.039.
305. M. Habich, J. L. Nagle, and P. Romatschke. Particle spectra and HBT radii for simulated central nuclear collisions of C + C, Al + Al, Cu + Cu, Au + Au, and Pb + Pb from $\sqrt{s} = 62.4 - 2760$ GeV. *Eur. Phys. J. C*, 75(1):15, 2015. doi:10.1140/epjc/s10052-014-3206-7.
306. Bjoern Schenke, Sangyong Jeon, and Charles Gale. (3+1)D hydrodynamic simulation of relativistic heavy-ion collisions. *Phys. Rev. C*, 82:014903, 2010. doi:10.1103/PhysRevC.82.014903.
307. H. Niemi, K. J. Eskola, and R. Paatelainen. Event-by-event fluctuations in a perturbative QCD + saturation + hydrodynamics model: Determining QCD matter shear viscosity in ultrarelativistic heavy-ion collisions. *Phys. Rev. C*, 93(2):024907, 2016. doi:10.1103/PhysRevC.93.024907.
308. D. Devetak, A. Dubla, S. Floerchinger, E. Grossi, S. Masciocchi, A. Mazeliauskas, and I. Selyuzhenkov. Global fluid fits to identified particle transverse momentum spectra from heavy-ion collisions at the Large Hadron Collider. *JHEP*, 06:044, 2020. doi:10.1007/JHEP06(2020)044.
309. Jonah E. Bernhard. *Bayesian parameter estimation for relativistic heavy-ion collisions*. PhD thesis, Duke U., 4 2018.
310. Scott Pratt, Evan Sangaline, Paul Sorensen, and Hui Wang. Constraining the Eq. of State of Super-Hadronic Matter from Heavy-Ion Collisions. *Phys. Rev. Lett.*, 114:202301, 2015. doi:10.1103/PhysRevLett.114.202301.
311. Jonah E. Bernhard, J. Scott Moreland, Steffen A. Bass, Jia Liu, and Ulrich Heinz. Applying Bayesian parameter estimation to relativistic heavy-ion collisions: simultaneous characterization of the initial state and quark-gluon plasma medium. *Phys. Rev. C*, 94(2):024907, 2016. doi:10.1103/PhysRevC.94.024907.
312. D. Everett et al. Multisystem Bayesian constraints on the transport coefficients of QCD matter. *Phys. Rev. C*, 103(5):054904, 2021. doi:10.1103/PhysRevC.103.054904.
313. J. E. Parkkila, A. Onnerstad, and D. J. Kim. Bayesian estimation of the specific shear and bulk viscosity of the quark-gluon plasma with additional flow harmonic observables. *Phys. Rev. C*, 104(5):054904, 2021. doi:10.1103/PhysRevC.104.054904.
314. J. E. Parkkila, A. Onnerstad, S. F. Taghavi, C. Mordasini, A. Bilandzic,

- M. Virta, and D. J. Kim. New constraints for QCD matter from improved Bayesian parameter estimation in heavy-ion collisions at LHC. *Phys. Lett. B*, 835:137485, 2022. doi:10.1016/j.physletb.2022.137485.
315. Matthew R. Heffernan, Charles Gale, Sangyong Jeon, and Jean-François Paquet. Bayesian quantification of strongly interacting matter with color glass condensate initial conditions. *Phys. Rev. C*, 109(6):065207, 2024. doi:10.1103/PhysRevC.109.065207.
316. J. Scott Moreland, Jonah E. Bernhard, and Steffen A. Bass. Bayesian calibration of a hybrid nuclear collision model using p-Pb and Pb-Pb data at energies available at the CERN Large Hadron Collider. *Phys. Rev. C*, 101(2):024911, 2020. doi:10.1103/PhysRevC.101.024911.
317. Govert Nijs, Wilke van der Schee, Umut Gürsoy, and Raimond Snellings. Transverse Momentum Differential Global Analysis of Heavy-Ion Collisions. *Phys. Rev. Lett.*, 126(20):202301, 2021. doi:10.1103/PhysRevLett.126.202301.
318. Govert Nijs, Wilke van der Schee, Umut Gürsoy, and Raimond Snellings. Bayesian analysis of heavy ion collisions with the heavy ion computational framework Trajectum. *Phys. Rev. C*, 103(5):054909, 2021. doi:10.1103/PhysRevC.103.054909.
319. Govert Nijs and Wilke van der Schee. Predictions and postdictions for relativistic lead and oxygen collisions with the computational simulation code Trajectum. *Phys. Rev. C*, 106(4):044903, 2022. doi:10.1103/PhysRevC.106.044903.
320. Moritz Greif, Carsten Greiner, Björn Schenke, Sören Schlichting, and Zhe Xu. Importance of initial and final state effects for azimuthal correlations in p+Pb collisions. *Phys. Rev. D*, 96(9):091504, 2017. doi:10.1103/PhysRevD.96.091504.
321. Zi-Wei Lin, Che Ming Ko, Bao-An Li, Bin Zhang, and Subrata Pal. A Multi-phase transport model for relativistic heavy ion collisions. *Phys. Rev. C*, 72:064901, 2005. doi:10.1103/PhysRevC.72.064901.
322. Chao Zhang, Liang Zheng, Feng Liu, Shusu Shi, and Zi-Wei Lin. Update of a multiphase transport model with modern parton distribution functions and nuclear shadowing. *Phys. Rev. C*, 99(6):064906, 2019. doi:10.1103/PhysRevC.99.064906.
323. Zi-Wei Lin and Liang Zheng. Further developments of a multi-phase transport model for relativistic nuclear collisions. *Nucl. Sci. Tech.*, 32(10):113, 2021. doi:10.1007/s41365-021-00944-5.
324. Zhe Xu and Carsten Greiner. Transport rates and momentum isotropization of gluon matter in ultrarelativistic heavy-ion collisions. *Phys. Rev. C*, 76:024911, 2007. doi:10.1103/PhysRevC.76.024911.
325. Jan Uphoff, Florian Senzel, Oliver Fochler, Christian Wesp, Zhe Xu, and Carsten Greiner. Elliptic flow and nuclear modification factor in ultrarelativistic heavy-ion collisions within a partonic transport model. *Phys. Rev. Lett.*, 114(11):112301, 2015. doi:10.1103/PhysRevLett.114.112301.
326. T. Pierog, Iu. Karpenko, J. M. Katzy, E. Yatsenko, and K. Werner.

- EPOS LHC: Test of collective hadronization with data measured at the CERN Large Hadron Collider. *Phys. Rev. C*, 92(3):034906, 2015. doi:10.1103/PhysRevC.92.034906.
327. Klaus Werner. Revealing a deep connection between factorization and saturation: New insight into modeling high-energy proton-proton and nucleus-nucleus scattering in the EPOS4 framework. *Phys. Rev. C*, 108(6):064903, 2023. doi:10.1103/PhysRevC.108.064903.
328. J. D. Bjorken. Highly Relativistic Nucleus-Nucleus Collisions: The Central Rapidity Region. *Phys. Rev. D*, 27:140–151, 1983. doi:10.1103/PhysRevD.27.140.
329. Dirk H. Rischke. Fluid dynamics for relativistic nuclear collisions. *Lect. Notes Phys.*, 516:21, 1999. doi:10.1007/BFb0107310.
330. Raphael E. Houtt and Pavel Kovtun. Stable and causal relativistic Navier-Stokes equations. *JHEP*, 06:067, 2020. doi:10.1007/JHEP06(2020)067.
331. Fabio S. Bemfica, Marcelo M. Disconzi, and Jorge Noronha. First-Order General-Relativistic Viscous Fluid Dynamics. *Phys. Rev. X*, 12(2):021044, 2022. doi:10.1103/PhysRevX.12.021044.
332. Peter Brockway Arnold, Guy D. Moore, and Laurence G. Yaffe. Effective kinetic theory for high temperature gauge theories. *JHEP*, 01:030, 2003. doi:10.1088/1126-6708/2003/01/030.
333. Peter Brockway Arnold, Guy D Moore, and Laurence G. Yaffe. Transport coefficients in high temperature gauge theories. 2. Beyond leading log. *JHEP*, 05:051, 2003. doi:10.1088/1126-6708/2003/05/051.
334. W. Israel and J. M. Stewart. Transient relativistic thermodynamics and kinetic theory. *Annals Phys.*, 118:341–372, 1979. doi:10.1016/0003-4916(79)90130-1.
335. Ingo Müller. Zum Paradoxon der Wärmeleitungstheorie. *Zeitschrift für Physik*, 198:329, 1967. doi:10.1007/BF01326412.
336. W. A. Hiscock and L. Lindblom. Stability and causality in dissipative relativistic fluids. *Annals Phys.*, 151:466–496, 1983. doi:10.1016/0003-4916(83)90288-9.
337. William A. Hiscock and Lee Lindblom. Generic instabilities in first-order dissipative relativistic fluid theories. *Phys. Rev. D*, 31:725–733, 1985. doi:10.1103/PhysRevD.31.725.
338. Azwinndini Muronga. Second order dissipative fluid dynamics for ultrarelativistic nuclear collisions. *Phys. Rev. Lett.*, 88:062302, 2002. doi:10.1103/PhysRevLett.88.062302. [Erratum: Phys.Rev.Lett. 89, 159901 (2002)].
339. Azwinndini Muronga. Causal theories of dissipative relativistic fluid dynamics for nuclear collisions. *Phys. Rev. C*, 69:034903, 2004. doi:10.1103/PhysRevC.69.034903.
340. Azwinndini Muronga. Shear viscosity coefficient from microscopic models. *Phys. Rev. C*, 69:044901, 2004. doi:10.1103/PhysRevC.69.044901.
341. G. S. Denicol, H. Niemi, E. Molnar, and D. H. Rischke. Derivation of transient relativistic fluid dynamics from the Boltzmann equation. *Phys. Rev. D*, 85:114047, 2012. doi:10.1103/PhysRevD.85.114047. [Erratum: Phys.Rev.D 91,

- 039902 (2015)].
342. Paul Romatschke. Retarded correlators in kinetic theory: branch cuts, poles and hydrodynamic onset transitions. *Eur. Phys. J. C*, 76(6):352, 2016. doi:10.1140/epjc/s10052-016-4169-7.
 343. Alekski Kurkela and Urs Achim Wiedemann. Analytic structure of nonhydrodynamic modes in kinetic theory. *Eur. Phys. J. C*, 79(9):776, 2019. doi:10.1140/epjc/s10052-019-7271-9.
 344. Stephan Ochsened and Sören Schlichting. Hydrodynamic and nonhydrodynamic excitations in kinetic theory — a numerical analysis in scalar field theory. *JHEP*, 09:186, 2023. doi:10.1007/JHEP09(2023)186.
 345. Xiaojian Du, Stephan Ochsened, and Sören Schlichting. Universality of energy-momentum response in kinetic theories. *Phys. Lett. B*, 845:138161, 2023. doi:10.1016/j.physletb.2023.138161.
 346. Melville S. Green. Markoff Random Processes and the Statistical Mechanics of Time-Dependent Phenomena. II. Irreversible Processes in Fluids. *J. Chem. Phys.*, 22(3):398, 1954. doi:10.1063/1.1740082.
 347. Ryogo Kubo. Statistical mechanical theory of irreversible processes. 1. General theory and simple applications in magnetic and conduction problems. *J. Phys. Soc. Jap.*, 12:570–586, 1957. doi:10.1143/JPSJ.12.570.
 348. Jacopo Ghiglieri, Guy D. Moore, and Derek Teaney. QCD Shear Viscosity at (almost) NLO. *JHEP*, 03:179, 2018. doi:10.1007/JHEP03(2018)179.
 349. Harvey B. Meyer. A Calculation of the bulk viscosity in SU(3) gluodynamics. *Phys. Rev. Lett.*, 100:162001, 2008. doi:10.1103/PhysRevLett.100.162001.
 350. Harvey B. Meyer. A Calculation of the shear viscosity in SU(3) gluodynamics. *Phys. Rev. D*, 76:101701, 2007. doi:10.1103/PhysRevD.76.101701.
 351. Guy D. Moore. Stress-stress correlator in ϕ^4 theory: poles or a cut? *JHEP*, 05:084, 2018. doi:10.1007/JHEP05(2018)084.
 352. Sayantani Bhattacharyya, Veronika E Hubeny, Shiraz Minwalla, and Mukund Rangamani. Nonlinear Fluid Dynamics from Gravity. *JHEP*, 02:045, 2008. doi:10.1088/1126-6708/2008/02/045.
 353. Johanna Erdmenger, Michael Haack, Matthias Kaminski, and Amos Yarom. Fluid dynamics of R-charged black holes. *JHEP*, 01:055, 2009. doi:10.1088/1126-6708/2009/01/055.
 354. D. E. Kharzeev, J. Liao, S. A. Voloshin, and G. Wang. Chiral magnetic and vortical effects in high-energy nuclear collisions—A status report. *Prog. Part. Nucl. Phys.*, 88:1–28, 2016. doi:10.1016/j.pnpnp.2016.01.001.
 355. Dam T. Son and Piotr Surowka. Hydrodynamics with Triangle Anomalies. *Phys. Rev. Lett.*, 103:191601, 2009. doi:10.1103/PhysRevLett.103.191601.
 356. Dam T. Son and Andrei O. Starinets. Minkowski space correlators in AdS / CFT correspondence: Recipe and applications. *JHEP*, 09:042, 2002. doi:10.1088/1126-6708/2002/09/042.
 357. Andrei O. Starinets. Quasinormal modes of near extremal black branes. *Phys. Rev. D*, 66:124013, 2002. doi:10.1103/PhysRevD.66.124013.

358. Sean A. Hartnoll and S. Prem Kumar. AdS black holes and thermal Yang-Mills correlators. *JHEP*, 12:036, 2005. doi:10.1088/1126-6708/2005/12/036.
359. Sašo Grozdanov, Nikolaos Kaplis, and Andrei O. Starinets. From strong to weak coupling in holographic models of thermalization. *JHEP*, 07:151, 2016. doi:10.1007/JHEP07(2016)151.
360. Jorge Casalderrey-Solana, Sašo Grozdanov, and Andrei O. Starinets. Transport Peak in the Thermal Spectral Function of $\mathcal{N} = 4$ Supersymmetric Yang-Mills Plasma at Intermediate Coupling. *Phys. Rev. Lett.*, 121(19):191603, 2018. doi:10.1103/PhysRevLett.121.191603.
361. Sašo Grozdanov and Andrei O. Starinets. Adding new branches to the “Christmas tree” of the quasinormal spectrum of black branes. *JHEP*, 04:080, 2019. doi:10.1007/JHEP04(2019)080.
362. L. D. Landau and E. M. Lifshitz. *Fluid Mechanics*. Pergamon, New York, 1959.
363. Harold Grad. On the kinetic theory of rarefied gases. *Commun. Pure Appl. Math.*, 2(4):331–407, 1949. doi:10.1002/cpa.3160020403.
364. G. Baym. THERMAL EQUILIBRATION IN ULTRARELATIVISTIC HEAVY ION COLLISIONS. *Phys. Lett. B*, 138:18–22, 1984. doi:10.1016/0370-2693(84)91863-X.
365. R. Baier, Alfred H. Mueller, D. Schiff, and D. T. Son. ‘Bottom up’ thermalization in heavy ion collisions. *Phys. Lett. B*, 502:51–58, 2001. doi:10.1016/S0370-2693(01)00191-5.
366. Alekski Kurkela and Egang Lu. Approach to Equilibrium in Weakly Coupled Non-Abelian Plasmas. *Phys. Rev. Lett.*, 113(18):182301, 2014. doi:10.1103/PhysRevLett.113.182301.
367. Alekski Kurkela and Yan Zhu. Isotropization and hydrodynamization in weakly coupled heavy-ion collisions. *Phys. Rev. Lett.*, 115(18):182301, 2015. doi:10.1103/PhysRevLett.115.182301.
368. Alekski Kurkela, Aleksas Mazeliauskas, Jean-François Paquet, Sören Schlichting, and Derek Teaney. Effective kinetic description of event-by-event pre-equilibrium dynamics in high-energy heavy-ion collisions. *Phys. Rev. C*, 99(3):034910, 2019. doi:10.1103/PhysRevC.99.034910.
369. Alekski Kurkela, Aleksas Mazeliauskas, Jean-François Paquet, Sören Schlichting, and Derek Teaney. Matching the Nonequilibrium Initial Stage of Heavy Ion Collisions to Hydrodynamics with QCD Kinetic Theory. *Phys. Rev. Lett.*, 122(12):122302, 2019. doi:10.1103/PhysRevLett.122.122302.
370. Alekski Kurkela, Robin Törnkvist, and Korinna Zapp. AMY Lorentz invariant parton cascade – the thermal equilibrium case. *Eur. Phys. J. C*, 84(1):74, 2024. doi:10.1140/epjc/s10052-024-12424-2.
371. Nicolas Borghini and Clement Gombeaud. Anisotropic flow far from equilibrium. *Eur. Phys. J. C*, 71:1612, 2011. doi:10.1140/epjc/s10052-011-1612-7.
372. Liang He, Terrence Edmonds, Zi-Wei Lin, Feng Liu, Denes Molnar, and Fuqiang Wang. Anisotropic parton escape is the dominant source of az-

- imuthal anisotropy in transport models. *Phys. Lett. B*, 753:506–510, 2016. doi:10.1016/j.physletb.2015.12.051.
373. Paul Romatschke. Azimuthal Anisotropies at High Momentum from Purely Non-Hydrodynamic Transport. *Eur. Phys. J. C*, 78(8):636, 2018. doi:10.1140/epjc/s10052-018-6112-6.
374. Simon Caron-Huot and Charles Gale. Finite-size effects on the radiative energy loss of a fast parton in hot and dense strongly interacting matter. *Phys. Rev. C*, 82:064902, 2010. doi:10.1103/PhysRevC.82.064902.
375. R. Baier, D. Schiff, and B. G. Zakharov. Energy loss in perturbative QCD. *Ann. Rev. Nucl. Part. Sci.*, 50:37–69, 2000. doi:10.1146/annurev.nucl.50.1.37.
376. Bjoern Schenke, Prithwish Tribedy, and Raju Venugopalan. Fluctuating Glasma initial conditions and flow in heavy ion collisions. *Phys. Rev. Lett.*, 108:252301, 2012. doi:10.1103/PhysRevLett.108.252301.
377. Bjoern Schenke, Prithwish Tribedy, and Raju Venugopalan. Event-by-event gluon multiplicity, energy density, and eccentricities in ultrarelativistic heavy-ion collisions. *Phys. Rev. C*, 86:034908, 2012. doi:10.1103/PhysRevC.86.034908.
378. Kevin Dusling and Raju Venugopalan. Azimuthal collimation of long range rapidity correlations by strong color fields in high multiplicity hadron-hadron collisions. *Phys. Rev. Lett.*, 108:262001, 2012. doi:10.1103/PhysRevLett.108.262001.
379. Kevin Dusling and Raju Venugopalan. Comparison of the color glass condensate to dihadron correlations in proton-proton and proton-nucleus collisions. *Phys. Rev. D*, 87(9):094034, 2013. doi:10.1103/PhysRevD.87.094034.
380. Mark Mace, Vladimir V. Skokov, Prithwish Tribedy, and Raju Venugopalan. Hierarchy of Azimuthal Anisotropy Harmonics in Collisions of Small Systems from the Color Glass Condensate. *Phys. Rev. Lett.*, 121(5):052301, 2018. doi:10.1103/PhysRevLett.121.052301. [Erratum: *Phys.Rev.Lett.* 123, 039901 (2019)].
381. J. L. Nagle and W. A. Zajc. Assessing saturation physics explanations of collectivity in small collision systems with the IP-Jazma model. *Phys. Rev. C*, 99(5):054908, 2019. doi:10.1103/PhysRevC.99.054908.
382. Sören Schlichting and Prithwish Tribedy. Collectivity in Small Collision Systems: An Initial-State Perspective. *Adv. High Energy Phys.*, 2016:8460349, 2016. doi:10.1155/2016/8460349.
383. Alex Kovner and Michael Lublinsky. Angular Correlations in Gluon Production at High Energy. *Phys. Rev. D*, 83:034017, 2011. doi:10.1103/PhysRevD.83.034017.
384. M. Gyulassy, P. Levai, I. Vitev, and T. S. Biro. Non-Abelian bremsstrahlung and azimuthal asymmetries in high energy p-A reactions. *Phys. Rev.*, D90(5):054025, 2014. doi:10.1103/PhysRevD.90.054025.
385. Larry McLerran and Vladimir V. Skokov. The eccentric collective BFKL pomeron. *Acta Phys. Polon.*, B46(8):1513, 2015.

- doi:10.5506/APhysPolB.46.1513.
386. Boris Blok, Christian D. Jäkel, Mark Strikman, and Urs Achim Wiedemann. Collectivity from interference. *JHEP*, 12:074, 2017. doi:10.1007/JHEP12(2017)074.
387. Boris Blok and Urs Achim Wiedemann. Collectivity in pp from resummed interference effects? *Phys. Lett. B*, 795:259–265, 2019. doi:10.1016/j.physletb.2019.05.038.
388. T. Lappi, B. Schenke, S. Schlichting, and R. Venugopalan. Tracing the origin of azimuthal gluon correlations in the color glass condensate. *JHEP*, 01:061, 2016. doi:10.1007/JHEP01(2016)061.
389. Bjoern Schenke, Soeren Schlichting, and Pragya Singh. Rapidity dependence of initial state geometry and momentum correlations in p+Pb collisions. *Phys. Rev. D*, 105(9):094023, 2022. doi:10.1103/PhysRevD.105.094023.
390. Björn Schenke, Sören Schlichting, and Raju Venugopalan. Azimuthal anisotropies in p+Pb collisions from classical Yang–Mills dynamics. *Phys. Lett. B*, 747:76–82, 2015. doi:10.1016/j.physletb.2015.05.051.
391. Bjoern Schenke, Chun Shen, and Prithwish Tribedy. Hybrid Color Glass Condensate and hydrodynamic description of the Relativistic Heavy Ion Collider small system scan. *Phys. Lett. B*, 803:135322, 2020. doi:10.1016/j.physletb.2020.135322.
392. Christian Bierlich, Gösta Gustafson, and Leif Lönnblad. A shoving model for collectivity in hadronic collisions. 12 2016. doi:10.48550/arXiv.1612.05132.
393. Christian Bierlich, Gösta Gustafson, and Leif Lönnblad. Collectivity without plasma in hadronic collisions. *Phys. Lett. B*, 779:58–63, 2018. doi:10.1016/j.physletb.2018.01.069.
394. Christian Bierlich, Gösta Gustafson, Leif Lönnblad, and Harsh Shah. The Angantyr model for Heavy-Ion Collisions in PYTHIA8. *JHEP*, 10:134, 2018. doi:10.1007/JHEP10(2018)134.
395. Edward Shuryak. Comments on the CMS discovery of the 'Ridge' in High Multiplicity pp collisions at LHC. 9 2010. doi:10.48550/arXiv.1009.4635.
396. James D. Bjorken, Stanley J. Brodsky, and Alfred Scharff Goldhaber. Possible multiparticle ridge-like correlations in very high multiplicity proton-proton collisions. *Phys. Lett. B*, 726:344–346, 2013. doi:10.1016/j.physletb.2013.08.066.
397. A. Capella, U. Sukhatme, C-I Tan, and J. Tran Thanh Van. Dual parton model. *Phys. Rept.*, 236:225–329, 1994. doi:10.1016/0370-1573(94)90064-7.
398. H. Sorge, Horst Stoecker, and W. Greiner. RELATIVISTIC QUANTUM MOLECULAR DYNAMICS APPROACH TO NUCLEAR COLLISIONS AT ULTRARELATIVISTIC ENERGIES. *Nucl. Phys. A*, 498:567C–576C, 1989. doi:10.1016/0375-9474(89)90641-6.
399. M. Bleicher et al. Relativistic hadron hadron collisions in the ultrarelativistic quantum molecular dynamics model. *J. Phys. G*, 25:1859–1896, 1999. doi:10.1088/0954-3899/25/9/308.
400. Stephen E. Vance and Miklos Gyulassy. Anti-hyperon enhancement

- through baryon junction loops. *Phys. Rev. Lett.*, 83:1735–1738, 1999. doi:10.1103/PhysRevLett.83.1735.
401. Denes Molnar. How AMPT generates large elliptic flow with small cross sections. 6 2019. doi:10.48550/arXiv.1906.12313.
402. M. G. Ryskin, A. D. Martin, and V. A. Khoze. Probes of multiparticle production at the LHC. *J. Phys. G*, 38:085006, 2011. doi:10.1088/0954-3899/38/8/085006.
403. K. Werner, Iu. Karpenko, T. Pierog, M. Bleicher, and K. Mikhailov. Evidence for hydrodynamic evolution in proton-proton scattering at 900 GeV. *Phys. Rev. C*, 83:044915, 2011. doi:10.1103/PhysRevC.83.044915.
404. Soeren Schlichting. New theoretical developments on the early-time dynamics and approach to equilibrium in Heavy-Ion collisions. In *30th International Conference on Ultrarelativistic Nucleus-Nucleus Collisions*, 1 2024. doi:10.48550/arXiv.2401.03841.
405. Aleksi Kurkela, Wilke van der Schee, Urs Achim Wiedemann, and Bin Wu. Early- and Late-Time Behavior of Attractors in Heavy-Ion Collisions. *Phys. Rev. Lett.*, 124(10):102301, 2020. doi:10.1103/PhysRevLett.124.102301.
406. Paul Romatschke. Relativistic Hydrodynamic Attractors with Broken Symmetries: Non-Conformal and Non-Homogeneous. *JHEP*, 12:079, 2017. doi:10.1007/JHEP12(2017)079.
407. Paul Romatschke. Relativistic Fluid Dynamics Far From Local Equilibrium. *Phys. Rev. Lett.*, 120(1):012301, 2018. doi:10.1103/PhysRevLett.120.012301.
408. Michael Strickland, Jorge Noronha, and Gabriel Denicol. Anisotropic nonequilibrium hydrodynamic attractor. *Phys. Rev. D*, 97(3):036020, 2018. doi:10.1103/PhysRevD.97.036020.
409. Jean-Paul Blaizot and Li Yan. Fluid dynamics of out of equilibrium boost invariant plasmas. *Phys. Lett. B*, 780:283–286, 2018. doi:10.1016/j.physletb.2018.02.058.
410. Michal P. Heller and Viktor Svensson. How does relativistic kinetic theory remember about initial conditions? *Phys. Rev. D*, 98(5):054016, 2018. doi:10.1103/PhysRevD.98.054016.
411. Alireza Behtash, Syo Kamata, Mauricio Martinez, and Haosheng Shi. Dynamical systems and nonlinear transient rheology of the far-from-equilibrium Bjorken flow. *Phys. Rev. D*, 99(11):116012, 2019. doi:10.1103/PhysRevD.99.116012.
412. Michael Strickland and Ubaid Tantiary. Exact solution for the non-equilibrium attractor in number-conserving relaxation time approximation. *JHEP*, 10:069, 2019. doi:10.1007/JHEP10(2019)069.
413. M. Strickland. The non-equilibrium attractor for kinetic theory in relaxation time approximation. *JHEP*, 12:128, 2018. doi:10.1007/JHEP12(2018)128.
414. Michał Spaliński. On the hydrodynamic attractor of Yang–Mills plasma. *Phys. Lett. B*, 776:468–472, 2018. doi:10.1016/j.physletb.2017.11.059.
415. Michał Spaliński. Universal behaviour, transients and attractors in

- supersymmetric Yang–Mills plasma. *Phys. Lett. B*, 784:21–25, 2018. doi:10.1016/j.physletb.2018.07.003.
416. Jürgen Berges, Michal P. Heller, Aleksas Mazeliauskas, and Raju Venugopalan. QCD thermalization: Ab initio approaches and interdisciplinary connections. *Rev. Mod. Phys.*, 93(3):035003, 2021. doi:10.1103/RevModPhys.93.035003.
417. Aleksis Kurkela and Aleksas Mazeliauskas. Chemical Equilibration in Hadronic Collisions. *Phys. Rev. Lett.*, 122:142301, 2019. doi:10.1103/PhysRevLett.122.142301.
418. Xiaojian Du and Sören Schlichting. Equilibration of the Quark-Gluon Plasma at Finite Net-Baryon Density in QCD Kinetic Theory. *Phys. Rev. Lett.*, 127(12):122301, 2021. doi:10.1103/PhysRevLett.127.122301.
419. Gabriel S. Denicol and Jorge Noronha. Divergence of the Chapman-Enskog expansion in relativistic kinetic theory. 8 2016. doi:10.48550/arXiv.1608.07869.
420. Michal P. Heller, Aleksis Kurkela, Michal Spaliński, and Viktor Svensson. Hydrodynamization in kinetic theory: Transient modes and the gradient expansion. *Phys. Rev. D*, 97(9):091503, 2018. doi:10.1103/PhysRevD.97.091503.
421. Alireza Behtash, C. N. Cruz-Camacho, and M. Martinez. Far-from-equilibrium attractors and nonlinear dynamical systems approach to the Gubser flow. *Phys. Rev. D*, 97(4):044041, 2018. doi:10.1103/PhysRevD.97.044041.
422. Gabriel S. Denicol and Jorge Noronha. Hydrodynamic attractor and the fate of perturbative expansions in Gubser flow. *Phys. Rev. D*, 99(11):116004, 2019. doi:10.1103/PhysRevD.99.116004.
423. Jasmine Brewer, Li Yan, and Yi Yin. Adiabatic hydrodynamization in rapidly-expanding quark-gluon plasma. *Phys. Lett. B*, 816:136189, 2021. doi:10.1016/j.physletb.2021.136189.
424. Aleksis Kurkela, Seyed Farid Taghavi, Urs Achim Wiedemann, and Bin Wu. Hydrodynamization in systems with detailed transverse profiles. *Phys. Lett. B*, 811:135901, 2020. doi:10.1016/j.physletb.2020.135901.
425. Victor E. Ambrus, S. Schlichting, and C. Werthmann. Development of transverse flow at small and large opacities in conformal kinetic theory. *Phys. Rev. D*, 105(1):014031, 2022. doi:10.1103/PhysRevD.105.014031.
426. Chandrodoy Chattopadhyay, Sunil Jaiswal, Lipei Du, Ulrich Heinz, and Subrata Pal. Non-conformal attractor in boost-invariant plasmas. *Phys. Lett. B*, 824:136820, 2022. doi:10.1016/j.physletb.2021.136820.
427. Nicolas Borghini, Marc Borrell, Nina Feld, Hendrik Roch, Sören Schlichting, and Clemens Werthmann. Statistical analysis of initial-state and final-state response in heavy-ion collisions. *Phys. Rev. C*, 107(3):034905, 2023. doi:10.1103/PhysRevC.107.034905.
428. Paul M. Chesler. Colliding shock waves and hydrodynamics in small systems. *Phys. Rev. Lett.*, 115(24):241602, 2015. doi:10.1103/PhysRevLett.115.241602.
429. Paul M. Chesler and Laurence G. Yaffe. Holography and off-center collisions of localized shock waves. *JHEP*, 10:070, 2015. doi:10.1007/JHEP10(2015)070.
430. Paul M. Chesler. How big are the smallest drops of quark-gluon plasma?

- JHEP*, 03:146, 2016. doi:10.1007/JHEP03(2016)146.
431. I. Bautista, L. Cunqueiro, J. Dias de Deus, and C. Pajares. Particle production azimuthal asymmetries in a clustering of color sources. *J. Phys. G*, 37:015103, 2010. doi:10.1088/0954-3899/37/1/015103.
432. L. Cunqueiro, J. Dias de Deus, and C. Pajares. Nuclear like effects in proton-proton collisions at high energy. *Eur. Phys. J. C*, 65:423–426, 2010. doi:10.1140/epjc/s10052-009-1215-8.
433. Matthew Luzum and Paul Romatschke. Viscous Hydrodynamic Predictions for Nuclear Collisions at the LHC. *Phys. Rev. Lett.*, 103:262302, 2009. doi:10.1103/PhysRevLett.103.262302.
434. G. Ortona, G. S. Denicol, Ph. Mota, and T. Kodama. Elliptic flow in high multiplicity proton-proton collisions at $\sqrt{s}(1/2) = 14$ -TeV as a signature of deconfinement and quantum energy density fluctuations. 11 2009. doi:10.48550/arXiv.0911.5158.
435. S. K. Prasad, Victor Roy, S. Chattopadhyay, and A. K. Chaudhuri. Elliptic flow (v_2) in pp collisions at energies available at the CERN Large Hadron Collider: A hydrodynamical approach. *Phys. Rev. C*, 82:024909, 2010. doi:10.1103/PhysRevC.82.024909.
436. Piotr Bozek. Elliptic flow in proton-proton collisions at $\sqrt{s}(S) = 7$ TeV. *Eur. Phys. J. C*, 71:1530, 2011. doi:10.1140/epjc/s10052-010-1530-0.
437. Jorge Casalderrey-Solana and Urs Achim Wiedemann. Eccentricity fluctuations make flow measurable in high multiplicity p-p collisions. *Phys. Rev. Lett.*, 104:102301, 2010. doi:10.1103/PhysRevLett.104.102301.
438. D. d’Enterria, G. Kh. Eyyubova, V. L. Korotkikh, I. P. Lokhtin, S. V. Petrushanko, L. I. Sarycheva, and A. M. Snigirev. Estimates of hadron azimuthal anisotropy from multiparton interactions in proton-proton collisions at $\sqrt{s} = 14$ TeV. *Eur. Phys. J. C*, 66:173–185, 2010. doi:10.1140/epjc/s10052-009-1232-7.
439. H. Von Gersdorff, Larry D. McLerran, M. Kataja, and P. V. Ruuskanen. Studies of the Hydrodynamic Evolution of Matter Produced in Fluctuations in anti-p p Collisions and in Ultrarelativistic Nuclear Collisions. *Phys. Rev. D*, 34:794, 1986. doi:10.1103/PhysRevD.34.794.
440. Adrian Dumitru, Kevin Dusling, Francois Gelis, Jamal Jalilian-Marian, Tuomas Lappi, and Raju Venugopalan. The Ridge in proton-proton collisions at the LHC. *Phys. Lett. B*, 697:21–25, 2011. doi:10.1016/j.physletb.2011.01.024.
441. Paul Romatschke. Light-Heavy Ion Collisions: A window into pre-equilibrium QCD dynamics? *Eur. Phys. J. C*, 75(7):305, 2015. doi:10.1140/epjc/s10052-015-3509-3.
442. Ryan D. Weller and Paul Romatschke. One fluid to rule them all: viscous hydrodynamic description of event-by-event central p+p, p+Pb and Pb+Pb collisions at $\sqrt{s} = 5.02$ TeV. *Phys. Lett.*, B774:351–356, 2017. doi:10.1016/j.physletb.2017.09.077.
443. You Zhou, Wenbin Zhao, Koichi Murase, and Huichao Song. One

- fluid might not rule them all. *Nucl. Phys. A*, 1005:121908, 2021. doi:10.1016/j.nuclphysa.2020.121908.
444. Wenbin Zhao, Che Ming Ko, Yu-Xin Liu, Guang-You Qin, and Huichao Song. Probing the Partonic Degrees of Freedom in High-Multiplicity $p - Pb$ collisions at $\sqrt{s_{NN}} = 5.02$ TeV. *Phys. Rev. Lett.*, 125(7):072301, 2020. doi:10.1103/PhysRevLett.125.072301.
445. Paul Romatschke. Collective flow without hydrodynamics: simulation results for relativistic ion collisions. *Eur. Phys. J. C*, 75(9):429, 2015. doi:10.1140/epjc/s10052-015-3646-8.
446. You Zhou, Xiangrong Zhu, Pengfei Li, and Huichao Song. Investigation of possible hadronic flow in $\sqrt{s_{NN}} = 5.02$ TeV $p - Pb$ collisions. *Phys. Rev. C*, 91:064908, 2015. doi:10.1103/PhysRevC.91.064908.
447. Kevin Welsh, Jordan Singer, and Ulrich W. Heinz. Initial state fluctuations in collisions between light and heavy ions. *Phys. Rev. C*, 94(2):024919, 2016. doi:10.1103/PhysRevC.94.024919.
448. Wenbin Zhao, You Zhou, Haojie Xu, Weitian Deng, and Huichao Song. Hydrodynamic collectivity in proton-proton collisions at 13 TeV. *Phys. Lett. B*, 780:495–500, 2018. doi:10.1016/j.physletb.2018.03.022.
449. Wenbin Zhao, You Zhou, Koichi Murase, and Huichao Song. Searching for small droplets of hydrodynamic fluid in proton-proton collisions at the LHC. *Eur. Phys. J. C*, 80(9):846, 2020. doi:10.1140/epjc/s10052-020-8376-x.
450. Zeming Wu, Baochi Fu, Shujun Zhao, Runsheng Liu, and Huichao Song. Collective flow and the fluid behavior in $p/d/{}^3\text{He} + \text{Au}$ collisions at $\sqrt{s_{NN}} = 200$ GeV. 7 2023. doi:10.48550/arXiv.2307.02995.
451. K. Werner, Iu. Karpenko, and T. Pierog. The 'Ridge' in Proton-Proton Scattering at 7 TeV. *Phys. Rev. Lett.*, 106:122004, 2011. doi:10.1103/PhysRevLett.106.122004.
452. K. Werner, M. Bleicher, B. Guiot, Iu. Karpenko, and T. Pierog. Evidence for Flow from Hydrodynamic Simulations of p -Pb Collisions at 5.02 TeV from ν_2 Mass Splitting. *Phys. Rev. Lett.*, 112(23):232301, 2014. doi:10.1103/PhysRevLett.112.232301.
453. K. Werner, B. Guiot, Iu. Karpenko, and T. Pierog. Analysing radial flow features in p -Pb and p -p collisions at several TeV by studying identified particle production in EPOS3. *Phys. Rev. C*, 89(6):064903, 2014. doi:10.1103/PhysRevC.89.064903.
454. Sascha Vogel, Pol Bernard Gossiaux, Klaus Werner, and Joerg Aichelin. Heavy Quark Energy Loss in High Multiplicity Proton Proton Collisions at LHC. *Phys. Rev. Lett.*, 107:032302, 2011. doi:10.1103/PhysRevLett.107.032302.
455. Fu-Ming Liu and Klaus Werner. Direct photons at low transverse momentum: A QGP signal in pp collisions at LHC. *Phys. Rev. Lett.*, 106:242301, 2011. doi:10.1103/PhysRevLett.106.242301.
456. Klaus Geiger and Berndt Muller. Dynamics of parton cascades in highly relativistic nuclear collisions. *Nucl. Phys. B*, 369:600–654, 1992. doi:10.1016/0550-

- 3213(92)90280-O.
457. G. Peter, D. Behrens, and C. C. Noack. Poincare covariant particle dynamics. 1: Intranuclear cascade model. *Phys. Rev. C*, 49:3253–3265, 1994. doi:10.1103/PhysRevC.49.3253.
458. Miklos Gyulassy, Yang Pang, and Bin Zhang. Transverse energy evolution as a test of parton cascade models. *Nucl. Phys. A*, 626:999–1018, 1997. doi:10.1016/S0375-9474(97)00604-0.
459. Bin Zhang. ZPC 1.0.1: A Parton cascade for ultrarelativistic heavy ion collisions. *Comput. Phys. Commun.*, 109:193–206, 1998. doi:10.1016/S0010-4655(98)00010-1.
460. Bin Zhang, Miklos Gyulassy, and Yang Pang. Equation of state and collision rate tests of parton cascade models. *Phys. Rev. C*, 58:1175–1182, 1998. doi:10.1103/PhysRevC.58.1175.
461. V. Borchers, J. Meyer, St. Gieseke, G. Martens, and C. C. Noack. A Poincare covariant parton cascade model for ultrarelativistic heavy ion reactions. *Phys. Rev. C*, 62:064903, 2000. doi:10.1103/PhysRevC.62.064903.
462. Denes Molnar and Miklos Gyulassy. New solutions to covariant nonequilibrium dynamics. *Phys. Rev. C*, 62:054907, 2000. doi:10.1103/PhysRevC.62.054907.
463. S. A. Bass, Berndt Muller, and D. K. Srivastava. Parton rescattering and screening in Au+Au collisions at RHIC. *Phys. Lett. B*, 551:277–283, 2003. doi:10.1016/S0370-2693(02)03068-X.
464. Adam Bzdak and Guo-Liang Ma. Elliptic and triangular flow in p +Pb and peripheral Pb+Pb collisions from parton scatterings. *Phys. Rev. Lett.*, 113(25):252301, 2014. doi:10.1103/PhysRevLett.113.252301.
465. Guo-Liang Ma and Adam Bzdak. Long-range azimuthal correlations in proton–proton and proton–nucleus collisions from the incoherent scattering of partons. *Phys. Lett. B*, 739:209–213, 2014. doi:10.1016/j.physletb.2014.10.066.
466. Piotr Bozek, Adam Bzdak, and Guo-Liang Ma. Rapidity dependence of elliptic and triangular flow in proton–nucleus collisions from collective dynamics. *Phys. Lett. B*, 748:301–305, 2015. doi:10.1016/j.physletb.2015.06.007.
467. J. D. Orjuela Koop, A. Adare, D. McGlinchey, and J. L. Nagle. Azimuthal anisotropy relative to the participant plane from a multiphase transport model in central $p + Au$, $d + Au$, and ${}^3\text{He} + Au$ collisions at $\sqrt{s_{NN}} = 200$ GeV. *Phys. Rev. C*, 92(5):054903, 2015. doi:10.1103/PhysRevC.92.054903.
468. Hanlin Li, Liang He, Zi-Wei Lin, Denes Molnar, Fuqiang Wang, and Wei Xie. Origin of the mass splitting of azimuthal anisotropies in a multiphase transport model. *Phys. Rev. C*, 96(1):014901, 2017. doi:10.1103/PhysRevC.96.014901.
469. Denes Molnar and Miklos Gyulassy. Saturation of elliptic flow and the transport opacity of the gluon plasma at RHIC. *Nucl. Phys. A*, 697:495–520, 2002. doi:10.1016/S0375-9474(01)01224-6. [Erratum: Nucl.Phys.A 703, 893–894 (2002)].
470. Hannah Petersen, Dmytro Oliinychenko, Markus Mayer, Jan Staudenmaier, and Sangwook Ryu. SMASH – A new hadronic transport approach. *Nucl.*

- Phys. A*, 982:399–402, 2019. doi:10.1016/j.nuclphysa.2018.08.008.
471. Christian Bierlich and Jesper Roy Christiansen. Effects of color reconnection on hadron flavor observables. *Phys. Rev. D*, 92(9):094010, 2015. doi:10.1103/PhysRevD.92.094010.
472. Klaus Werner. Core-corona separation in ultra-relativistic heavy ion collisions. *Phys. Rev. Lett.*, 98:152301, 2007. doi:10.1103/PhysRevLett.98.152301.
473. Naoto Tanji and Juergen Berges. Nonequilibrium quark production in the expanding QCD plasma. *Phys. Rev. D*, 97(3):034013, 2018. doi:10.1103/PhysRevD.97.034013.
474. T. S. Biro, E. van Doorn, Berndt Muller, M. H. Thoma, and X. N. Wang. Parton equilibration in relativistic heavy ion collisions. *Phys. Rev. C*, 48:1275–1284, 1993. doi:10.1103/PhysRevC.48.1275.
475. Duncan M. Elliott and Dirk H. Rischke. Chemical equilibration of quarks and gluons at RHIC and LHC energies. *Nucl. Phys. A*, 671:583–608, 2000. doi:10.1016/S0375-9474(99)00840-4.
476. Zhe Xu and Carsten Greiner. Thermalization of gluons in ultrarelativistic heavy ion collisions by including three-body interactions in a parton cascade. *Phys. Rev. C*, 71:064901, 2005. doi:10.1103/PhysRevC.71.064901.
477. Jean-Paul Blaizot, Bin Wu, and Li Yan. Quark production, Bose–Einstein condensates and thermalization of the quark–gluon plasma. *Nucl. Phys. A*, 930:139–162, 2014. doi:10.1016/j.nuclphysa.2014.07.041.
478. Marco Ruggieri, Salvatore Plumari, Francesco Scardina, and Vincenzo Greco. Quarks production in the quark–gluon plasma created in relativistic heavy ion collisions. *Nucl. Phys. A*, 941:201–211, 2015. doi:10.1016/j.nuclphysa.2015.07.004.